UiT
THE ARCTIC UNIVERSITY OF NORWAY

Faculty of Science and Technology

Department of Engineering and Safety

Thermal and Mechanical Properties of SK One Component Polyurethane (SKOCP)

Determining the Thermal and Mechanical properties of SKOCP in Colder Conditions

—

Hans-Kristian Norum Eidesen

TEK-3901 Master thesis in Technology and Safety in the High North
June 2017

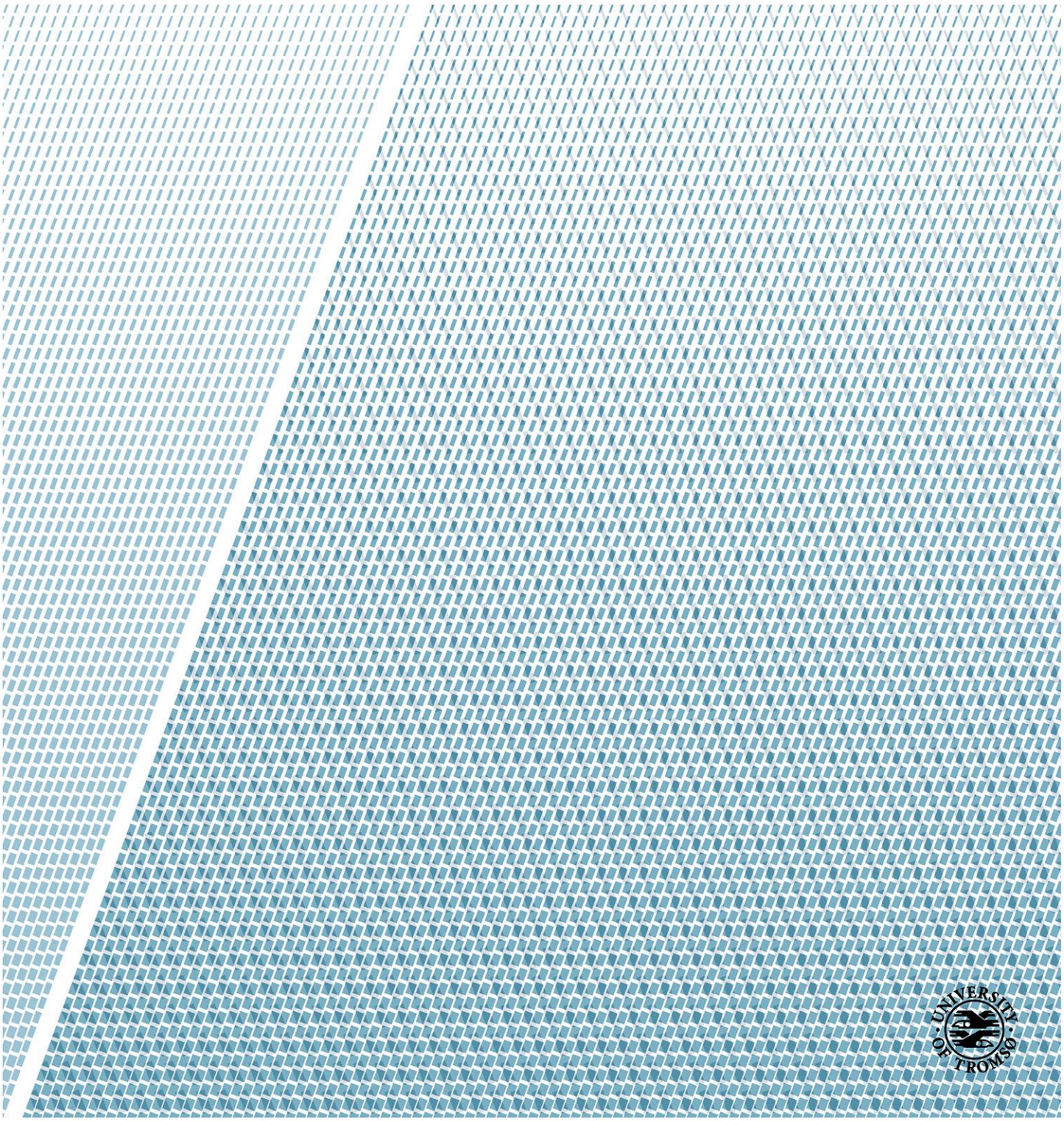

Abstract

Polymers have an extreme wide range of potential applications. From artificial heart valves, computer hardware, coating materials, noise damping materials and so on. Polyurethane is one of the such materials with a broad range of applications. A few such applications and properties are, but not limited to, treatment of leakage of an expansion joint, abrasion resistance, anti-freezing performance and so on (Zhiheng, 2015). Additionally, the fish farm industry uses feed pipes and cages made of polyurethane. The Norwegian oil and gas industry have their eyes set on the Arctic region of the Norwegian continental shelf. If polyurethane is to be used in such conditions, knowledge on how the material changes it properties is needed. Properties that are expected to change are tensile properties, ice adhesion, thermal conductivity and more.

The master thesis focuses on two aspects, namely mechanical and thermal properties of SK One Component Polyurethane (SKOCP). The SKOCP samples are provided by China Institute of Water Resources and Hydropower Research, Beijing, China. There are two different variants known as anti-seepage and anti-abrasion. The thesis is divided into three parts. First part focuses on determining the Young's moduli. Second part investigates ice adhesion, and the third part investigates the thermal properties of SKOCP.

The first part investigates how SKOCP behaves in cold temperatures (for e.g. changes in Young's moduli). In this work, the mechanical behavior of SKOCP was investigated using a four-point bending test. The same phenomenon was simulated in ANSYS workbench. Results revealed the Young's moduli of the samples.

The second part presents ice adhesion to the polyurethane surface. These tests were also performed using four-point bending test. In these, water was poured on the SKOCP surface and allowed to freeze. Upon loading in four-point test, the ice separated. The load indicates the adhesion strength of the ice. Same phenomenon was also simulated in ANSYS workbench for clarity of results.

The third part looks into the thermal properties of SKOCP. In this study two parameters were focused heat transfer coefficient and thermal conductivity. This was done using experiments (IR imaging) compared with numerical solution.

UiT
THE ARCTIC
UNIVERSITY
OF NORWAY

Faculty of Science and Technology

Department of Engineering and Safety

Part A

Determining the Youngs Modulus of SKOCP at Colder Temperatures using Euler-Bernoulli Beam Theory and Four-Point Bending Test

—

Hans-Kristian Norum Eidesen

TEK-3901 Master thesis (Part 1 of 3) in Technology and Safety in the High North
June 2017

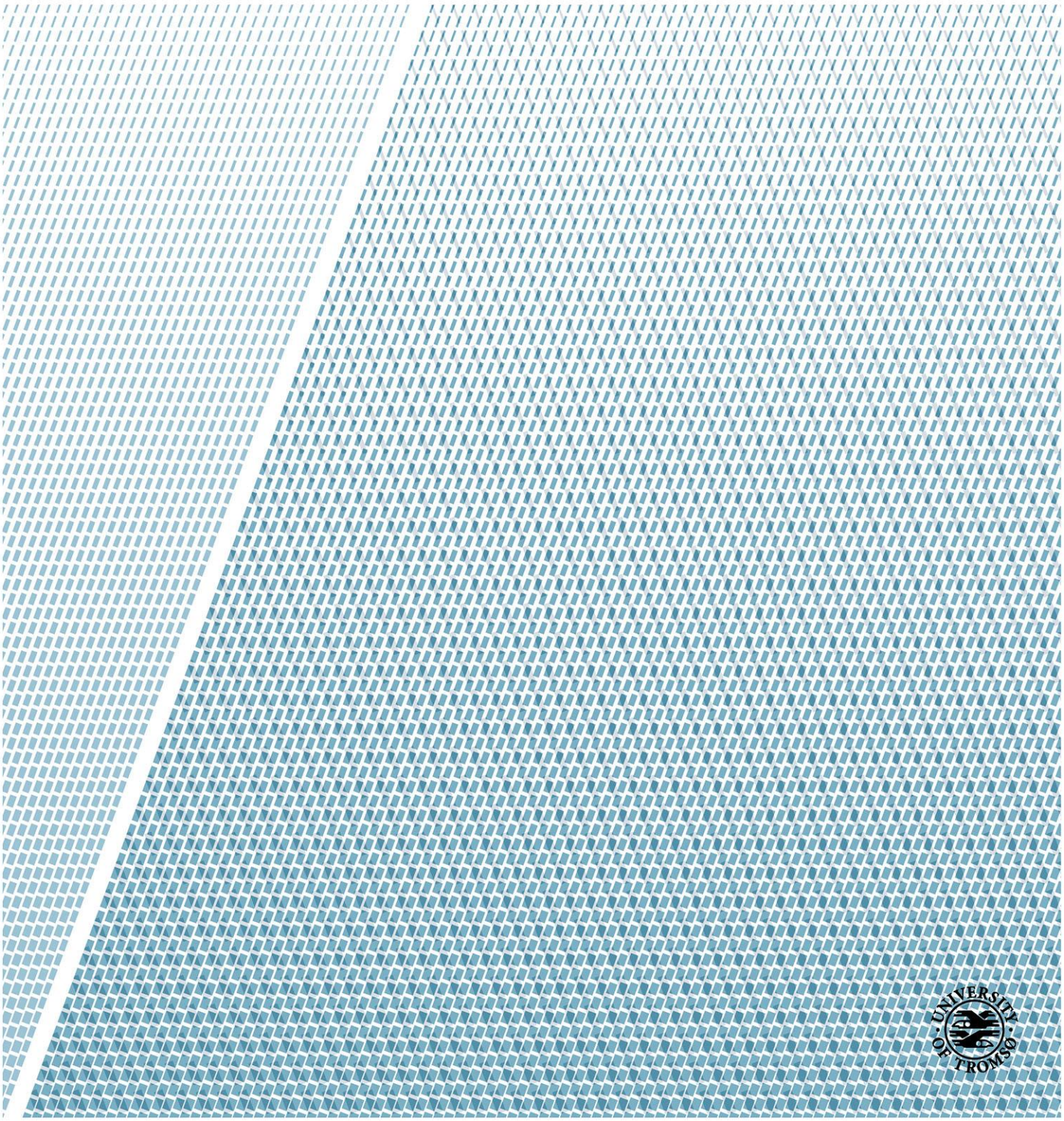

Abstract

By the use of four-point bending and the solution to Euler-Bernoulli beam theory, Young's modulus for SKOCP have been estimated. The results revealed that the Young's modulus had a non-linear behavior, meaning that it was not constant, and was changing with the applied load on the four-point bending. This is because the atomic structure of the polymers. When the specimen is subjected to bending, the long chains that make up the material will be stretched out. However, when a material have a hysteresis behavior, the chains will not return to its original shape.

Table of Contents

List of Figures

List of Tables

Nomenclature

Description	Symbol	Unit
Stress	σ	Pa
Strain	ε	$1\ or\ radian$
Modulus of elasticity	E	Pa
Length	L, L_1 and L_2	m
Shear stress	τ_x	Pa
Shear force	V	N
Longitudinal stress	σ_x	Pa
Bending moment	M	Nm
Distance to the neutral axis	c	m
Second moment of inertia	I	m^4
Slope of a bending beam	θ	$radian$
Radius of a bending beam	R	m
Force of a bending beam	ΔP	N
Differential in $y-direction$	dy	m
The distance to dy to neutral axis	z	m
The distance where the moment is calculated	x	m
Unknowns constants from solving PDEs	C_1 to C_6	N/A
Length of specimen	l	mm
Thickness of specimen	t_s	mm
Width of specimen	b	mm
Cubic fitted curve from MATLAB®	y	kg

Outline

The paper is divided into 5 chapters. The content of each chapter is listed below:

- Chapter 1 gives an introduction to the goal of the paper.
- Chapter 2 is a literature review on ice adhesion, and previous done work in the area..
- Chapter 3 introduces the method that was elected to govern the solutions that was obtained in this paper. Additionally, this chapter gives a mathematically introduction to Euler-Bernoulli beam theory, which a fundamental method to estimate some necessary parameters, such as longitudinal stress.
- Chapter 4 presents the results that was obtain in MATLAB® and ANSYS®.
- Chapter 5 gives the discussion and conclusion.
- Appendix I contains the MATLAB® code that was used to calculate and plot the Young's Modulus for anti-abrasion polyurethane (copy/paste safe).

Chapter 1: Introduction

When materials are utilized in cold climates areas, their material properties, such as the Modulus of Elasticity (Young's Modulus) can change compered to warmer climates. This is dependent on the atomic structure of the material, and how it changes. When a body is subjected to negative heat change, the atoms and molecules that make up the body will have a lower net motion. And thus, how the force that's applied will behave differently compared to warmer surroundings. This paper will determine the Young's modulus of anti-abrasion polyurethane at and anti-seepage polyurethane $-20°C$. This will be done using a four-point stress test bench. The results obtained from the bench will be interpreted and solved with mathematical models based on Euler-Bernoulli beam theory, and by results obtained from simulation in the ANSYS ® Mechanical software bundle.

Chapter 2: Literature Review

2.1. Polyurethane

Polyurethane was invented by Otto Bayer and Heinrich Rinke, in Germany in 1937 (Bayer, 1947), (Prisacariu, 2011) and some of the first use of this plastic was during WWII, where it was applied as a coating of the German airplanes (Seymore & Kauffman, 1992). However, some of the first commercially available products made from polyurethane was rigids foams and rubbers for different purposes. It was discovered that by the addition of different materials (e.g. mica and other processed mineral fibers, and other), the polyurethane got stiffer (Young's modulus) and better heat properties. In 1983, a US car making company made the Pontiac Fiero, where the entire body was made from polyurethane with special additives. As of 2011, the use of polyurethane is spread from construction materials to clothing (Prisacariu, 2011).

Table 1: the distribution of different applications that use polyurethane

Polyurethane use	Amounts (millions of kg)	Percentage (%)
Building and construction	662	26.8
Transportation	589	23.8
Furniture and bedding	511	20.7
Appliances	126	5.1
Packaging	113	4.6
Textile, fibers and apparel	82	3.3
Machinery and Foundry	80	3.3
Electronics	34	1.4
Footwear	17	0.7
Other use	253	10.2
Total	2467	100

2.1.1. Chemistry of Polyurethane

Polyurethane is in the chemical class called reaction polymers (Gum, et al., 1992), (Harrington & Hock, 1991) and (Woods, 1990). The process of making polyurethane involves reaction an isocyanate containing two or more isocyanate groups per molecule $(R - N = C = O)_n$ (Soto, et al., 2014) with a polyol containing hydroxyl groups $(R' - (OH)_n)$ (Soto, et al., 2014) that contain on average two or more molecules. In addition to these molecules, the urethane groups

are introduced $(-NHCO-O)$. These three groups are then put under an ultraviolet light or with a presence of a catalyst, and thus, polyurethane is made. See figure 1 below. Naturally, the process is more complicated than that. It is, however, not the scope of this paper to investigate all the steps in creating polyurethane.

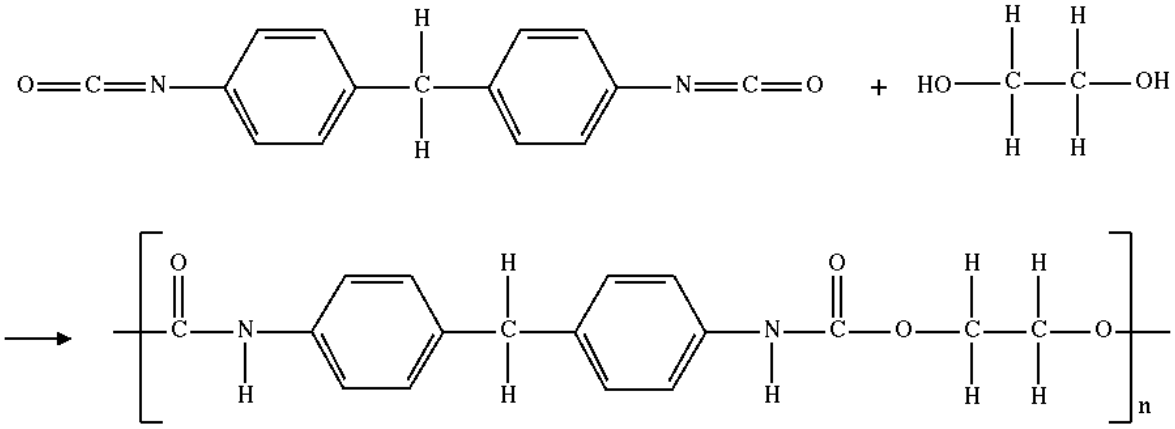

Figure 1: the creation of polyurethane

2.1.2. SK One Component Polyurethane

In this paper, the polyurethane that's tested is developed by China Institute of Water Resources & Hydropower Research Beijing IWHR-KHL Co. Ltd. The product name is SK One Component Polyurethane, however, polyurethane is the name that will be used in the following chapters and sections in this paper. The company provided two distinct types of polyurethane for testing, namely anti-seepage polyurethane and anti-abrasion polyurethane. Anti-seepage polyurethane is suggested to be used as a sealant in either chemical tanks, as it has good resistance to chemical corrosion (Zhiheng, 2015) or in dams to prevent water leaks through the concrete. Anti-abrasion polyurethane can be used on locations where high corrosion is expected. Locations of such can be water ducts from dams, on ships, due to the force of water while ship is in transit, and so forth.

2.3. Modulus of Elasticity

The modulus of elasticity, or Young's Modulus, named after the British scientist Thomas Young, when he published his paper "*A Course of Lectures on Natural Philosophy and the Mechanical Arts*" in 1807. Young's modulus is describing the stiffness of an elastic material (Petrescu, et al., 2011), and also, Young's modulus describes the materials ability to resist elastic deformation, in either compressive or tensile load.

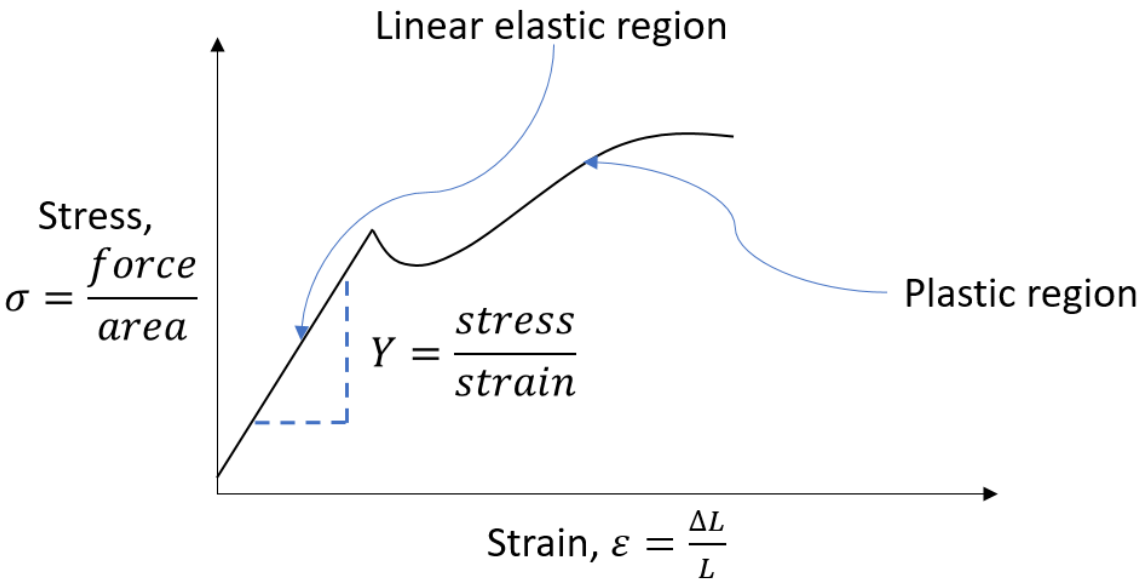

Figure 2: Young's modulus (Y) for materials and different regions. The plastic region is exaggerated.

Materials that are subjected to stresses, and the stresses are not high enough to enter the plastic region, the material will "go back" to its original shape when the stress is removed. However, when materials enter the plastic region, the material will be permanently deformed after the stress is removed.

2.3.1. Hysteresis

It is expected that the Young's modulus of polyurethane will behave according to the plastic region, as seen in figure 2 above. Additionally, some polymers have different Young's modulus when the load is removed. E.g., it will behave differently if, let's say, $5N$, is *applied* versus when the same load is *removed*. This behavior is called hysteresis. Imagine a regular balloon. Initially, to blow up the balloon, it is rather difficult. However, if the same balloon where stretched before attempting to blow it up, it will be much easier. The reason behind this behavior is due the fact that the polymer loses energy (heat) when the load is applied and then removed (Meyers & Chawla, 1999). This loss of energy is due to the fact that the molecular structure of the polymer rearranges the long chains when load is applied (McCrum, et al., 2003). Since the behavior is because of loss of heat, with lower temperatures the necessary work needed to displace an equal distance is less compared to higher temperatures (Atanackovic & Guran, 2012). There are different mathematical model that can describe the hysteris behavior, whereas some are

- Maxwell model
- Kelvin-Voigt model
- Standard linear solid model
- Generalized Maxwell model

It is, however, not the scope of this paper to describe or include these models.

Chapter 3: Methodology

To determine how polyurethane behaves in cold climates, comparison of experimental data and simulated data can be applied. For this technique to be viable, fundamental knowledge of how materials behave when subjected to load (force) is necessary. In this paper, the Euler-Bernoulli beam equation will be solved analytically for a four-point bending setup. The simple definition of the Euler-Bernoulli beam theory states that the stress varies linearly with the distance from the neutral axis.

To determine the elasticity of polyurethane in cold climates, there are two main steps,

- Theoretical analysis of Euler-Bernoulli beam theory
- Experiments

The theoretical study will introduce the equations necessary to estimate Young's modulus. Based on the results from the experiments, the displacement as a function of the applied loads are given. Thus, Young's modulus can be estimated.

The experiments will be done at the cold lab at UiT The Arctic University of Norway. A four-point test bench will be constructed, and based on this bench, the results will be obtained.

3.1. Beam Theory

To calculate the theoretical displacement y in a beam, Euler-Bernoulli beam theory can be applied. The following section will introduce the basic equations that are used to calculate the displacement, theoretical load, and so on. This derivation considers the moment M about the neutral axis c. See the figure on the next page.

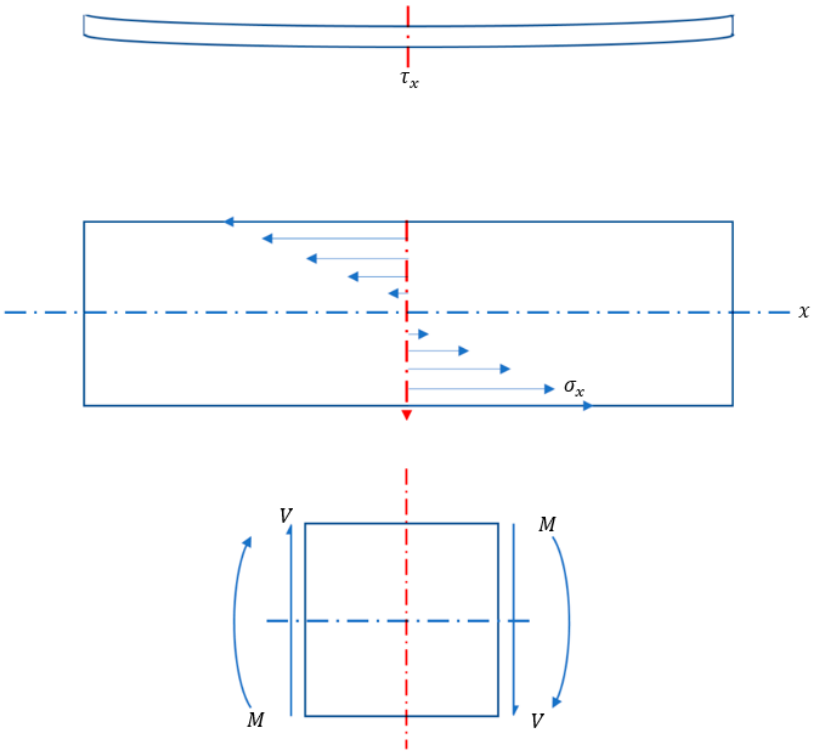

Figure 3: Longitudinal stress (σ_x), shear stress (τ_x), shear force (V) and bending moment (M) in a beam, as seen in (Khawaja & Xue, 2016)

To calculate the longitudinal stress, σ_x, equation 1 below can be used (Khawaja & Xue, 2016)

$$\sigma_x = \frac{M|c|}{I} \tag{1}$$

Where

- M is the moment
- c is the distance to the neutral axis
- I is the second moment of inertia.

The strain in a beam undergoing deflection (bending) is a function of the radius of the neutral axis and the distance of the surface from the neutral axis (Khawaja & Xue, 2016), as shown in figure 4 on the next page.

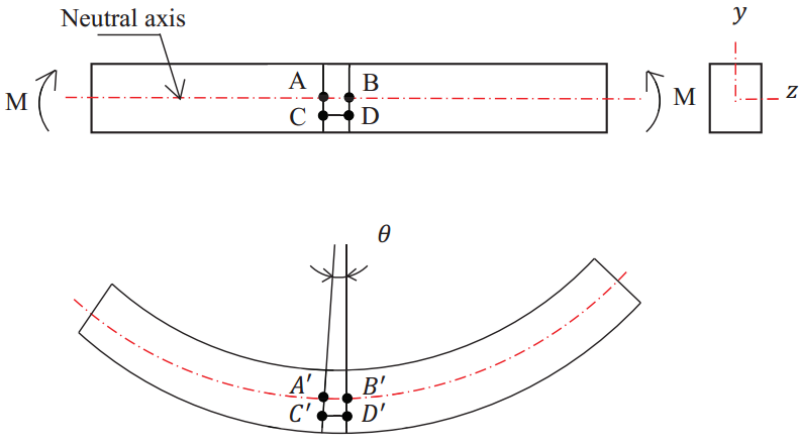

Figure 4: the longitudinal strain (ε_x) in a beam undergoing bending (Khawaja & Xue, 2016)

Based on figure 4, to express the relationship between $\frac{C'D'}{A'B'}$, basic geometrical rules can be applied. This relationship is displayed in eq. 2 below.

$$\frac{C'D'}{A'B'} = \frac{(R+c)\theta}{R\theta} = \frac{R+c}{R} \tag{2}$$

Where

- R is the radius of the neutral axis
- θ is the slope, in radians

Thus, the strain, ε_x, at layer $C'D'$ can be expressed as the change in length, e.g. $(C'D' - CD)$ divided by the original length (CD). Remember that the distance AB and CD originates from the initial layer, so $AB = CD$. In addition, AB is on the neutral axis, so there will not be any changes in the length, e.g. $AB = A'B'$. Thus, the strain at layer $C'D'$ is displayed in equation 3 below

$$\varepsilon_x = \frac{C'D' - CD}{CD} = \frac{C'D' - CD}{AB} = \frac{C'D'}{AB} - 1 \tag{3}$$

By substituting eq. 2 and 3 into eq. 4, we get

$$\varepsilon_x = \frac{c}{R} \tag{4}$$

Since the beam is only subjected to moments, due to the location of where forces are applied, and the beam is in static equilibrium, the forces across the surface of the cross-section is

longitudinal. Remember that moment is simply $force$ multiplied by $distance$. Thus, the force at each of the cross-section areas in the beam can be expressed as (Khawaja & Xue, 2016)

$$\Delta P = \sigma_x \cdot b \cdot dy \tag{5}$$

And the moment can be described as

$$\Delta M = \Delta P \cdot c = (\sigma_x \cdot b \cdot dy) \cdot c \tag{6}$$

Where

- dy is the differential in the $y - direction$.

Further, to create an expression for the entire cross-section area at a given location, simply summarize from $z = +c/2$ to $z = -c/2$ (z being the distance to dy from the neutral axis c) over the cross-section area in $y - direction$:

$$M = \sum (\sigma_x \cdot b \cdot dy) \cdot c \tag{7}$$

Now, remember Hooke's Law (Atanackovic & Guran, 2012), $\sigma_x = E\varepsilon_x$,

Where

- E is Young's Modulus

Substituting the strain that was found in eq. 3, Hooke's Law can be rewritten to

$$\sigma_x = E\frac{c}{R} \tag{8}$$

When a beam undergoes bending, the neutral axis will naturally also bend. The angle, $d\theta$, is described as the two points in between dy where the slope of the neutral axis intersects on top and bottom of dy.

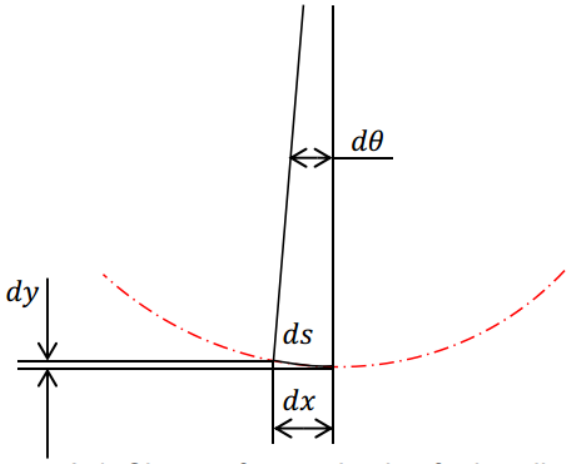

Figure 5: shape of the neutral axis of a beam undergoing bending (Khawaja & Xue, 2016)

It is known that for very small angles, $\tan\theta = \frac{dy}{dx}$ can be rewritten to $\theta = \frac{dy}{dx}$. Note that θ is in radians, and thus, $\theta = \frac{s}{R}$. Further, ds is very small, so that $ds = dx$. Therefore (Khawaja & Xue, 2016),

$$\frac{1}{R} = \frac{d\theta}{ds} = \frac{d\theta}{dx} = \frac{d^2y}{dx^2} \tag{9}$$

In addition, the moment of inertia, I, for the beam can be written as (Khawaja & Xue, 2016)

$$I = \sum c^2 \cdot b \cdot dy \tag{10}$$

By substituting eq. 8, eq. 9 and eq. 10, into eq. 11, we get:

$$\frac{d^2y}{dx^2} = \frac{M}{EI} \tag{11}$$

Now, the expression for the theoretical displacement in $y - direction$ can be constructed. Remember that $\theta = \frac{dy}{dx}$, thus

$$\theta = \int \frac{M}{EI} dx \rightarrow y = \int \theta dx \rightarrow y = \int \int \frac{M}{EI} dx \tag{12}$$

It has now been established equation that can be applied to describe the theoretical displacement, y, for a beam that is subjected to force. In this paper, a four-point bending problem will be analyzed. That means that the beam is supported by two points, and loaded with two points, see the figure below. The advantages to use a four-point load is that the moment is constant between the two loads points. To determine the different parameters seen in figure 3, different test methods can be applied. Further, the bending moment and shear force diagram of a four-point bending beam can be seen in figure 6 below (Khawaja & Xue, 2016).

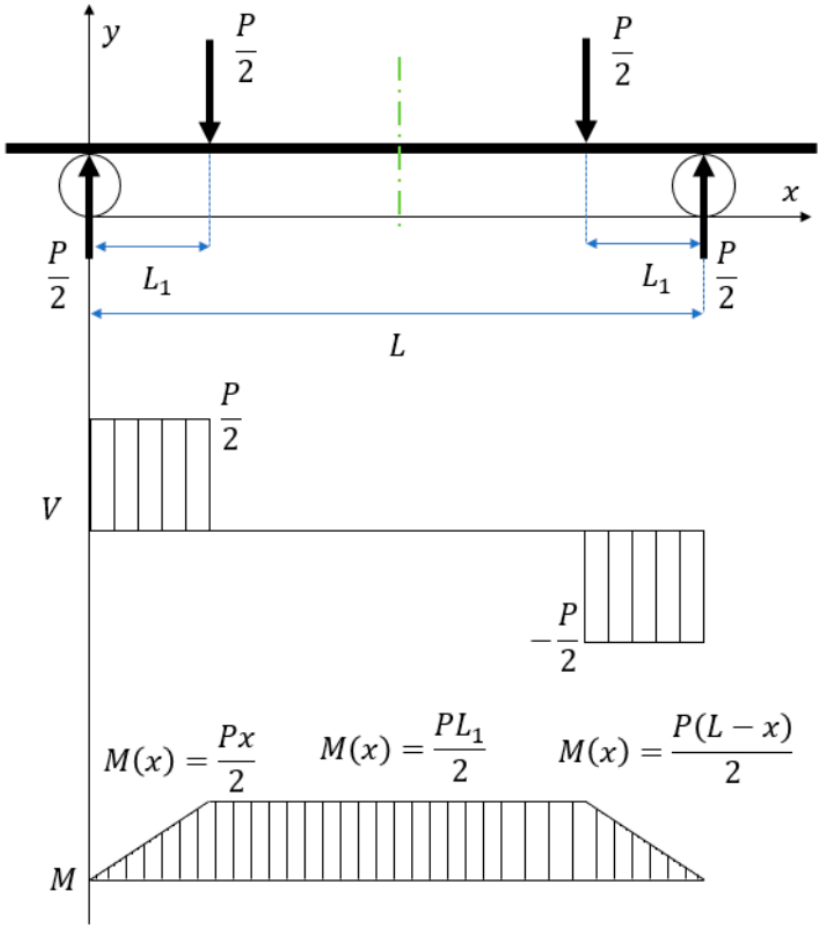

Figure 6: Bending moment (M) and shear force (V) diagrams of a four-point bending beam, as seen in (Khawaja & Xue, 2016).

Where

- P is the load on the (N)
- L is the distance between the support joints (m)
- L_1 is the distance between the support joints and loading points (m)

- x is the distance of which the moment is calculated (m).

The moment is a function of x, e.g. the distance from the load to the support (Wachtman, et al., 2009), and the advantage to use a four-point test bench is that the moment is constant in the middle of the beam (Xue, 2015), e.g.:

$$\begin{aligned} M(x) &= \frac{Px}{2} && 0 \le x \le L_1 \\ M &= \frac{PL_1}{2} && L_1 \le x \le (L - L_1) \\ M(x) &= \frac{P(L-x)}{2} && (L - L_1) \le x \le L \end{aligned} \quad (13)$$

Thus, multiple correlations based on equations 11, 12 and 13, can be derived. For the case where $0 \le x \le L_1$, and $M(x) = \frac{Px}{2}$, we get equations 14 and 15:

$$\theta_1 = \frac{Px^2}{4EI} + C_1 \quad (14)$$

$$\delta_1 = \frac{Px^3}{12EI} + C_1 x + C_2 \quad (15)$$

Further, for the case where $L_1 \le x \le (L - L_1)$, and $M = \frac{PL_1}{2}$, equations 16 and 17 can be obtained:

$$\theta_2 = \frac{PL_1 x}{2EI} + C_3 \quad (16)$$

$$\delta_2 = \frac{PL_1 x}{4EI} + C_3 x + C_4 \quad (17)$$

For the last case, where $(L - L_1) \le x \le L$, and $M(x) = \frac{P(L-x)}{2}$, the last set of equations can be derived:

$$\theta_3 = -\frac{Px^2}{4EI} + \frac{PL_x}{2EI} + C_5 \quad (18)$$

$$\delta_3 = -\frac{Px^3}{12EI} + \frac{PLx^2}{4EI} + C_5 x + C_6 \quad (19)$$

In equations 14 to 19, there are six unknows, C_1, C_2, C_3, C_4, C_5 and C_6. To solve the equations, boundary conditions are needed. These boundary conditions are given in equations 20 to 24:

$$x = 0, \qquad \delta_1 = 0 \tag{20}$$

$$x = L, \qquad \delta_1 = \delta_2, \qquad \theta_1 = \theta_2 \tag{21}$$

$$x = \frac{L}{2}, \qquad \theta_2 = 0 \tag{22}$$

$$x = L - L_1, \qquad \theta_2 = 0, \qquad \theta_2 = \theta_3 \tag{23}$$

$$x = L, \qquad \delta_3 = 0 \tag{24}$$

By solving the equations (Young & Budynas, 2002) with the respective boundary conditions, we get the following set of equations:

$$\theta_1 = \frac{Px^2}{4EI} + \frac{PL_1^2}{4EI} - \frac{PL_1L}{4EI} \tag{25}$$

$$\delta_1 = \frac{Px^3}{12EI} + \frac{PL_1^2x}{4EI} - \frac{PL_1Lx}{4EI} \tag{26}$$

$$\theta_2 = \frac{PL_1x}{4EI} - \frac{PLL_1}{4EI} \tag{27}$$

$$\delta_2 = \frac{PL_1x^2}{4EI} - \frac{PLL_1x}{4EI} + \frac{PL_1^3}{12EI} \tag{28}$$

$$\theta_3 = -\frac{Px^2}{4EI} + \frac{PLx}{2EI} - \frac{PL_1^2}{4EI} - \frac{PL^2}{4EI} + \frac{PLL_1}{4EI} \tag{29}$$

$$\delta_3 = -\frac{Px^3}{12EI} + \frac{PLx^2}{4EI} - \frac{PL_1^2x}{4EI} - \frac{PL^2x}{4EI} + \frac{PLL_1x}{4EI} + \frac{PL^3}{12EI} + \frac{PL_1^2L}{4EI} - \frac{PL^2L_1}{4EI} \tag{30}$$

Where eq. 25 and 26 are in the region $0 \leq x \leq L_1$, eq. 27 and 28 are in the region $L_1 \leq x \leq (L - L_1)$, and eq. 29 and 30 are in the region $(L - L_1) \leq x \leq L$, and

- L is the distance between the supports
- P is the total load from the four-point bending
- E is the Young's modulus
- I is the moment of inertia.

Thus, in equations 25 to 30, a relationship between L, P, E and I has been established. Depending on what parameters are given, the equations can be rearranged to be solve a missing parameter.

3.2. Experimental Work

The experimental work consists of two parts, setup of the testing apparatus (four-point bench), preparing the polyurethane sample, and data gathering. The following sections will describe these steps.

3.2.1. Four-point Test Bench Setup

To obtain the necessary numbers that are needed to estimate the Young's modulus of polyurethane, a four-point bench can be used. A four-point bench have two loading points, and two support points. A rendered image of the bench that was used to obtain the number is this paper, can be seen in figure 7 on the next page. In this figure, (a) is the load points, and (b) is the support joints. The parameters of the four-point test bench are shown in table 3 below. The parameters of the four-point test bench are shown in table 2 below.

Table 2: parameters of the four-point test bench and the polyurethane specimen

Description	Variable	Value (mm)
Length of specimen	l	260
Width of specimen	b	60
Thickness of specimen	t_s	90
Distance between support and load points	L_1	20
Distance between the loads points	L_2	160
Distance between support points	L	200

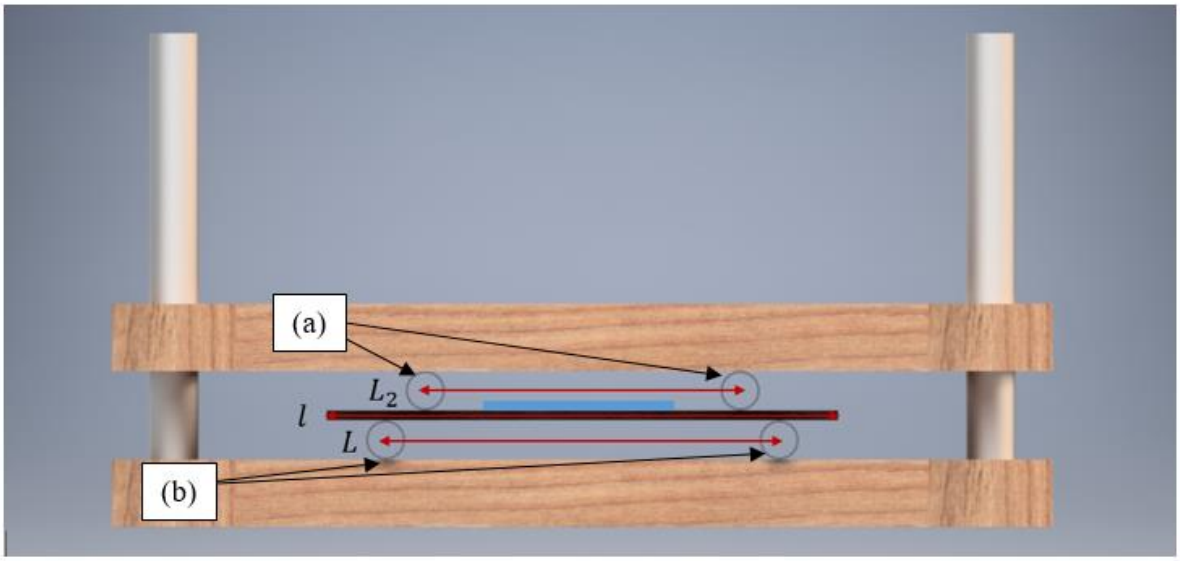

Figure 7: schematic figure of four-point stress bench. Rendered in Autodesk Inventor Professional 2017.

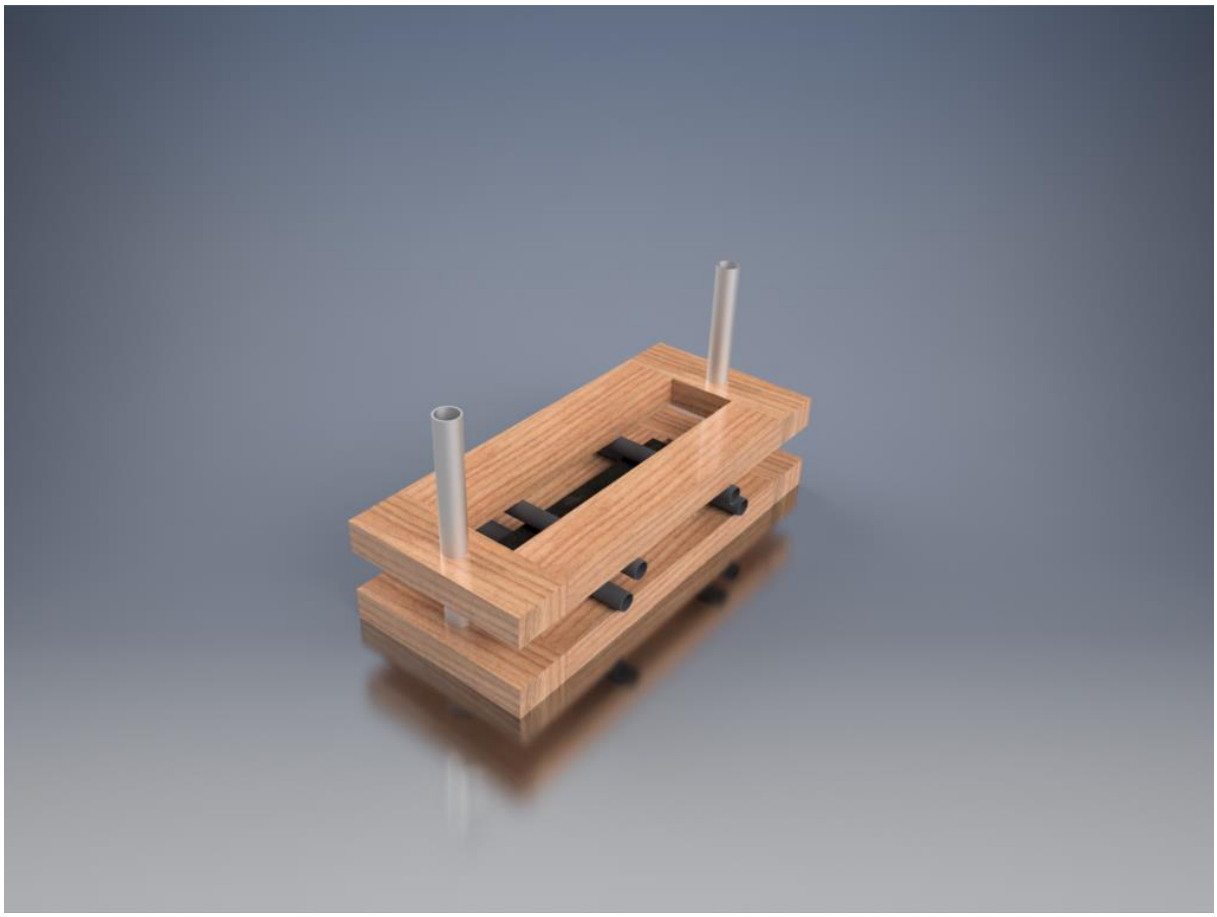

Figure 8: top view of the four-point test bench. The polyurethane specimen in the middle. The renders in fig. 5 and 6 are both modelled in Autodesk Inventor Professional 2017.

By the use of this test method, the parameters *"load"* and *"displacement"* are recorded. Other parameters, such as the area moment of inertia are calculated by the use of well-established equations. See eq. 31 below.

$$I = b \cdot \frac{t^3}{12} \tag{31}$$

Where

- I is the area moment of inertia
- b is the breadth of the specimen
- t is the thickness of the specimen.

3.2.2. Preparation of Sample

The polyurethane sample was cut in appropriate sizes $(260mm\ x\ 60mm)$. Both the sample and the four-point bench was put in the freezer $(-25°C)$ over-night to ensure even temperature in the entire specimen. In the design of the test bench, there are two support rods. These were added to the system to ensure that the load joints did not move when load was applied, and hence, ensure more accurate results.

The entire apparatus, and the anti-abrasion polyurethane, was put inside the cold room over-night. When the objects were properly cold, masses were added on the four-point bench, while still inside the cold room.

3.2.3. Data Gathering

The load and deflection data was gathered while both the apparatus and the specimen where still inside the cold room. The initial load from the loading frame (see fig. 7 and 8), was 1.25 kg. The added mass came from iron weights, and the added mass had an increment of 1.25 kg each time. The initial displacement was recorded before the first 1.25 kg iron weight was added, in the middle of the upper frame. At each time more weight was added, the new displacement was recorded. See figure 9 on the next page. When the upper frame had reached the lower frame, the experiment was concluded.

Figure 9: recording of displacement using a Vernier caliper. At this instant, the only load is from the upper frame alone. The middle of the frame is marked with a circle.

3.3. Analytical Study in MATLAB®

The analytical study was done based on the equations obtained in section 3.1. Equation 26 (constant moment in the middle of the beam) was used because of the location where the data was gathered (see fig. 9). However, remember that eq. 26 is the equation for displacement, thus the equation needed to be modified to calculate the Young's modulus. This equation can be seen below

$$E = \frac{Px}{4 \cdot \delta_1 \cdot I}\left(\frac{x^2}{3} + L_1(L_1 - L)\right) \tag{32}$$

Where

- E is the Young's modulus (Pa)
- P is the load (N)
- x is the distance where the moment is calculated ($x = L_1$ in this case) (m)
- δ_1 is the recorded displacement (m)
- I is the area moment of inertia
- L_1 is the distance to the load joint
- L is the total length of the specimen.

Chapter 4: Results and Discussion

4.1. Four-point Stress Test and Analytical Study

The experimental data to determine Young's modulus for anti-abrasive polyurethane and anti-seepage polyurethane is displayed in the table on the next page

Table 3: force vs. displacement. This data was used to estimate Young's modulus for anti-abrasive polyurethane

Mass (kg)	Displacement (anti-abrasion) (mm)		Displacement (anti-seepage) (mm)	
	Loading	Unloading	Loading	Unloading
1.25	2.91	2.98	4.32	7.2
2.50	4.1	4.63	6.79	8.88
3.75	4.53	5.65	9.08	10.36
5.00	4.92	5.85	10.32	11.62
6.25	5.61	5.59	11.48	12.62

What was found when comparing the results shown in table 3 and the analytical study using eq. 26, was that there was only a correlation between simulated data and experimental data one data point at a time. E.g., the simulated displacement with $E = E_1$ did only fit the first experimental data point, and $E = E_2$ only fit the second data point ($E_1 \neq E_2$). This suggest that Young's modulus, E, is a function of the applied force (hysteresis). Thus, by using eq. 31., where Young's modulus was solved with respect to the displacement. It was found that Young's modulus of polyurethane had a nonlinear behavior when subjected to cold temperatures. This nonlinear behavior is called *hysteresis.*

Table 4: the Young's modulus at loading and unloading versus the load. Results for anti-abrasion polyurethane.

Load (kg)	Young's modulus (MPa)	
	Loading	Unloading
1.25	20.1	13.9
2.50	29.1	22.1
3.75	38.8	29.9
5.00	47.6	39.9
6.25	52.1	52.2

Table 5: the Young's modulus at loading and unloading versus the load. Results for anti-seepage polyurethane

Load (kg)	Young's modulus (MPa)	
	Loading	Unloading
1.25	18.1	10.9
2.50	23.1	17.7
3.75	25.9	27.3
5.00	30.4	27.0
6.25	34.2	31.1

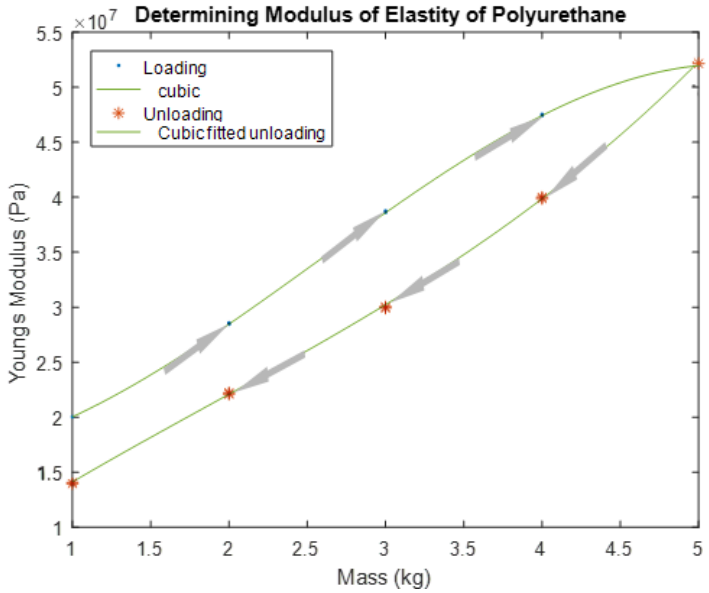

Figure 10: Young's Modulus of anti-abrasion polyurethane showing hysteresis behavior.

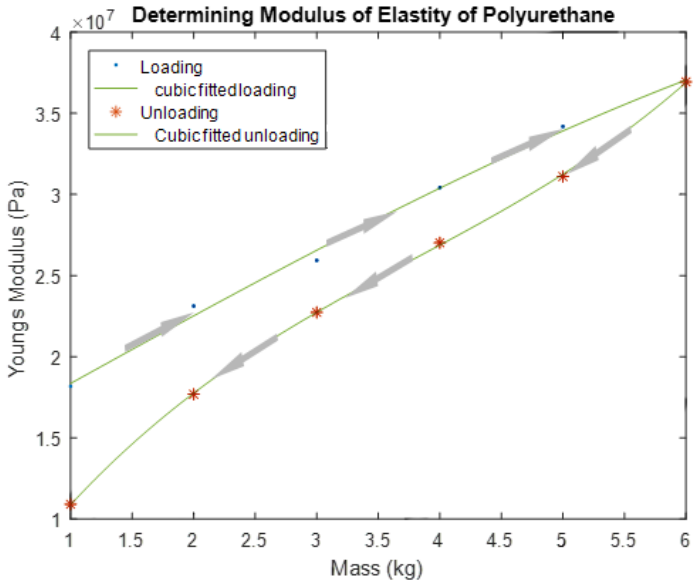

Figure 11: Young's Modulus of anti-abrasion polyurethane showing hysteresis behavior.

The figure above have clearly illustrates the hysteresis behavior of anti-abrasion polyurethane. The grey arrows illustrates the loading (arrow going up) and unloading (arrow going down). To illustrate the behavior better, the green lines have been added using the basic data fitting tool in MATLAB®. The area within the loop represents the loss of energy within the polyurethane.

The method of reading the results on the Vernier caliper are not as reliable as one could want. Additionally, the human factor plays an important role in these measurements, seeing as they were read while inside the cold room. Consequently, the person doing the reading are exposed (not directly!) to the cold temperatures, and this could affect the reading accuracy.

Chapter 5: Conclusions and Future Work

5.1. Conclusions

The conclusions that can be drawn from this report is

- The Young's modulus of anti-abrasion and anti-seepage polyurethane, when tested in cold room is dependent on the applied mass, or the applied load. This feature is called hysteresis. However, the Young's modulus for anti-abrasion is from 15 to 20 MPa, whereas for anti-seepage, the Young's modulus is from 10 to 17 MPa, at loads from 1.25kg to 6.5 kg.
- Equation 34 can be applied to determine the Young's modulus, for applied loads between $1.25\ kg$ and $6.25\ kg$, regardless of what material, as long as appropriate constants are used.

5.2. Future work

This report found the Young's modulus for anti-abrasion polyurethane, and indeed, the Young's modulus had a hysteresis behavior, which was expected due to the internal atomic structure of the material. However, what could have been done could be to investigate if the modulus changes with *time* as well. If the load was kept on the bench for example $2\ minutes$ before a different load was put on.

References

Adeeb, S., 2015. *Beam Structures - Plane Beam Approximations.* [Online] Available at: http://sameradeeb.srv.ualberta.ca/beam-structures/plane-beam-approximations/ [Accessed 16 03 2017].

Atanackovic, T. M. & Guran, A., 2012. *Theory of Elasticity for Scientists and Engineers.* Boston: Birkhäuser Boston.

Bayer, O., 1947. Das Di-Isocyanat-Polyadditionsverfahren (Polyurethane). *Angewandte Chemie,* 59(9), pp. 257 - 272.

Döppenschmidt, A. & Butt, H.-J., 2000. Measuring the Thickness of the Liquid-like Layer on Ice Surfaces with Atomic Force Microscopy. *Langmuir,* 16(16), pp. 6709 - 6714.

Dulong, P. L. & Petit, A. T., 1819. Recherches sur quelques points importants de la Théorie de la Chaleur. *Annales de Chimie et de Physique,* Issue 10, pp. 395 - 413.

Fourier, J., 2007 (1822). *The Analytical Theory of Heat.* s.l.:Cosimo Classics.

Gebhart, B., 1993. *Heat conduction and mass diffusion.* 1st ed. New York: McGraw-Hill.

Goertz, M. P., Zhu, X. Y. & Houston, J. E., 2009. Exploring the Liquid-like Layer on the Ice Surface. *Langmuir,* 25(12), p. 6905–6908.

Griffin, R. & Krishnan, S., 2000. *A Four-Point Bend Test Experiment for Use in the Classroom, and Procedures for Evaluating Results,* Texas: Texas A&M University at Qatar.

Gum, W., Wolfram, R. & Ulrich, H., 1992. *Reaction Polymers.* New York: Oxford University Press.

Harrington, R. & Hock, K., 1991. *Flexible Polyurethane Foams.* Midland: The Dow Chemical Company.

Jellink, H. H. G., 1967. Liquid-Like (Transition) Layer on Ice. *Journal of Colloid and Interface Science,* Issue 25, pp. 192 - 205.

Jellinks, H. H. G., 1959. Adhesive Properties of Ice. *Journal of Colloid Science,* Issue 14, pp. 268 - 280.

Khawaja, H. A. & Xue, H., 2016. Analytical and Case Studies of a Sandwich Structure using Euler-Bernoulli Beam Equation. *Mathematics in Engineering, Science and Aerospace,* 7(4), pp. 599 - 612.

Kulinich, S. A. & Farzaneh, M., 2009. Ice adhesion on super-hydrophobic surfaces. *Applied Surface Science,* 18(255), p. 8153–8157.

Landy, M. & Freiberger, A., 1967. Studies of Ice Adhesion. *Journal of Colloid and Interface Science,* Issue 25, pp. 231 - 244.

Michael Faraday, 1850. Occasional Papers on the Theory of Glaciers. *Forbes, J.D.,* p. 640.

Moran, M. J., Shaprio, H. N., Munson, B. R. & DeWitt, D. P., 2003. *Introduction to Thermal systems Engineering. Thermodynamics, Fluid Mechanics, and Heat Transfer.* 1st ed. s.l.:Wiley & Sons, Inc..

National International Conference, 1973. Permafrost. In: *North American Contribution: Permafrost.* Washington, D.C.: National Acadamy of Science.

Nave, R., 2016. *hyperphysics.phy-astr.gsu.* [Online] Available at: http://hyperphysics.phy-astr.gsu.edu/hbase/thermo/Dulong.html#c1 [Accessed 11 02 2017].

Özisik, N. M., 1993. *Heat Conduction.* 2nd ed. New York: John Wiley & Sons, Inc..

Petrescu, I., Mohora, C. & Ispas, C., 2011. Determination of Young'S Modulus For CFRP Using the Three – Point Bending Test. *Proceedings in Manufacturing Systems,* 6(4), pp. 255 - 261.

Pipe Flow Software, 2010. *Pipe Flow Software.* [Online] Available at: http://www.pipeflow.com/sitemap/pipe-roughness [Accessed 30 01 2017].

Prisacariu, C., 2011. *Polyurethane Elastomers. From Morphology to Mechanical Aspects.* Wien: Springer.

Rashid, T., Khawaja, H. & Edvardsen, K., 2016. Determination of Thermal Properties of Fresh Water and Sea Water Ice using Multiphysics Analysis. *International Journal of Multiphysics,* 10(3), pp. 277 - 290.

Recktenwald, G. W., 2004. *Finite-Difference Approximations to the Heat Equation,* s.l.: s.n.

Roberts, P. W., 1951. *Effect of Extreme Arctic Cold on Materials.* Dartmouth: Dartmouth College Library.

Seymore, R. B. & Kauffman, G. B., 1992. Polyurethanes: A class of modern versatile materials. *Journal of Chemical Education,* 69(11), p. 909.

Smith, R., Inomata, H. & Peters, C., 2013. Chapter 8 – Heat Transfer and Finite-Difference Methods. *Supercritical Fluid Science and Technology,* Volume 4, pp. 557-615.

Snoke, D. W., 2009. *Solid State Physics: Essential Concepts.* 1st ed. s.l.:Addison-Wesley.

Soto, M., Sebastián, R. M. & Marquet, J., 2014. Photochemical Activation of Extremely Weak Nucleophiles: Highly Fluorinated Urethanes and Polyurethanes from Polyfluoro Alcohols. *The Journal of Organic Chemistry,* 11(79), pp. 5019 - 5027.

Wachtman, J. B., Cannon, W. R. & Matthewson, M. J., 2009. *Mechanical properties of ceramics.* s.l.:John Wiley & Sons.

Wayl, W. A., 1951. Surface Structure of Water and Some of its Physical and Chemical Manifestations. *Journal of Colloid Science,* 6(5), pp. 389-405.

Weisstein, E. W., 2011. *Mean-Value Theorem.* [Online] Available at: http://mathworld.wolfram.com/Mean-ValueTheorem.html [Accessed 15 03 2017].

Woods, G., 1990. *The ICI Polyurethanes Book.* New York: John Wiley & Sons.

Xue, H., 2015. *Ice Shedding Processes,* Narvik: Department of Technology, Narvik University College.

Young, W. C. & Budynas, R. G., 2002. *Roark's Formulas for Stress and Strain.* 1st ed. New York: McGraw Hill.

Zhiheng, S., 2015. *The SK one component polyurea and its application in hydraulic and hydropower project structures.* Beijing, China Institute of Water Resources & Hydropower Research.

Appendix I

```
clear all
close all

Load = [1.25,2.5,3.75,5,6.25];   %kg

Exp_disp = [2.91,4.1,4.53,4.92,5.61]/-1000;  % mm and negative for keep signs
consistent

P = Load*9.81;  %N

L1 = 0.02;  %m

L = 0.2;  %m

t = 9e-3;  %m

b = 6e-2;  %m

I = b*t^3/12;  %m^4 (area moment of inertia)

E = 40e6;  %Pa

x = L1;


E_exp = P.*x^3/12./(Exp_disp)/I+P.*L1^2*x/4./(Exp_disp)/I-
P.*L1*L*x/4./(Exp_disp)/I;
figure()
plot (E_exp,'.')
title('Determining Modulus of Elastity of Polyurethane')
xlabel('Mass (kg)')
ylabel('Youngs Modulus (Pa)')
legend('Youngs Modulus vs. load','location','northwest')'

hold on


Unload = sort(Load, 'ascend');   %kg
Exp_disp_2 = [2.98,4.63,5.65,5.85,5.59]/-1000;  % mm and negative for keep signs
consistent

E_exp_2 = P.*x^3/12./(Exp_disp_2)/I+P.*L1^2*x/4./(Exp_disp_2)/I-
P.*L1*L*x/4./(Exp_disp_2)/I;

plot (E_exp_2,'*')
title('Determining Modulus of Elastity of Polyurethane')
xlabel('Mass (kg)')
ylabel('Youngs Modulus (Pa)')
legend('Loading','Unloading','location','northwest')'
```

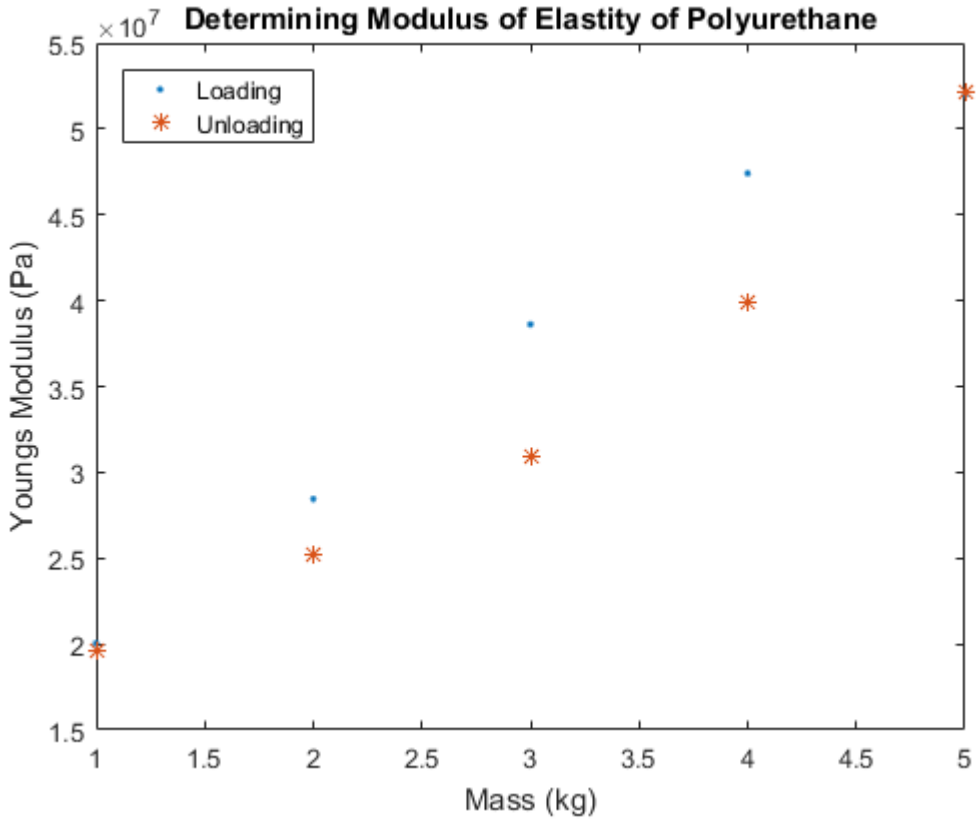
Determining Modulus of Elastity of Polyurethane
×10^7
5.5
5
4.5
4
3.5
3
2.5
2
1.5
Youngs Modulus (Pa)
Loading
Unloading
1
1.5
2
2.5
3
3.5
4
4.5
5
Mass (kg)

UiT
THE ARCTIC
UNIVERSITY
OF NORWAY

Faculty of Science and Technology

Department of Engineering and Safety

Part B

Investigation of ice separation between ice and Polyurethane surface due to bending using FEM and Euler-Bernoulli beam theory

—

Hans-Kristian Norum Eidesen

TEK-3901 Master thesis (part 2 of 3) in Technology and Safety in the High North
June 2017

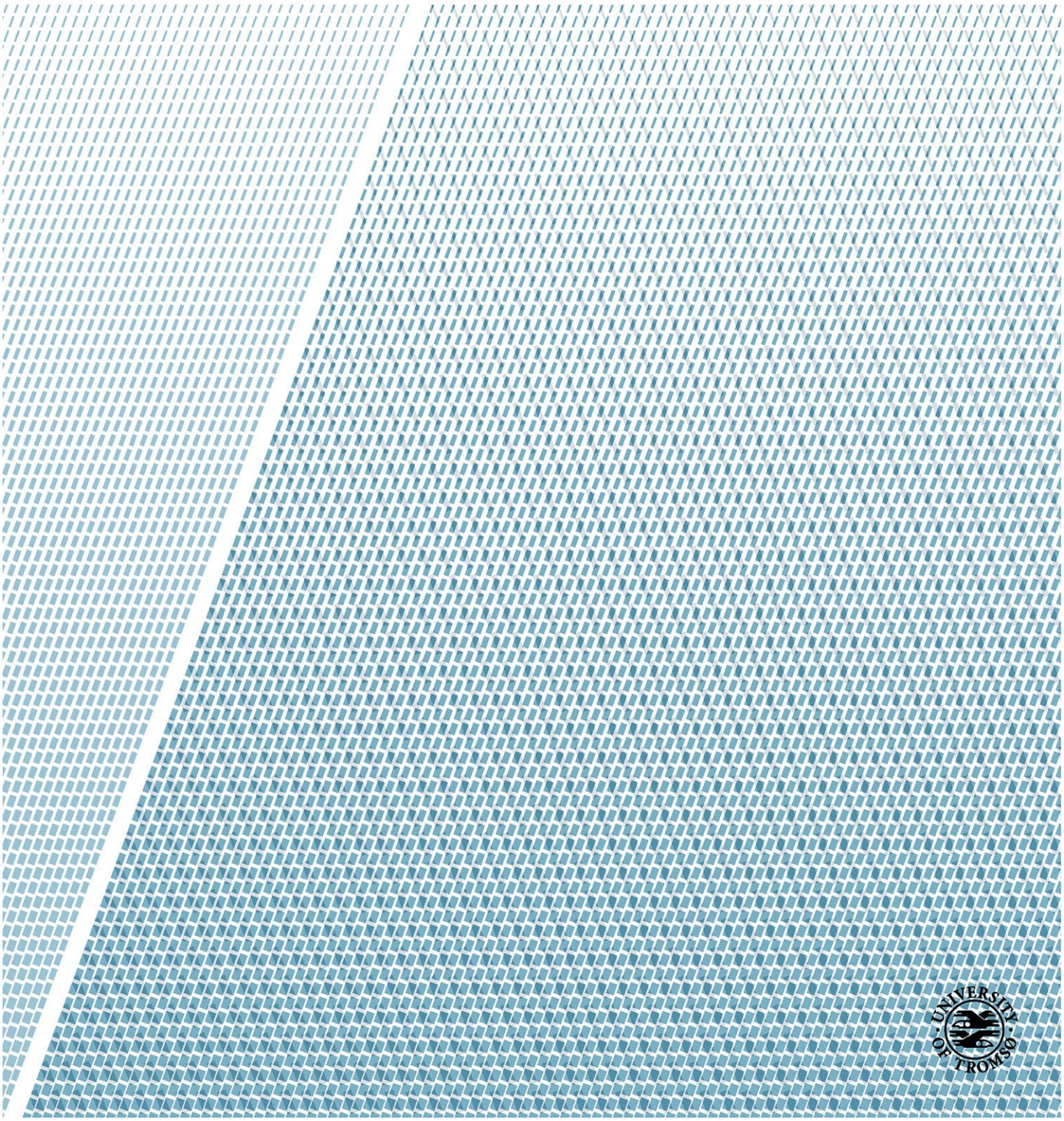

Abstract

The strength of ice adhesion between the surface of the SKOCP and ice was found using four-point bending, with the addition to numerical solutions to Euler-Bernoulli bending theory and simulations in ANSYS® Work package. In the experiment, masses were added on the four-point bench until the ice had separated from the surface. The displacement at the time of separation was read, and the same displacement were feed into the ANSYS® Work package. From this, the longitudinal stress was found. Additionally, from the theory based on Euler-Bernoulli bending, the longitudinal stress was calculated. The results revealed that the ice adhesion on the surface of polyurethane is in the same range as other polymers.

Table of Contents

List of Figures

List of Tables

Nomenclature

Description	Symbol	Unit
Stress	σ	Pa
Strain	ε	$1\ or\ radian$
Modulus of elasticity	E	Pa
Length	L, L_1 and L_2	m
Shear stress	τ_x	Pa
Shear force	V	N
Longitudinal stress	σ_x	Pa
Bending moment	M	Nm
Distance to the neutral axis	c	m
Second moment of inertia	I	m^4
Slope of a bending beam	θ	$radian$
Radius of a bending beam	R	m
Force of a bending beam	ΔP	N
Differential in $y-direction$	dy	m
The distance to dy to neutral axis	z	m
The distance where the moment is calculated	x	m
Unknowns constants from solving PDEs	C_1 to C_6	N/A
Length of specimen	l	mm
Thickness of specimen	t_s, t_1 and t_2	m
Width of specimen	b	mm
Cross section area	A_1, A_2	m
Balance coefficient	n	1
Centroid	C_y	m
Centroid coordinates	D_i and D_{i+1}	m
Total moment of inertia	I_t	m^4
The position where stress is calculated	y	m

Outline

This paper is divided into 5 chapters. The goals in each chapter is described below:

- Chapter 1 gives an introduction to the goal of the paper.
- Chapter 2 is a literature review on ice adhesion, and previous done work in the area.
- Chapter 3 introduces the method that was elected to govern the solutions that was obtained in this paper. Additionally, this chapter gives a mathematically introduction to Euler-Bernoulli beam theory, which is a fundamental method to estimate some necessary parameters, such as longitudinal stress.
- Chapter 4 presents the results that was obtain in MATLAB® and ANSYS®.
- Chapter 5 gives the discussion and conclusion.
- Appendix J contains the MATLAB® codes that were used to calculate and plot the normal stress on the surface of polyurethane at ice separation.

Chapter 1: Introduction

Most manmade infrastructures and structures are not created to have ice on them. Therefore, time, money and energy are spent to remove the ice from the respectable surfaces. When ice have accumulated on roads, powerful machinery scrapes the ice off. When ice accumulates on pipes, it needs to be hacked off. When ice have accumulated on constructions where the accessibility is difficult or non-existence, let it be the blades of a wind turbine, icing can be very dangerous. All-in-all, the effect of ice accumulation, if not handled well, is dangerous, and can even be fatal. Most materials that are used in the Arctic region are designed in climates where the probability of icing is low. Take asphalt as an example. Amongst the first nations to use asphalt as a road coating materials were the US (Gerhard, 1908) in 1876. During the winter time in the Arctic, the temperature will be sub-zero. Thus, ice will start to accumulate. Due to the structure of asphalt, liquid water will seep into every small crack and groove, see figure 1 on the next page. Here, the greyish area represents the surface, and the blueish area represents ice. Basically, no surface is perfectly polished, and with a rougher surface, more water will stick to the surface, and thus, the adhesion force ice will be bigger. When icing accumulates on wind turbine blades, thermal energy is applied to melt away the ice. This is a process which takes time, and is costly.

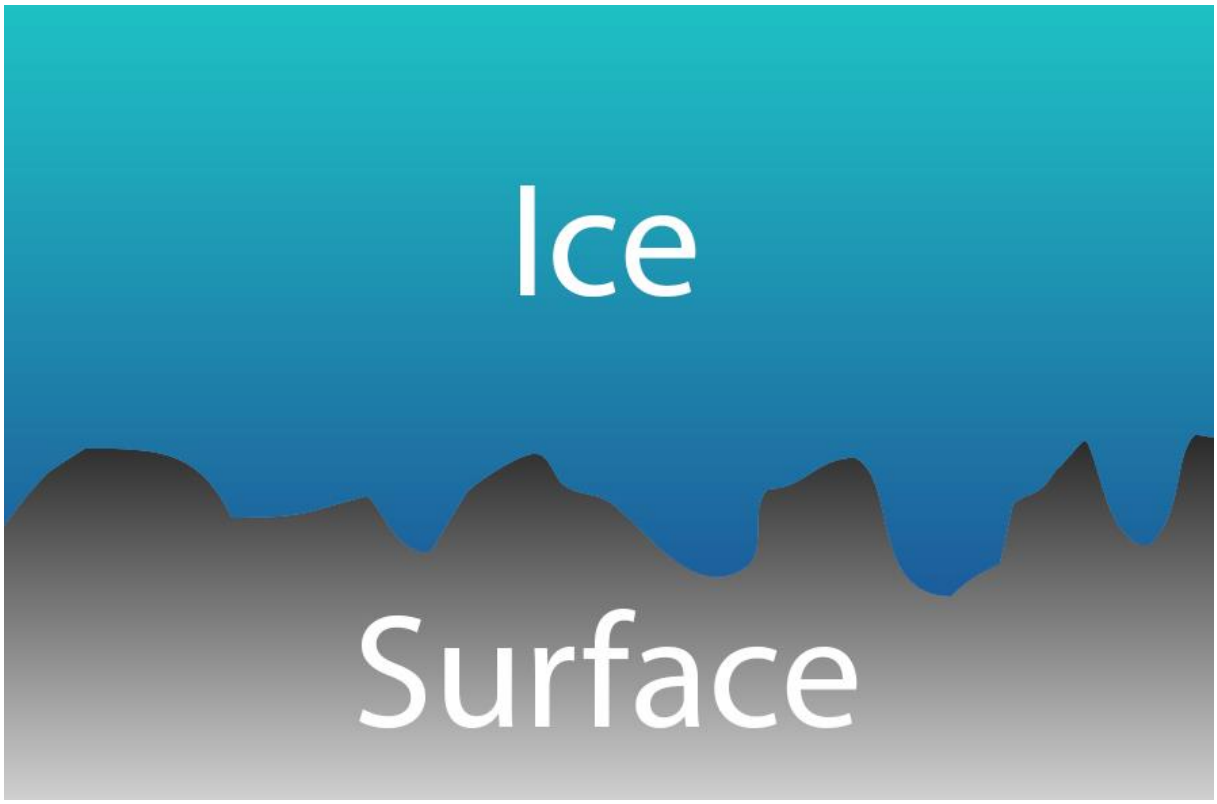

Figure 1: ice adhesion

The figure above represents how ice adhere to a surface (mechanical adhesion, see section 2.2.3). The grooves is a representation of the roughness. Cast iron has an approximate 0.26 mm groove height, whereas glass has approximately 0.0015 mm groove height (Pipe Flow Software, 2010). Within the grooves, the pressure will be higher compared to the pressure that are on the rims of the grooves. Because of this, liquids that expands when going to solid state, adhere well. This type of adhesion is called *mechanical adhesion* (Landy & Freiberger, 1967).

The scope of this paper is thus to investigate the force required to separate the ice from the surface of polyurethane.

1.1. Different types of icing

Icing can occur based on several factors, whereas some are:

- Location (locally and globally)
- Wind
- Air and sea surface temperature
- Salinity
- Humidity.

The type of ice that adheres best, is ice from pure water. Salt water, rain water, dirty water will all have impaired ice adhesion properties.

When the surface of which icing have occurred starts to deform, from stresses or strain, the ice adhesion will seize. If icing has occurred on metal surfaces, a relatively large load will be necessary to break the ice. Whereas surfaces that deform easily, e.g. polymers, the ice will shed rather quickly.

Chapter 2: Literature Review

2.1. Polyurethane

Polyurethane was invented by Otto Bayer and Heinrich Rinke, in Germany in 1937 (Bayer, 1947), (Prisacariu, 2011) and some of the first use of this plastic was during WWII, where it was applied as a coating of the German airplanes (Seymore & Kauffman, 1992). However, some of the first commercially available products made from polyurethane was rigids foams and rubbers for different purposes. It was discovered that by the addition of different materials (e.g. mica and other processed mineral fibers), the polyurethane got stiffer (Young's modulus) and better heat properties. In 1983, a US car making company made the Pontiac Fiero, where the entire body was made from polyurethane with special additives. As of 2011, the use of polyurethane is spread from construction materials to clothing (Prisacariu, 2011).

Table 1: the distribution of different applications that use polyurethane

Polyurethane use	Amounts (millions of kg)	Percentage (%)
Building and construction	662	26.8
Transportation	589	23.8
Furniture and bedding	511	20.7
Appliances	126	5.1
Packaging	113	4.6
Textile, fibers and apparel	82	3.3
Machinery and Foundry	80	3.3
Electronics	34	1.4
Footwear	17	0.7
Other use	253	10.2
Total	2467	100

2.1.1. Chemistry of polyurethane

Polyurethane is in the chemical class called reaction polymers (Gum, et al., 1992), (Harrington & Hock, 1991) and (Woods, 1990). The process of making polyurethane involves reaction an isocyanate containing two or more isocyanate groups per molecule $(R - N = C = O)_n$ (Soto, et al., 2014) with a polyol containing hydroxyl groups $(R' - (OH)_n)$ (Soto, et al., 2014)that

contain on average two or more molecules. In addition to these molecules, the urethane groups are introduced $(-NHCO-O)$. These three groups are then put under an ultraviolet light or with a presence of a catalyst, and thus, polyurethane is made. See figure 1 below. Naturally, the process is more complicated than that. It is, however, not the scope of this paper to investigate all the steps in creating polyurethane.

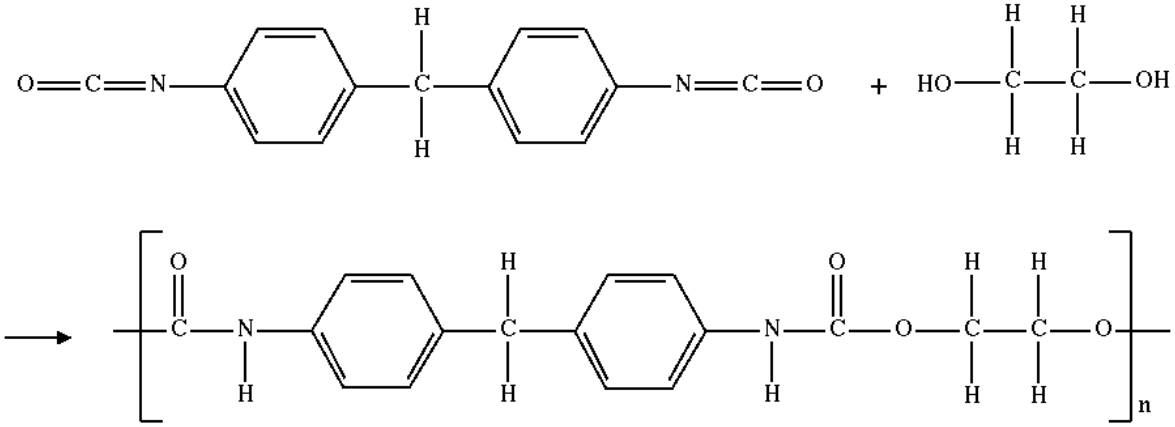

Figure 2: the creation of polyurethane

2.1.2. SK One Component Polyurethane

In this paper, the polyurethane developed by China Institute of Water Resources & Hydropower Research Beijing IWHR-KHL Co. Ltd is being tested. The product name is SK One Component Polyurethane, however, polyurethane is the name that will be used in the following chapters and sections in this paper. The company provided two distinct types of polyurethane, namely anti-seepage polyurethane and anti-abrasion polyurethane. Anti-seepage polyurethane are suggested to be used as a sealant in ether chemical tanks, as it has good hesitance to chemical corrosion (Zhiheng, 2015) or in dams to prevent water leaks through the concrete. Anti-abrasion polyurethane can be used on locations where high corrosion is expected. Locations of such can be water ducts from dams, on ships, due to the force of water while ship is in transit, and so forth.

2.2. Ice Adhesion

There is currently no exact method to calculate the force of ice adhesion of materials (Xue, 2015). However, there are a number of different theories on ice adhesion (Jellinks, 1959) and (Landy & Freiberger, 1967). The different theories have cataloged the force of ice adhesion into four different categories. These categories are shown below

2.2.1. Electrostatic Adhesion

When the adhesion force is due to electrostatic forces, the electrostatic charges between the ice and the surface it adheres to, hold them in place (Krotova, et al., 1965). Such adhesive force is generally found when there are positive ions in the water (Ryzhkin & Petrenko, 1997), and subsequently, the ice surface has a charge different that the surface.

2.2.2. Diffusive Adhesion

When the water and the surface diffuses across the interface, the resulting adhesion type is diffusive adhesion (Xue, 2015).

2.2.3. Mechanical Adhesion

The type of ice adhesion that was introduced in the introduction of this paper is called mechanical adhesion. The water flows into microscopic pores in the material, and when the water freezes, an interlocking mechanism holds the ice to the surface (Xue, 2015)

2.2.4. Chemical Adhesion

This type of ice adhesion is a results of when the chemical compounds of the two bodies (ice and surface) bonds with each other (Xue, 2015).

2.2.5. Strength of Ice Adhesion of Different Types of Surfaces

As it was mentioned in the introduction to this paper, the roughness of the surface where ice adhere plays an important role on the strength of ice adhesion. There are a number of different studies on ice adhesion force, where some reported described methods uses air pressure to separate the ice from the surface, some methods involves using probes to force the ice from the surface (He, et al., 2017), (Davis, et al., 2014). Most of these testes were done in room temperature.

Table 2: captured strength of ice separation from different literature

Material	Author	Temperature	Strength at ice separation (kPa)
Steel	(He, et al., 2017)	Room temperature	713
Aluminum	(He, et al., 2017)	Room temperature	486
Polymer based coating	(He, et al., 2017)	Room temperature	$7 - 355$
Polyvinyl chloride (PVC)	(Xue, 2015)	Cold room	$1500 - 2000$

What can be seen in table 2, is that the force of separation plays and important role on ice adhesion. This suggest that the ice adhesion is sensitive to temperature.

Chapter 3: Methodology

The methodology in this paper consist of three parts,

- theoretical analysis of beam theory,
- experiments
- numerical simulations using ANSYS©.

The theoretical part uses Euler-Bernoulli beam theory, and the focus in on a four-point setup. The resulting equations are coded in MATLB©.

How the real-life numbers (displacements) was recorded will be described in this section. The construction of the four-point test bench will also be briefly described in this section.

The last part, simulations in ANSYS©, will describe the steps to simulate a four-point problem.

3.1. Theoretical analysis

To calculate the theoretical displacement y in a beam, Euler-Bernoulli beam theory can be applied. The following section will introduce the basic equations that are used to calculate the displacement. This derivation considers the moment M about the neutral axis c.

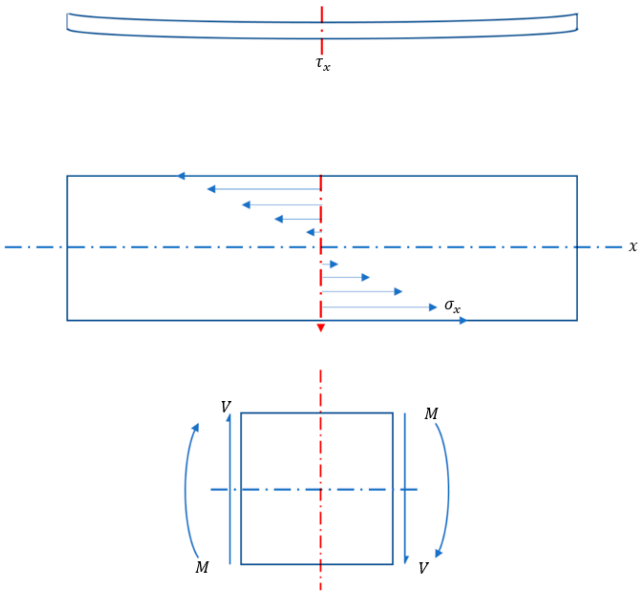

Figure 3: Longitudinal stress (σ_x), shear stress (τ_x), shear force (V) and bending moment (M) in a beam, as seen in (Khawaja & Xue, 2016)

To calculate the longitudinal stress, σ_x, equation 1 below can be used (Khawaja & Xue, 2016)

$$\sigma_x = \frac{M|c|}{I} \tag{1}$$

Where

- M is the moment
- c is the distance to the neutral axis
- I is the second moment of inertia.

The strain in a beam undergoing deflection (bending) is a function of the radius of the neutral axis and the distance of the surface from the neutral axis (Khawaja & Xue, 2016), as shown in figure 3 below

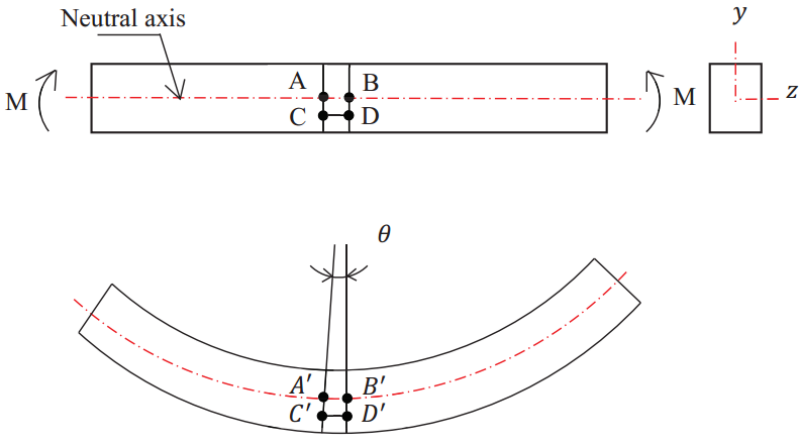

Figure 4: the longitudinal strain (ε_x) in a beam undergoing bending (Khawaja & Xue, 2016)

Based on figure 2, to express the relationship between $\frac{C'D'}{A'B'}$, basic geometrical rules can be applied. This relationship is displayed in eq. 2 below.

$$\frac{C'D'}{A'B'} = \frac{(R+c)\theta}{R\theta} = \frac{R+c}{R} \tag{2}$$

Where

- R is the radius of the neutral axis
- θ is the slope, in radians
- Thus, the strain, ε_x, at layer $C'D'$ can be expressed as the change in length, e.g. $(C'D' - CD)$ divided by the original length (CD). Remember that the distance AB and CD originates from the initial layer, so $AB = CD$. In addition, AB is on the neutral axis, so there will not be any changes in the length, e.g. $AB = A'B'$. Thus, the strain at layer $C'D'$ is displayed in equation 3 below

$$\varepsilon_x = \frac{C'D' - CD}{CD} = \frac{C'D' - CD}{AB} = \frac{C'D'}{AB} - 1 \tag{3}$$

- By substituting eq. 2 and 3 into eq. 4, we get

$$\varepsilon_x = \frac{c}{R} \tag{4}$$

Since the beam is only subjected to moments, due to the location of where forces are applied, and the beam is in static equilibrium, the forces across the surface of the cross-section is

longitudinal. Remember that moment is simply $force\ x\ distance$. Thus, the force at each of the cross-section areas in the beam can be expressed as (Khawaja & Xue, 2016)

$$\Delta P = \sigma_x \cdot b \cdot dy \tag{4}$$

And the moment can be described as

$$\Delta M = \Delta P \cdot c = (\sigma_x \cdot b \cdot dy) \cdot c \tag{5}$$

Where

- dy is the differential in the $y - direction$.

Further, to create an expression for the entire cross-section area at a given location, simply summarize from $z = +c/2$ to $z = -c/2$ over the cross-section area in $y - direction$:

$$M = \sum (\sigma_x \cdot b \cdot dy) \cdot c \tag{6}$$

Where

- z is the distance to dy from the neutral axis c

Now, remember Hooke's Law (Atanackovic & Guran, 2012) $\sigma_x = E\varepsilon_x$,

Where

- E is Young's Modulus

Substituting the strain that was found in eq. 3, Hooke's Law can be rewritten to

$$\sigma_x = E\frac{c}{R} \tag{7}$$

When a beam undergoes bending, the neutral axis will naturally bend. The angle, $d\theta$, is described as the two points in between dy where the neutral axis intersects on top and bottom of dy.

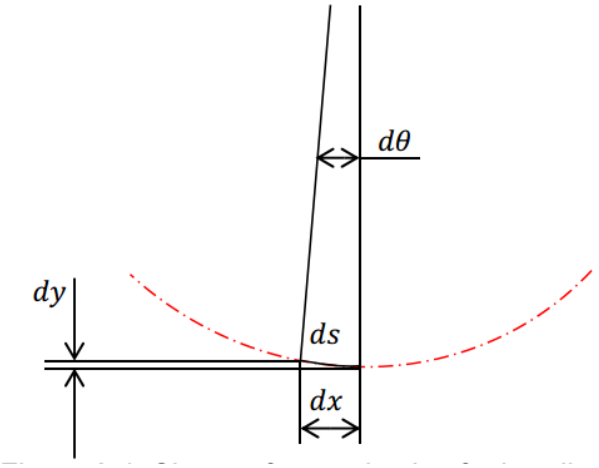

Figure 5: shape of the neutral axis of a beam undergoing bending (Khawaja & Xue, 2016)

It is known that for very small angles, $\tan\theta = \frac{dy}{dx}$ can be rewritten to $\theta = \frac{dy}{dx}$. Note that θ is in radians, and thus, $\theta = \frac{s}{R}$. Further, ds is very small, so that $ds = dx$. Therefore (Khawaja & Xue, 2016),

$$\frac{1}{R} = \frac{d\theta}{ds} = \frac{d\theta}{dx} = \frac{d^2y}{dx^2} \tag{8}$$

In addition, the moment of inertia, I, for the beam can be written as (Khawaja & Xue, 2016)

$$I = \sum c^2 \cdot b \cdot dy \tag{9}$$

By substituting eq. 7, eq. 8 and eq. 9, into eq. 10:

$$\frac{d^2y}{dx^2} = \frac{M}{EI} \tag{10}$$

Now, the expression for the theoretical displacement in $y - direction$ can be constructed. Remember that $\theta = \frac{dy}{dx}$, thus

$$\theta = \int \frac{M}{EI} dx \rightarrow y = \int \theta dx \rightarrow y = \int \int \frac{M}{EI} dx \tag{11}$$

It has now been established equation that can be applied to describe the theoretical displacement for a beam that is subjected to force. For this case, four-point bending will be applied. That means that the beam is supported by two points, and loaded with two points, see the figure on the next page. The advantages to use a four-point load is that the moment is constant between the two loads points. To determine the different parameters seen in figure 1, different test methods can be applied. Further, the bending moment and shear force diagram of a four-point bending beam can be seen in figure 2 below (Khawaja & Xue, 2016).

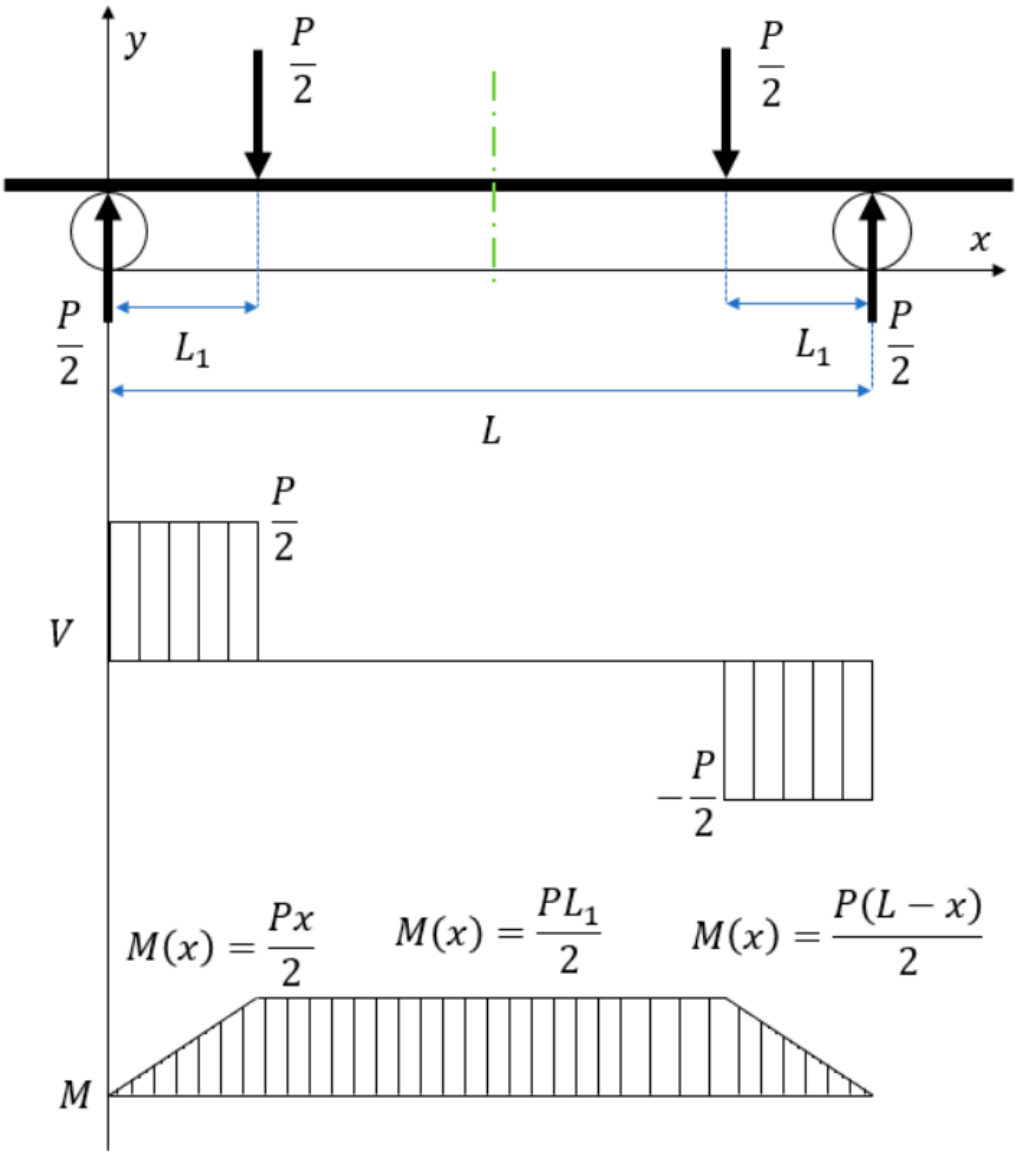

Figure 6: Bending moment (M) and shear force (V) diagrams of a four-point bending beam, as seen in (Khawaja & Xue, 2016).

Where

- P is the load on the (N)
- L is the distance between the support joints (m)
- L_1 is the distance between the support joints and loading points (m)
- x is the distance of which the moment is calculated (m).

The moment is a function of x, e.g. the distance from the load to the support (Wachtman, et al., 2009), and the advantage to use a four-point test bench is that the moment is constant in the middle of the beam (Xue, 2015), e.g.:

$$\begin{aligned} M(x) &= \frac{Px}{2} && 0 \le x \le L_1 \\ M &= \frac{PL_1}{2} && L_1 \le x \le (L - L_1) \\ M(x) &= \frac{P(L-x)}{2} && (L - L_1) \le x \le L \end{aligned} \quad (12)$$

Thus, multiple correlations based on equations 10, 11 and 12, can be derived. For the case where

$0 \le x \le L_1$, and $M(x) = \frac{Px}{2}$, we get equations 13 and 14:

$$\theta_1 = \frac{Px^2}{4EI} + C_1 \quad (13)$$

$$\delta_1 = \frac{Px^3}{12EI} + C_1 x + C_2 \quad (14)$$

Further, for the case where $L_1 \le x \le (L - L_1)$, and $M = \frac{PL_1}{2}$, equations 15 and 16 can be obtained:

$$\theta_2 = \frac{PL_1 x}{2EI} + C_3 \quad (15)$$

$$\delta_2 = \frac{PL_1 x}{4EI} + C_3 x + C_4 \quad (16)$$

For the last case, where $(L - L_1) \le x \le L$, and $M(x) = \frac{P(L-x)}{2}$, the last set of equations can be derived:

$$\theta_3 = -\frac{Px^2}{4EI} + \frac{PL_x}{2EI} + C_5 \tag{17}$$

$$\delta_3 = -\frac{Px^3}{12EI} + \frac{PLx^2}{4EI} + C_5 x + C_6 \tag{18}$$

In equations 13 to 18, there are six unknows, C_1, C_2, C_3, C_4, C_5 and C_6. To solve the equations, boundary conditions are needed. These boundary conditions are given in equations 19 to 23:

$$x = 0, \qquad \delta_1 = 0 \tag{19}$$

$$x = L, \qquad \delta_1 = \delta_2, \qquad \theta_1 = \theta_2 \tag{20}$$

$$x = \frac{L}{2}, \qquad \theta_2 = 0 \tag{21}$$

$$x = L - L_1, \qquad \theta_2 = 0, \qquad \theta_2 = \theta_3 \tag{22}$$

$$x = L, \qquad \delta_3 = 0 \tag{23}$$

By solving the equations (Young & Budynas, 2002) with the respective boundary conditions, we get the following set of equations:

$$\theta_1 = \frac{Px^2}{4EI} + \frac{PL_1^2}{4EI} - \frac{PL_1 L}{4EI} \tag{24}$$

$$\delta_1 = \frac{Px^3}{12EI} + \frac{PL_1^2 x}{4EI} - \frac{PL_1 Lx}{4EI} \tag{25}$$

$$\theta_2 = \frac{PL_1 x}{4EI} - \frac{PLL_1}{4EI} \tag{26}$$

$$\delta_2 = \frac{PL_1 x^2}{4EI} - \frac{PLL_1 x}{4EI} + \frac{PL_1^3}{12EI} \tag{27}$$

$$\theta_3 = -\frac{Px^2}{4EI} + \frac{PLx}{2EI} - \frac{PL_1^2}{4EI} - \frac{PL^2}{4EI} + \frac{PLL_1}{4EI} \tag{28}$$

$$\delta_3 = -\frac{Px^3}{12EI} + \frac{PLx^2}{4EI} - \frac{PL_1^2 x}{4EI} - \frac{PL^2 x}{4EI} + \frac{PLL_1 x}{4EI} + \frac{PL^3}{12EI} + \frac{PL_1^2 L}{4EI} - \frac{PL^2 L_1}{4EI} \tag{29}$$

Where eq. 24 and 25 are in the region $0 \leq x \leq L_1$, eq. 26 and 27 are in the region $L_1 \leq x \leq (L - L_1)$, and eq. 28 and 29 are in the region $(L - L_1) \leq x \leq L$, and

- L is the distance between the supports
- P is the total load from the four-point bending
- E is the Young's modulus

- I is the moment of inertia.

Thus, in equations 24 to 29, a relationship between L, P, E and I has been established, and deflections can be calculated.

3.1.1. Rule of Mixture

This study focuses on the correlation of load/deflection where there is a system of two different materials, and their Young's modulus of each material is non-equal, e.g. $E_1 \neq E_2$. To estimate the Young's modulus for the system, eq. 30 can be used:

$$E = E_1 \frac{A_1}{A} + E_2 \frac{A_2}{A} \tag{30}$$

Where

- A, with respective subscripts, are the net cross section area

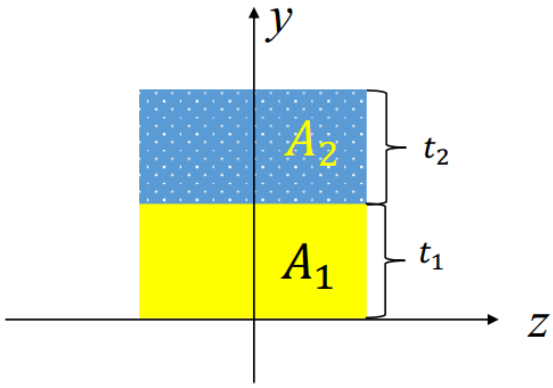

Figure 7: cross-section area of a system of two different materials (Khawaja & Xue, 2016)

In figure 7 above, the constant $t_1 + t_2$ represents the thickness of each specimen that make up the total system. The method to analyze the system with different materials, known as a composite beam, is to use equivalent areas to represent the change in stiffness (Khawaja & Xue, 2016). This can be done by introducing a balance coefficient n. The balance coefficient is given by equation 31

$$n = \frac{E_2}{E_1} \tag{31}$$

This method, with a new equivalent cross-section, is assumed to be entirely of the first material (polyurethane), and the balance coefficient n is multiplied by the area of the second material (ice) for scaling the difference in stiffness in the system (Hibbeler, 2013), (Khawaja & Xue, 2016). Furthermore, since the Young's modulus changes, the location of the centroid and the moment of inertia will also change (Khawaja & Xue, 2016). The new centroid can be calculated using equation 32

$$C_y = \frac{A_1 \sum D_i + nA_2 \sum D_{i+1}}{s(A_1 + nA_2)} \tag{32}$$

Where $i = 1, 3, 5, 7, \dots, 2s - 1$. The constant s represents how many times the total system (see fig. 7) was divided. Thus, $s = 1$ for this case, and consequently, $i = 1$. D_i and D_{i+1} are the centroid coordinates of each layer (Khawaja & Xue, 2016). These variables are calculated below:

$$\begin{aligned} D_1 &= \frac{t_1}{2s} \\ D_2 &= \frac{t_1}{s} + \frac{t_2}{2s} \end{aligned} \tag{33}$$

The new moment of inertia can be calculated the parallel axis theorem (Hibbeler, 2013), (Eshbach & Tapley, 1990), as seen below

$$I = I_{N.A} + y^2 A \tag{34}$$

Where

- I is the moment of inertia for each layer
- $I_{N.A}$ is the moment of inertia of each layer
- y is the distance from the neutral axis
- A is the cross-section area of the layer.

To calculate the longitudinal stress in the ice/polyurethane layer, equation 35 below can be used.

$$\sigma_x = \frac{M|y - C_y|}{I_t} \tag{35}$$

Where

- M is the bending moment
- y is position of where the stress is calculated
- C_y is the centroid
- I_t is the total moment of inertia.

The total moment of inertia, I_t, can be calculated by adding the moment of inertia for polyurethane and ice (Khawaja & Xue, 2016). The method to calculate the longitudinal stress has thus been established.

3.2.2. Ice adhesion in MATLAB®

In MATLAB®, the equation for longitudinal stress (eq. 35), was solved. The moment, as seen in eq. 12 was solved with the use of the displacement from eq. 25 and the total load, P.

3.2. Experimental Setup

To obtain the necessary numbers to estimate the ice adhesion, a four-point bench can be used. A four-point bench have two loading points, and two support points. A rendered image of the bench that was used to obtain the number is this paper, can be seen in figure 9 on the next page. In this figure, (a) is the load points, and (b) is the support joints. The parameters of the four-point test bench are shown in table 3 below.

Table 3: parameters of the four-point test bench and the polyurethane specimen

Description	Variable	Value (mm)
Length of specimen	l	260
Width of specimen	b	60
Thickness of specimen	t_s	90
Thickness of ice	t_i	$0.9 - 1.0$
Distance between support and load points	L_1	20
Distance between the loads points	L_2	160
Distance between support points	L	200

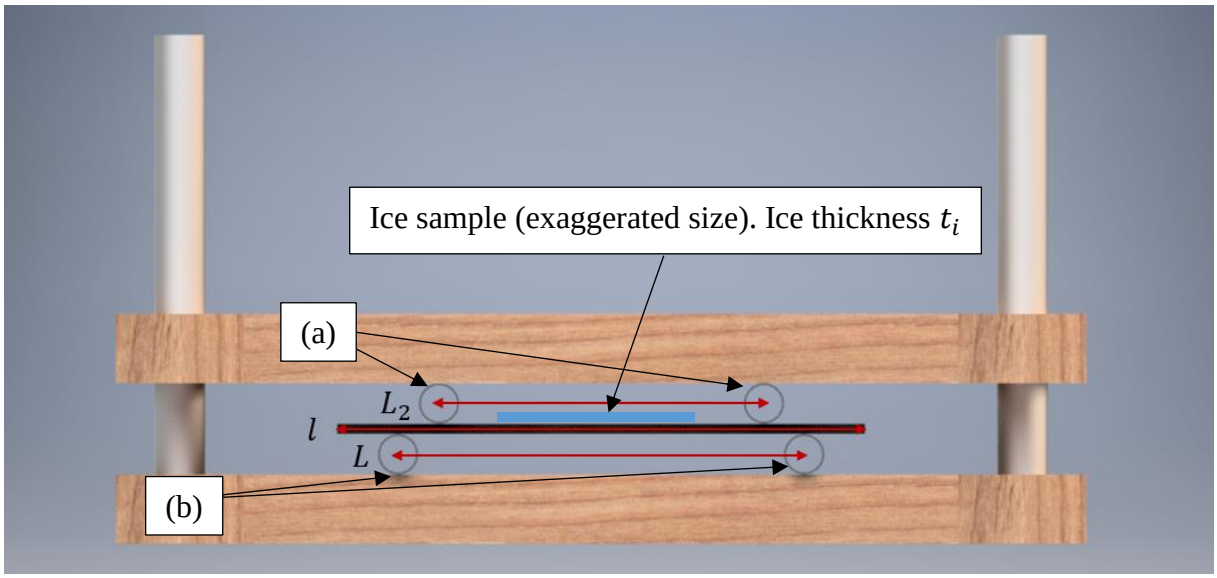

Figure 8: schematic figure of four-point stress bench. Rendered in Autodesk Inventor Professional 2017.

Figure 9: top view of the four-point test bench. The polyurethane specimen in the middle. The renders in fig. 8 and 9 are both modelled in Autodesk Inventor Professional 2017.

3.2.1. Preparation of Sample

The polyurethane sample was cut in appropriate sizes ($260mm\ x\ 60mm$). Both the sample and the four-point bench was put in the freezer ($-25°C$) over-night to ensure even temperature in the entire specimen. In the design of the test bench, there are two support rods. These were added to the system to ensure that the load joints only could move downwards when load was applied, and hence, ensure more accurate results.

The entire apparatus, and the anti-abrasion polyurethane, was put inside the cold room over-night. When the objects were properly cold, masses were added on the four-point bench, while still inside the cold room.

When the preparation for ice adhesion, liquid water was poured on the surface of the anti-abrasion polyurethane. This was done while the polyurethane specimens was inside the freezer, to minimize errors due to moving the specimen to the freezer from the ambient room. Errors can be that the water did not stick to the surface, and so on. The reason the water did not float everywhere was due to the surface tension between the water and surface of the polyurethane. Consequently, a decent slab of ice was obtained on top of the polyurethane. After approximately 6 hours the liquid water had turned to solid ice. See fig. 9 of the ice on the specimen on polyurethane. This specimen has been placed on the four-point test bench.

Figure 10: ice on polyurethane

3.2.2. Data Gathering

The load and deflection data was gathered while both the apparatus and the specimen where still inside the cold room. The initial load from the loading frame (see fig. 7 and 8), was 1.25 kg. The added mass came from iron weights, and the added mass had an increment of 1.25 kg each time. The initial displacement was recorded before the first 1.25 kg iron weight was added, in the middle of the upper frame. At each time more weight was added, the new displacement was recorded. See figure 11 on the next page.

Figure 11: recording of displacement using a Vernier caliper. At this instant, the only load is from the upper frame alone. The middle of the frame is marked with a circle.

When the ice had separated from the surface, the experiment was concluded. At each time more weight was added, the ice was gently poked on the side to check if for ice adhesion.

3.2.3. Conditions of Experimental Location

To ensure that the experimental setup was true to nature, most experiments was done while inside the cold room $(-30°C)$ at the Cold Room at the Arctic University of Tromsø. However, some experiments were done in room temperature. This was done so that data that could be compared to other work with different materials.

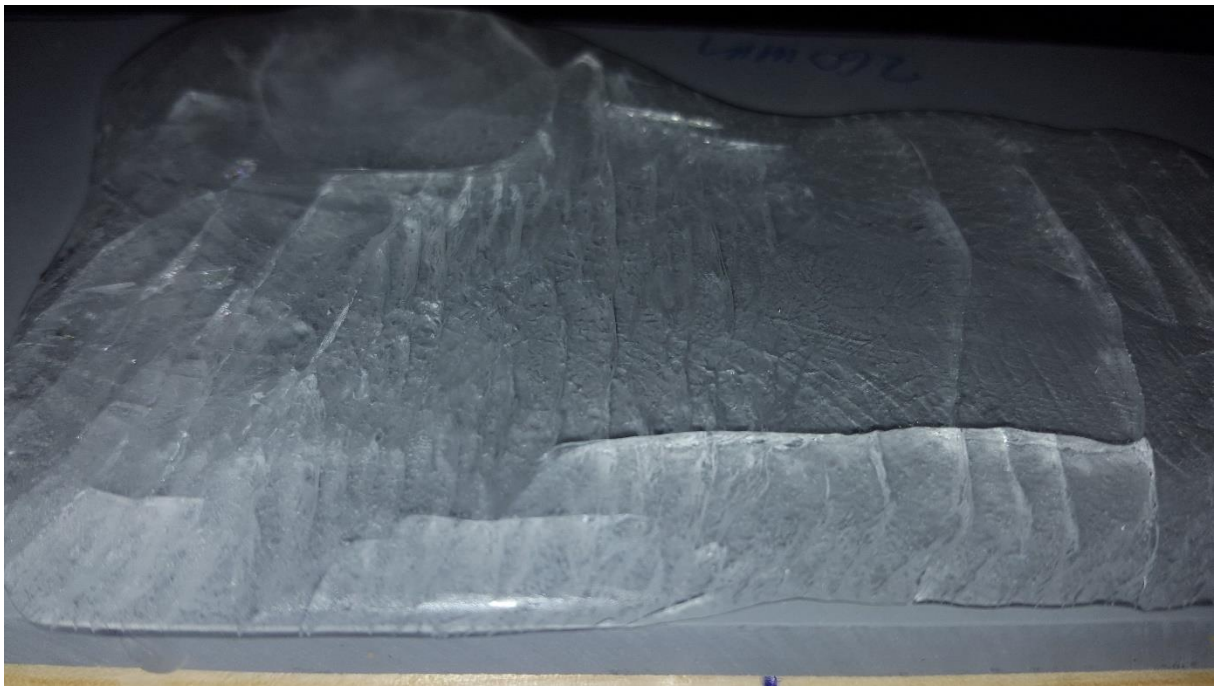

Figure 12: ice have broken due to shear stress, and there are no forces restraining the ice to the polyurethane.

When the displacement when the ice adhesion seized to exist was measured, the experiment was concluded. The identical experiment was done multiple times to ensure that substantial amounts of data was gathered. For each time water was poured, the ice had different areas, which was expected. However, all areas were recorded prior to the experiment started. When the masses were added on the four-point bench, the deflection at point L_1 was recorded using a Vernier caliper. This was done after each time where the added load was increased on the bench. Additionally, after each time where the load had increased, the ice was gently poked on the side to see if ice adhesion was still present.

3.3. Ice adhesion in ANSYS®

In ANSYS®, a setup of the four-point test was modelled. See figure 13 below.

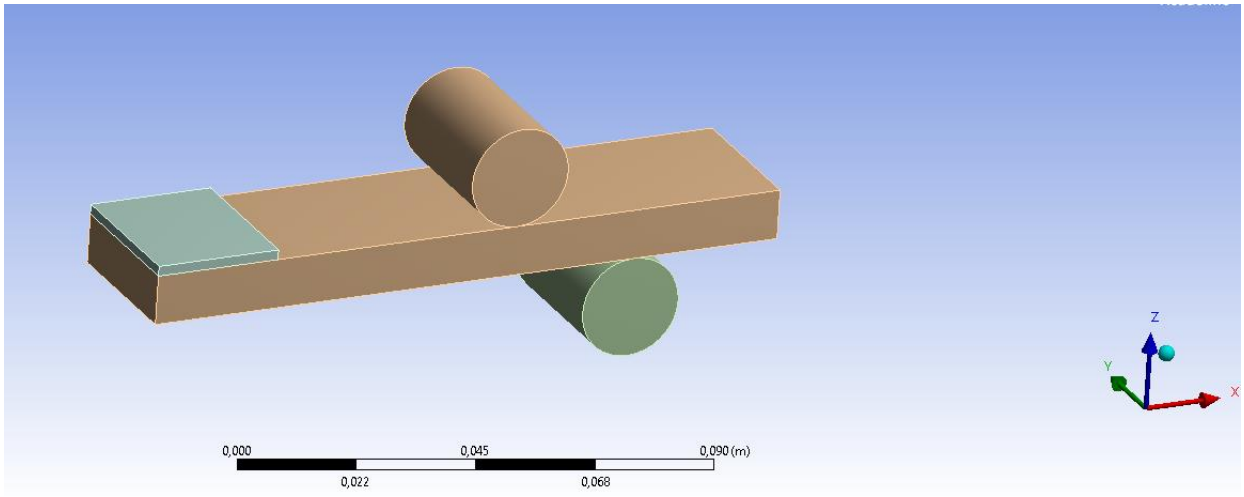

Figure 13: ice adhesion test in ANSYS®. The light-colored blue box on the left side represents the ice.

This model represents ¼ of the complete system. The reason to why only a quarter of the complete system was modelled is to minimize the computational load when solving the model. Inside the software, symmetry regions were put on the sides, so that the final model was appropriate, according to fig. 8 and 9. In figure 14 below, symmetry and the mesh have been added. The light shaded block between the load points represents the ice. For each run, the area of the ice was modelled according to table 4 in section 4.1.

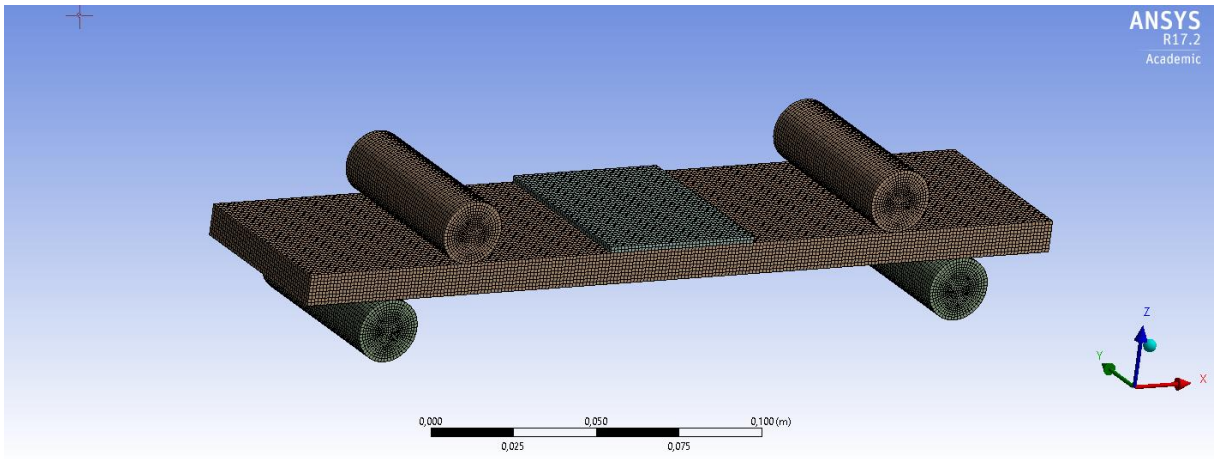

Figure 14: mesh and symmetry applied.

In this figure, the mesh has been applied to the system and symmetry was applied. In the setup, prior to running the simulation in the ANSYS®-software, the maximum displacement, in $z - direction$ was set according to the displacement at the point ice separated from the polyurethane surface in the experiments . See these results in table 4 in chapter 4. The recorded longitudinal stress from the simulation was recorded in the middle of the system. In ANSYS®, displacement in $z - direction$ was applied, according to the experimental results. These results can be viewed in table 1 in section 4.2, and appendix B. As it can be seen in figure 9 and 10, the ice in the ANSYS® model have not been modelled according to the real ice shape of the ice (ref. fig. 7). What was done, however, is that the area of the ice was estimated using basic math and trigonometry. Trigonometry where applied if the frozen ice had triangles at some point of the surface. Based on these results, it was possible to approximate the area of ice on the surface of polyurethane.

Chapter 4: Results and Discussion

4.1. Experimental Data

The sections 4.1.1 and 4.1.2. will present the results from the four-point test bench. In the tables below, the point of when the ice separated from the surface is highlighted in bold.

4.1.1. Anti-abrasion Polyurethane

The data obtained using a Vernier caliper to obtain the displacement and the added mass from experiments on anti-abrasion polyurethane is shown below.

Table 4: data from experiments with ice adhesion on anti-abrasion polyurethane

Experiment #1 (area $A = 59.7cm^2$)	
Mass (kg)	Displacement (mm)
1.25	1.30
2.50	1.46
3.75	1.92
5.00	2.03
6.25	2.48
7.50	**3.01**

Experiment #2 (area $A = 57.4cm^2$)	
Mass (kg)	Displacement (mm)
1.25	1.28
2.50	1.84
3.75	2.43
5.00	2.91
6.25	3.30
7.50	**3.85**

Experiment #3 (area $A = 56.4cm^2$)	
Mass (kg)	Displacement (mm)
1.25	1.25
2.50	1.35
3.75	1.51
5.00	**2.31**
6.25	-
7.50	-

Experiment #5 (area $A = 58.5cm^2$)	
Mass (kg)	Displacement (mm)
1.25	1.30
2.50	2.05
3.75	2.42
5.00	2.93
6.25	3.30
7.50	**3.83**

Experiment #6 (area $A = 59.8cm^2$)	
Mass (kg)	Displacement (mm)
1.25	1.30
2.50	1.85
3.75	2.62
5.00	2.93
6.25	3.21
7.50	**3.73**

Experiment #7 (area $A = 58.8cm^2$)	
Mass (kg)	Displacement (mm)
1.25	1.21
2.50	1.45
3.75	2.52
5.00	**2.73**
6.25	-
7.50	-

Experiment #8 (area $A = 56.9cm^2$)	
Mass (kg)	Displacement (mm)
1.25	1.59
2.50	2.90
3.75	3.73
5.00	3.60
6.25	**3.62**
7.50	-

Experiment #9 (area $A = 58.0cm^2$)	
Mass (kg)	Displacement (mm)
1.25	1.52
2.50	1.60
3.75	2.90
5.00	3.37
6.25	**3.63**
7.50	-

As it can be seen, the ice adhesion seized to exist at different loads, but it was never necessary to have a load bigger than 7.5 kg. The lowest load was 5 kg. In all, the experiment resulted in 9 successful results.

4.2.2. Anti-seepage Polyurethane

Table 5: data from experiments with ice adhesion on anti-seepage polyurethane

Experiment #1 (area $A = 52.7cm^2$)	
Mass (kg)	Displacement (mm)
1.25	1.28
2.50	1.52
3.75	1.95
5.00	2.12
6.25	2.57
7.50	**3.07**

Experiment #2 (area $A = 51.4cm^2$)	
Mass (kg)	Displacement (mm)
1.25	1.13
2.50	1.74
3.75	2.85
5.00	3.21
6.25	3.30
7.50	**3.95**

Experiment #3 (area $A = 58.4cm^2$)	
Mass (kg)	Displacement (mm)
1.25	1.27
2.50	1.45
3.75	1.61
5.00	2.71
6.25	**3.12**
7.50	-

Experiment #5 (area $A = 59.5cm^2$)	
Mass (kg)	Displacement (mm)
1.25	1.42
2.50	2.15
3.75	2.52
5.00	3.03
6.25	3.38
7.50	**4.01**

Experiment #6 (area $A = 51.8cm^2$)		Experiment #7 (area $A = 52.9cm^2$)	
Mass (kg)	Displacement (mm)	Mass (kg)	Displacement (mm)
1.25	1.28	1.25	1.17
2.50	1.45	2.50	1.55
3.75	2.32	3.75	2.62
5.00	2.84	**5.00**	**2.93**
6.25	3.41	6.25	-
7.50	**3.73**	7.50	-

The results reveals that ice adhesion to polyurethane is generally in the same region as was found in PVC (Xue, 2015). As for the ice adhesion to metals and other tested polymers (table 1), the method that was used in this paper could not obtain any quantifiable data. When the frozen polyurethane/ice where taken out in room temperature, the ice had already separated from the surface. This suggests that the ice adhesion force when tested in room temperature is low. Additionally, the numbers obtained from both the analytical study and simulations for both materials, are similar. This suggests that both materials will behave somewhat similar when subjected to cold climates.

4.2. Analytical Study and Simulations in ANSYS®

4.2.1 Anti-abrasion Polyurethane

Both the results from the analytical study (beam theory in MATLAB©) and simulations will be presented in this section.

The resulting normal stress from the simulations of experiment #1 (from table 4) in ANSYS® can be seen in figure 14, and table 3 below (run #1):

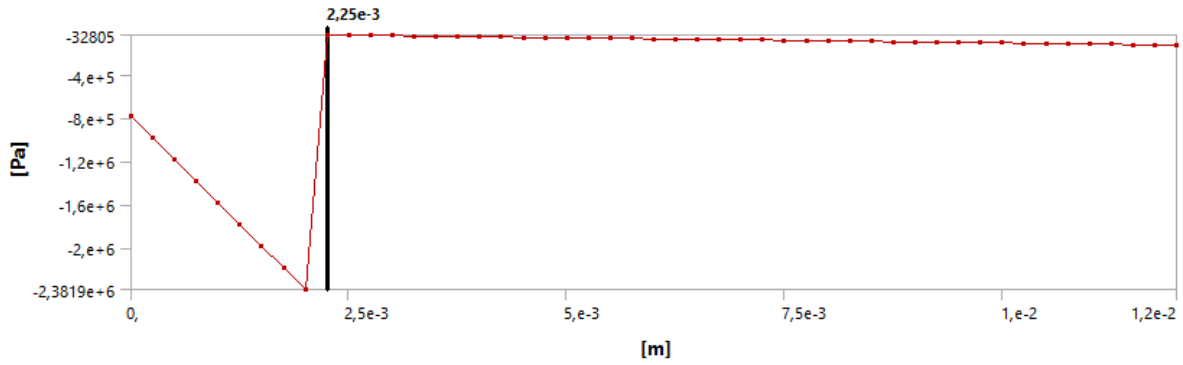

Figure 15: simulation of normal stress inside ANSYS®.

In figure 14 above, the distance between 0 and 2.5mm represents the ice cross-section area. The rest (2.5mm and beyond) is the cross-section area of polyurethane. To determine the ice adhesion, the normal stress at the black line is subtracted to the data point the adjacent point to the left. Thus, the normal stress between the ice and polyurethane is:

Table 6: normal stress between the ice layer and anti-abrasion polyurethane from simulations in ANSYS® and analytical simulations in MATLAB®.

Run #	Normal stress (MPa)		Area (cm^2)
	ANSYS®	Analytical	
1	1.91	1.99	56.4
2	1.99	2.10	56.9
3	2.35	2.15	57.4
4	2.24	2.23	58.0
5	2.35	2.39	58.4
6	2.35	2.47	58.9
7	2.38	2.55	58.9
8	2.38	2.66	59.7
9	2.56	2.63	56.8

The plotted figure based on table can be seen in figure 15 below.

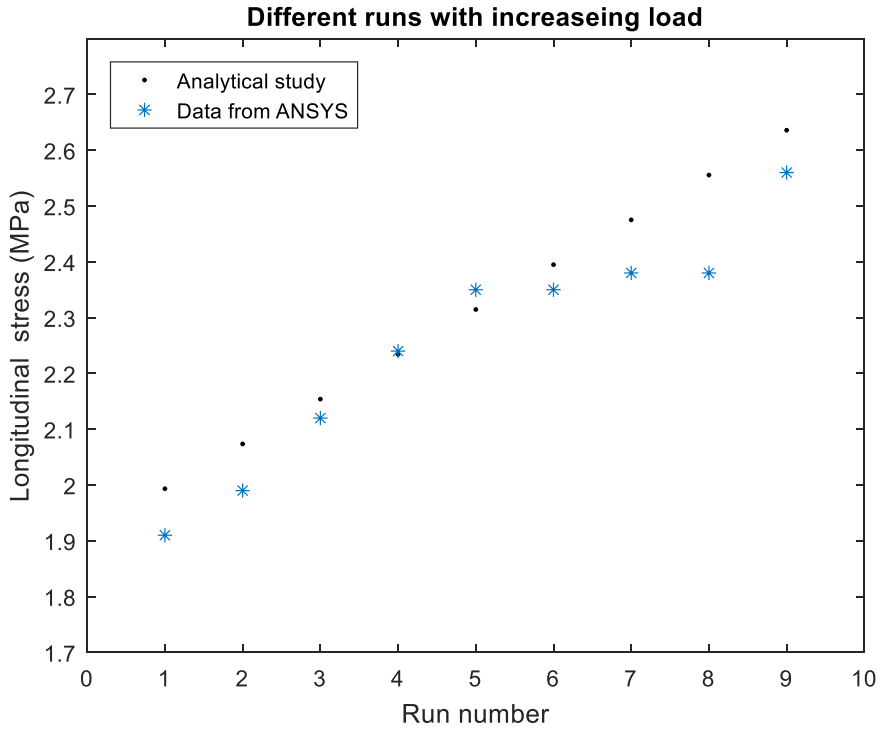

Figure 16:pl plotted (dots) values of the recorded data from the analytical study and data from ANSYS®

By multiplying the recorded area (m^2) in table 4 with the stress (Pa), the pressure of ice adhesion can be found.

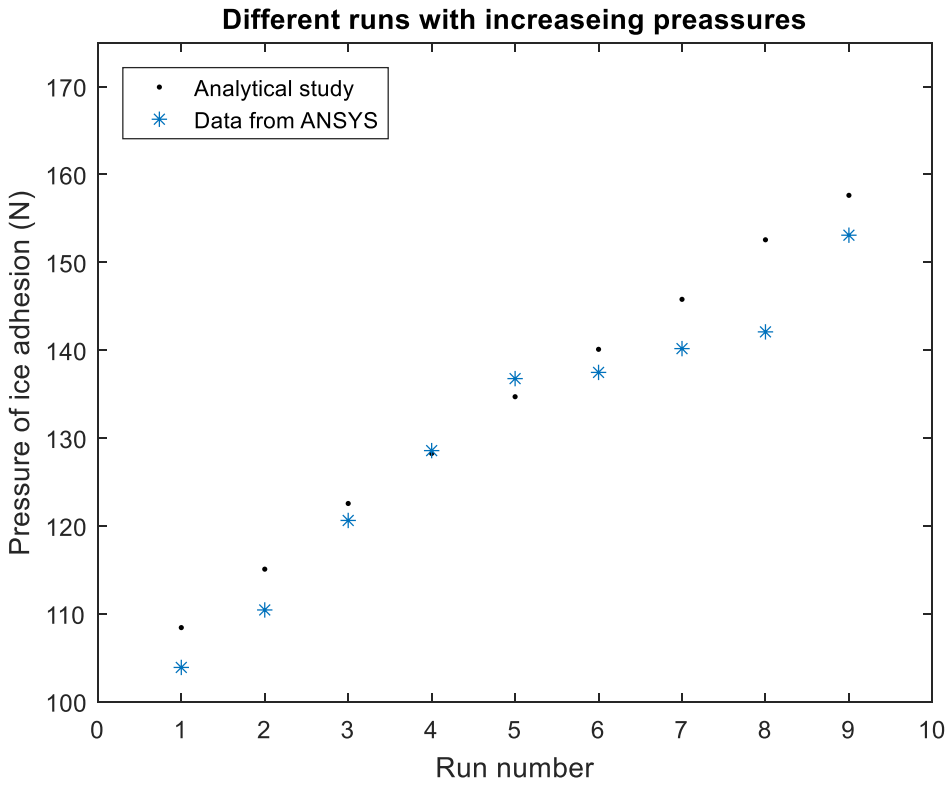

Figure 17: the pressure of the ice adhesion on anti-seepage polyurethane.

4.2.2. Anti-seepage Polyurethane

The results from the analytical study and simulations on anti-seepage polyurethane is displayed below.

Run #	Normal stress (MPa)		Area (cm^2)
	ANSYS®	Analytical	
1	1.42	1.55	51.4
2	1.52	1.61	51.8
3	1.65	1.76	52.1
4	1.85	1.97	52.7
5	2.19	2.22	52.9
6	2.25	2.29	58.4
7	2.29	2.32	55.9
8	2.38	2.39	56.1
9	2.48	2.51	56.9

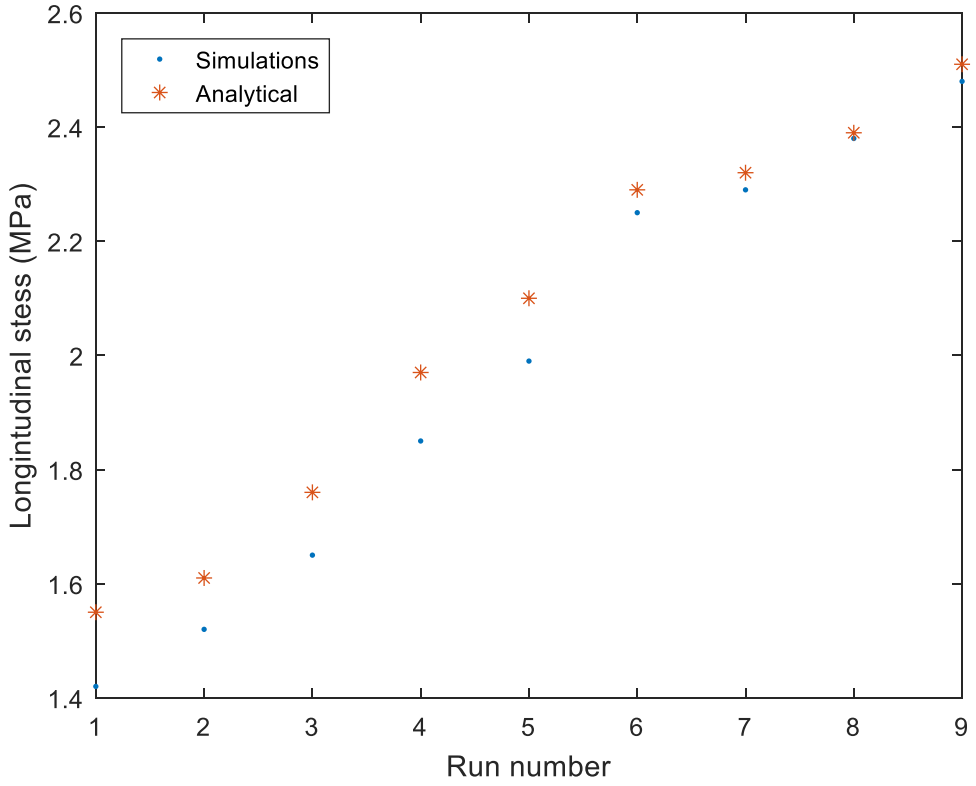

Figure 18: plotted (dots) values of the recorded data from the analytical study and data from ANSYS®

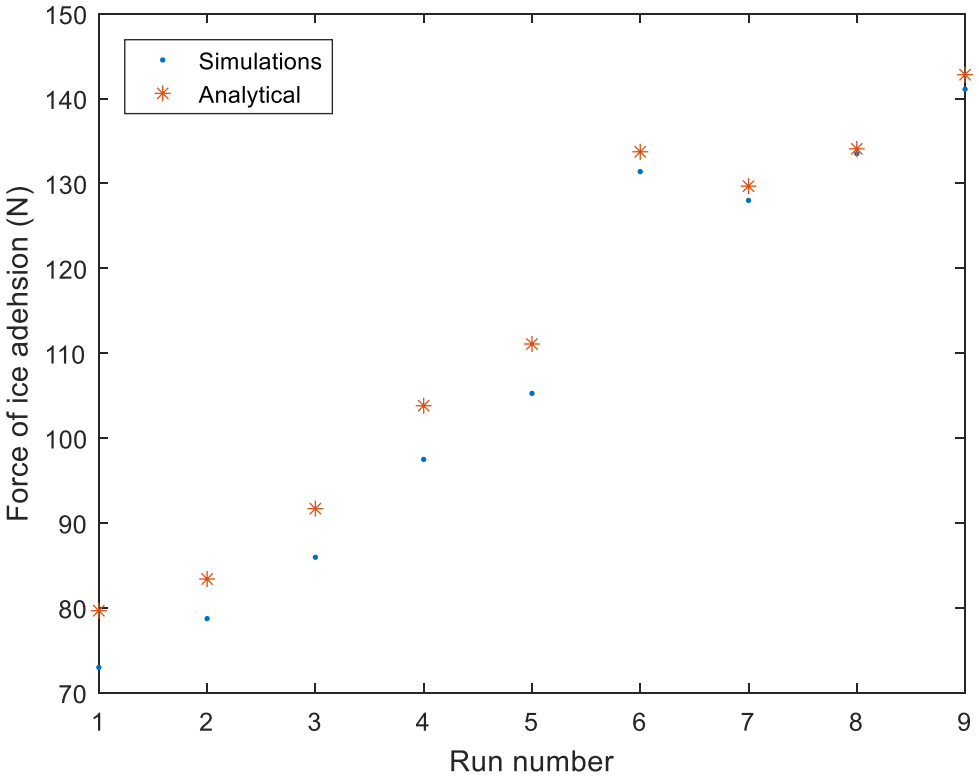

Figure 19: the pressure of the ice adhesion on anti-seepage polyurethane.

When the ice/polyurethane sample was tested in room temperature, the ice separated usually before the experiment could start. Therefore, there are no quantitative data to report.

Chapter 5: Conclusions and Future work

5.1. Conclusions

What was found in this study it the ice adhesion strength between polyurethane and ice when tested in a cold atmosphere. What can be said about the ice adhesion is that the temperature of where the experiment is done is important. This can also be seen in table 1 where the strength of ice adhesion between varied materials were tested. The ice adhesion force when the test is done in room temperature is way lower compared to when tests are done in cold room. This was also observed when polyurethane with ice was tested in room temperature. In addition, the added mass on the four-point bench, when the ice separated, varied from $7.5\ kg$ to $5\ kg$.

5.2. Future work

- More sophisticated method to determine the ice adhesion can be developed. Methods of such could be the use of a sensors to determine the instance when ice separated from the surface (e.g. ultrasonic waves detection).
- How these materials could be used in areas where icing is a problem, based on the results from the relatively low ice adhesion.

References

Adeeb, S., 2015. *Beam Structures - Plane Beam Approximations.* [Online] Available at: http://sameradeeb.srv.ualberta.ca/beam-structures/plane-beam-approximations/ [Accessed 16 03 2017].

Atanackovic, T. M. & Guran, A., 2012. *Theory of Elasticity for Scientists and Engineers.* Boston: Birkhäuser Boston.

Bayer, O., 1947. Das Di-Isocyanat-Polyadditionsverfahren (Polyurethane). *Angewandte Chemie,* 59(9), pp. 257 - 272.

Davis, A. et al., 2014. Superhydrophobic Nanocomposite Surface Topography and Ice. *Applied Materials & Interface,* Issue 6, pp. 9272 - 9279.

Döppenschmidt, A. & Butt, H.-J., 2000. Measuring the Thickness of the Liquid-like Layer on Ice Surfaces with Atomic Force Microscopy. *Langmuir,* 16(16), pp. 6709 - 6714.

Dulong, P. L. & Petit, A. T., 1819. Recherches sur quelques points importants de la Théorie de la Chaleur. *Annales de Chimie et de Physique,* Issue 10, pp. 395 - 413.

Eshbach, O. W. & Tapley, B. D., 1990. *Eshback's Handbook of Engineering Fundamentals.* s.l.:John Wiley & Sons.

Fourier, J., 2007 (1822). *The Analytical Theory of Heat.* s.l.:Cosimo Classics.

Gebhart, B., 1993. *Heat conduction and mass diffusion.* 1st ed. New York: McGraw-Hill.

Gerhard, W. M., 1908. *Modern Baths and Bath Houses.* New York: John Wiley and Sons.

Goertz, M. P., Zhu, X. Y. & Houston, J. E., 2009. Exploring the Liquid-like Layer on the Ice Surface. *Langmuir,* 25(12), p. 6905–6908.

Griffin, R. & Krishnan, S., 2000. *A Four-Point Bend Test Experiment for Use in the Classroom, and Procedures for Evaluating Results,* Texas: Texas A&M University at Qatar.

Gum, W., Wolfram, R. & Ulrich, H., 1992. *Reaction Polymers.* New York: Oxford University Press.

Harrington, R. & Hock, K., 1991. *Flexible Polyurethane Foams.* Midland: The Dow Chemical Company.

He, Z. et al., 2017. Room Temperature Characteristics of Polymer-Based Low Ice Adhesion Surfaces. *Scientific Reports*, Issue 7.

Hibbeler, R. C., 2013. *Statics and Mechanics of Materials.* s.l.:Pearson Higher Ed.

Jellink, H. H. G., 1967. Liquid-Like (Transition) Layer on Ice. *Journal of Colloid and Interface Science,* Issue 25, pp. 192 - 205.

Jellinks, H. H. G., 1959. Adhesive Properties of Ice. *Journal of Colloid Science,* Issue 14, pp. 268 - 280.

Jones, R. M., 1975. *Mechanics of Composite Materials.* Washington D.C.: Scripta Book Company.

Khawaja, H. A. & Xue, H., 2016. Analytical and Case Studies of a Sandwich Structure using Euler-Bernoulli Beam Equation. *Mathematics in Engineering, Science and Aerospace,* 7(4), pp. 599 - 612.

Krotova, N. A. et al., 1965. Investigation of Various Types of Adhesion Bonds. *DTIC Document.*

Kulinich, S. A. & Farzaneh, M., 2009. Ice adhesion on super-hydrophobic surfaces. *Applied Surface Science,* 18(255), p. 8153–8157.

Landy, M. & Freiberger, A., 1967. Studies of Ice Adhesion. *Journal of Colloid and Interface Science,* Issue 25, pp. 231 - 244.

Michael Faraday, 1850. Occasional Papers on the Theory of Glaciers. *Forbes, J.D.,* p. 640.

Moran, M. J., Shaprio, H. N., Munson, B. R. & DeWitt, D. P., 2003. *Introduction to Thermal systems Engineering. Thermodynamics, Fluid Mechanics, and Heat Transfer.* 1st ed. s.l.:Wiley & Sons, Inc..

National International Conference, 1973. Permafrost. In: *North American Contribution: Permafrost.* Washington, D.C.: National Acadamy of Science.

Nave, R., 2016. *hyperphysics.phy-astr.gsu.* [Online]
Available at: http://hyperphysics.phy-astr.gsu.edu/hbase/thermo/Dulong.html#c1
[Accessed 11 02 2017].

Özisik, N. M., 1993. *Heat Conduction.* 2nd ed. New York: John Wiley & Sons, Inc..

Petrescu, I., Mohora, C. & Ispas, C., 2011. Determination of Young'S Modulus For CFRP Using the Three – Point Bending Test. *Proceedings in Manufacturing Systems,* 6(4), pp. 255 - 261.

Pipe Flow Software, 2010. *Pipe Flow Software.* [Online]
Available at: http://www.pipeflow.com/sitemap/pipe-roughness
[Accessed 30 01 2017].

Prisacariu, C., 2011. *Polyurethane Elastomers. From Morphology to Mechanical Aspects.* Wien: Springer.

Rashid, T., Khawaja, H. & Edvardsen, K., 2016. Determination of Thermal Properties of Fresh Water and Sea Water Ice using Multiphysics Analysis. *International Journal of Multiphysics,* 10(3), pp. 277 - 290.

Recktenwald, G. W., 2004. *Finite-Difference Approximations to the Heat Equation,* s.l.: s.n.

Roberts, P. W., 1951. *Effect of Extreme Arctic Cold on Materials.* Dartmouth: Dartmouth College Library.

Ryzhkin, I. A. & Petrenko, V. F., 1997. Physical Mechanisms Responsible for Ice Adhesion. *Journal of Physical Chemistry,* Issue 101, pp. 6267 - 6270.

Seymore, R. B. & Kauffman, G. B., 1992. Polyurethanes: A class of modern versatile materials. *Journal of Chemical Education,* 69(11), p. 909.

Smith, R., Inomata, H. & Peters, C., 2013. Chapter 8 – Heat Transfer and Finite-Difference Methods. *Supercritical Fluid Science and Technology,* Volume 4, pp. 557-615.

Snoke, D. W., 2009. *Solid State Physics: Essential Concepts.* 1st ed. s.l.:Addison-Wesley.

Soto, M., Sebastián, R. M. & Marquet, J., 2014. Photochemical Activation of Extremely Weak Nucleophiles: Highly Fluorinated Urethanes and Polyurethanes from Polyfluoro Alcohols. *The Journal of Organic Chemistry,* 11(79), pp. 5019 - 5027.

Wachtman, J. B., Cannon, W. R. & Matthewson, M. J., 2009. *Mechanical properties of ceramics.* s.l.:John Wiley & Sons.

Wayl, W. A., 1951. Surface Structure of Water and Some of its Physical and Chemical Manifestations. *Journal of Colloid Science,* 6(5), pp. 389-405.

Weisstein, E. W., 2011. *Mean-Value Theorem.* [Online]
Available at: http://mathworld.wolfram.com/Mean-ValueTheorem.html
[Accessed 15 03 2017].

Woods, G., 1990. *The ICI Polyurethanes Book.* New York: John Wiley & Sons.

Xue, H., 2015. *Ice Shedding Processes,* Narvik: Department of Technology, Narvik University College.

Young, W. C. & Budynas, R. G., 2002. *Roark's Formulas for Stress and Strain.* 1st ed. New York: McGraw Hill.

Zhiheng, S., 2015. *The SK one component polyurea and its application in hydraulic and hydropower project structures.* Beijing, China Institute of Water Resources & Hydropower Research.

Appendix J

The MATLAB® code that was used in the analytical study

```
clc

clear all
close all

E_1 = 50e6;                                 %% Young's modulus for PE at -
30degC, Pa
E_2 = 4e9;                                  %% Young's moduls for ice (Helen
report), Pa

x = 20e-3;                                  %% distance to the support joint,
meter
n = E_2/E_1;                                %% Balance coefficient
s = 1;
% P = [5:0.25:7.5].*9.81;                   %% Recored force, N
o = [2.73:0.11:3.63]*1e-3;                  %% measured deflection (\delta), m
```

Polyurethane data

```
t_p = 8.5e-3;                               %% Thickness of polyurethane, m
l_p = 60e-3;                                %% width of polyurethane, m
```

Ice data

```
t_i = 0.91e-3;                                  %% Thickness of ice, m
l_t = 50e-3;                                    %% width of ice, m
A_1 =  t_p*l_p;                                 %% cross-section area of PU, m2
A_2 =  t_i*l_t;                                 %% cross-section area of ice, m2

A = A_1 + A_2;                                  %% Total cross-section area, m2
E = E_1*(A_1/A) + E_2*(A_2/A);                  %% Rule of mixture Young's modulus,
Pa

D_1 = t_p/2*s;                                  %% See report
D_2 = t_p/s + t_i/2*s;                          %% See report

c_y = (A_1*D_1 + n*A_2*D_2)/(s*(A_1 + n*A_2));

I_PU = l_p*t_p^3/12 + l_p*t_p/s*(D_1-c_y)^2;    %% Moment of inertia of
polyurethane, m4
I_ice = l_t*t_p^3/12+ l_t*t_i/s*(D_2-c_y)^2;    %% Moment of inertia of ice, m4

I_t = I_ice + I_PU;                             %% Total moment of inertia, m4
L_1 = x;                                        %% Distane to load joint, m
L = 260e-3;                                     %% Distanece between loading joints,
m

theo_P =  o.*((12*E*I_t)/(x^3) + (E*I_t)/(x*L_1^2) - 4*E*I_t/(L_1*L*x));  %%
theoretical applied force, N


y = t_p;                                        %% The distance from zero where we
find the longitudinal stress, m


M = L_1.*theo_P/2;


long_stress_1 = (M*abs(y-c_y)/I_t)/1e6;        %% The longitundinal stress in the
first (PU) material, in MPa
long_stress_2 = (n*M*abs(y-c_y)/I_t)/1e6;      %% The longitundinal stress in the
second (ice) material, in MPa

figure()
plot(long_stress_1,'.k')
axis([0 10 1.7 2.8])
hold on

data = sort([ 1.91, 2.35, 2.35, 2.38, 2.12, 1.99, 2.56 2.38 2.24]);
plot(data,'*')

legend('Analytical study','Data from ANSYS','location','northwest')


xlabel('Run number')
ylabel('Longitudinal  stress (MPa)')
```

```
title('Different runs with increaseing load')
```

UiT
THE ARCTIC UNIVERSITY OF NORWAY

Faculty of Science and Technology

Department of Engineering and Safety

Part C

Determining thermal properties of Polyurethane by solving the Heat equation and IR imaging

—

Hans-Kristian Norum Eidesen

TEK-3901 Master thesis (part 3 of 3) in Technology and Safety in the High North
June 2017

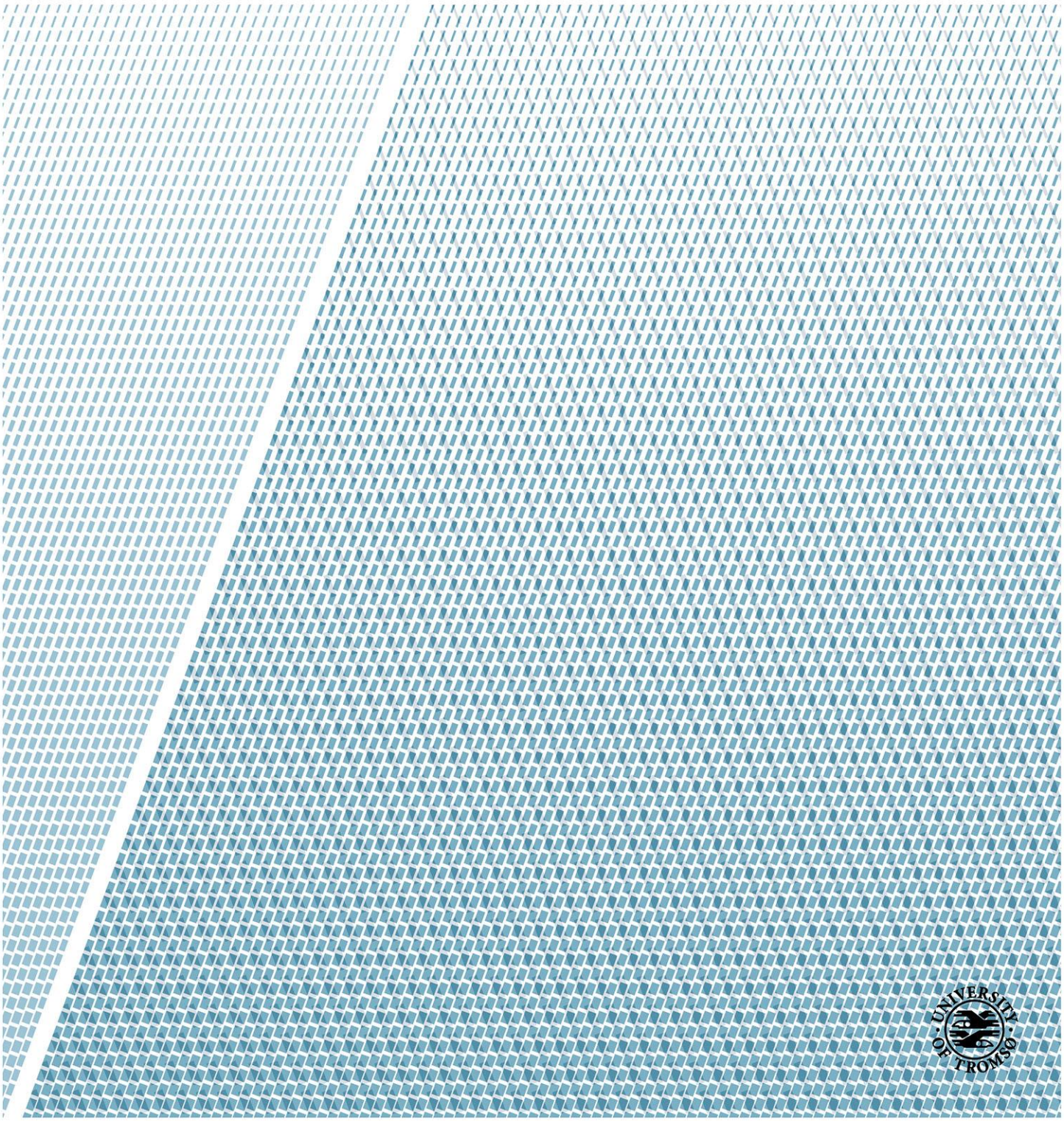

Abstract

By capturing the infrared signature using a FLIR Infrared camera (FLIR T1030Sc) of a cold ($app. -20°C$) specimen of SKOCP and comparing the results with a simulated result, the thermal properties of the material have been estimated. The simulation were carried out in MATLAB®, and the solution is based upon the Heat equation. In this paper, the driving mechanisms behind the Heat equation, as well as how the approximated solution to the Heat equation is obtained will be described.

Table of Contents

List of Figures

List of Tables

Nomenclature

Description	Symbol	Unit
Thermal conductivity	k	$W \cdot K^{-1} \cdot m^{-1}$
Heat transfer	h	$W \cdot K^{-1} \cdot m^{-2}$
Fourier's Law/heat flux	q_x''	W/m^2
Time	t	s
Spatial coordinates	x, y, z	m
Derivation in the cartesian space	$dx, dy. dz$	m
Internal energy	u	J
Specific heat capacity	C_p	$J/kg \cdot K$
Density of material	ρ	kg/m^3
Volumetric energy generation	$\dot{q}$	W/m^3
Volumetric heat capacity	α	$J/m^3 \cdot K$
Partial differential equation	$\frac{\partial \varphi}{\partial x}$	N/A
Truncation error	ξ	N/A

Outline

The paper is divided into 5 chapters. The content of each chapter is listed below:

- Chapter 1 introduces the goal of the paper.
- Chapter 2 is a literature review on what polyurethane is, a brief overview of the chemistry of polyurethane.
- Chapter 3 introduces the method that was elected to govern the solutions that was obtained in this paper. Additionally, this chapter describes what heat is. Mathematical models and theories, such as Fourier's Law, the derivation of the Heat equation, and the approximation ("solution") to the Heat equation are found in this chapter.
- Chapter 4 presents the results that was obtain by solving the Heat equation in MATLAB®.
- Chapter 5 gives the discussion and conclusion.
- Appendix I contains the MATLAB© code that was used to solve the Heat equation and compare the experimental results. It was constructed two similar set of codes, however, only one set of code are included, because of the obvious similarities between the two.

Chapter 1: Introduction

All materials have different and unique thermal properties, and there are two important constants that determine how the temperature changes when a material is subjected to a temperature difference. These constants are named the thermal conductivity and the heat transfer coefficient. By solving the Heat equation and by using infrared camera technology, these factors can be estimated. This paper will introduce the basic concepts of heat, introduce Fourier's Law, and how the Heat equation is derived. The solution the Heat equation is currently not available, therefore, *approximations* or *numerical solutions* will be applied. The approximation the is used in this paper is called the Finite Difference Method (FDM), and Forward-Time Central-Space (FTCS). By comparing the thermal images captured by an IR camera with the results from the FDM/FTCS analysis, the thermal properties can be estimated.

This study will investigate the thermal properties of a plastic called polyurethane. This plastic is unique in that sense that it can be applied to close-to anything. Depending on what additives the manufacturer decides to put in the production of polyurethane, the material characteristics will change. This paper will, however, focus on anti-seepage polyurethane and anti-abrasion polyurethane. If these materials where to be put in Arctic regions, let it be as a coating material for pipes used by the oil and gas industry, their thermal properties must be adequate with regards to current standards. The paper will, however, not suggest if these materials be used as listed, it will purely focus on determining the thermal properties.

1.2. Thermal Properties of Materials

As mentioned, each material have unique thermal properties, and some thermal properties of common materials are listed below (Engineering Toolbox, 2017)

Material	Thermal conductivity $(W/m^{-1} \cdot K^{-1})$	Coefficient of heat transfer $(W/m^{-2} \cdot K^{-1})$
Cast iron	58	5.7
Stainless steel	16	7.9
Wood	0.23	–

Note that the coefficient of heat transfer is dependent of different factors (fluid velocity over material surface etc.). These factors are not studied in this paper.

Chapter 2: Literature Review

2.1. Polyurethane

Polyurethane was invented by Otto Bayer and Heinrich Rinke, in Germany in 1937 (Bayer, 1947), (Prisacariu, 2011) and some of the first use of this plastic was during WWII, where it was applied as a coating of the German airplanes (Seymore & Kauffman, 1992). However, some of the first commercially available products made from polyurethane was rigids foams and rubbers for different purposes. It was discovered that by the addition of different materials (e.g. mica and other processed mineral fibers), the polyurethane got stiffer and better heat properties (thermal conductivity and heat transfer). In 1983, a US car making company made the Pontiac Fiero, where the entire body was made from polyurethane with special additives. As of 2011, the use of polyurethane is spread from construction materials to clothing (Prisacariu, 2011).

Table 1: the distribution of different applications that use polyurethane

Polyurethane use	Amounts (millions of kg)	Percentage (%)
Building and construction	662	26.8
Transportation	589	23.8
Furniture and bedding	511	20.7
Appliances	126	5.1
Packaging	113	4.6
Textile, fibers and apparel	82	3.3
Machinery and Foundry	80	3.3
Electronics	34	1.4
Footwear	17	0.7
Other use	253	10.2
Total	2467	100

2.1.1. Chemistry of Polyurethane

Polyurethane is in the chemical class called reaction polymers (Gum, et al., 1992), (Harrington & Hock, 1991) and (Woods, 1990). The process of making polyurethane involves reaction an isocyanate containing two or more isocyanate groups per molecule $(R - N = C = O)_n$ (Soto, et al., 2014) with a polyol containing hydroxyl groups $(R' - (OH)_n)$ (Soto, et al., 2014)that contain on average two or more molecules. In addition to these molecules, the urethane groups are introduced $(-NHCO - O)$. These three groups are then put under an ultraviolet light or with a presence of a catalyst, and thus, polyurethane is made. See figure 1 below. Naturally, the process is more complicated than that. It is, however, not the scope of this paper to investigate all the steps in creating polyurethane.

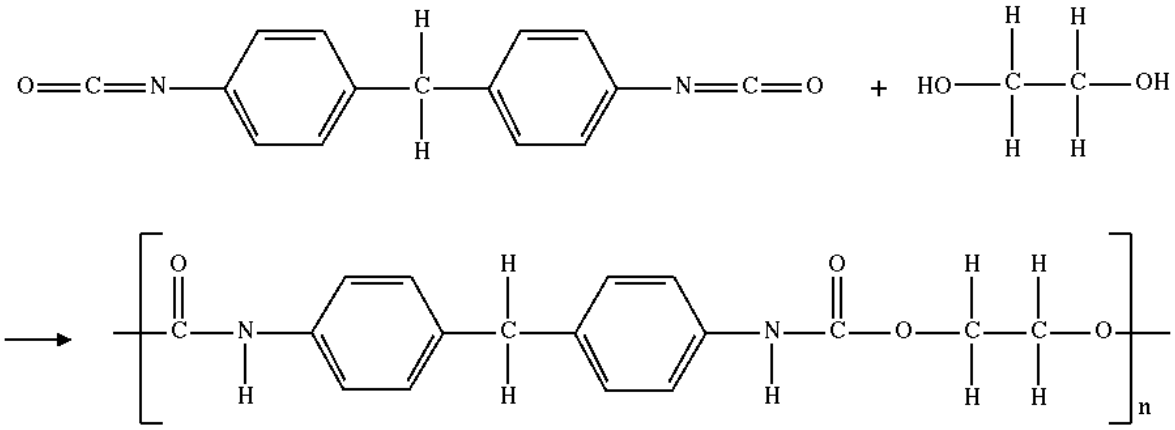

Figure 1: the creation of polyurethane

2.1.2. SK One Component Polyurethane

In this paper, the polyurethane developed by China Institute of Water Resources & Hydropower Research Beijing IWHR-KHL Co. Ltd. The product name is SK One Component Polyurethane, however, polyurethane is the name that will be used in the following chapters and sections in this paper. The company provided two distinct types of polyurethane, namely anti-seepage polyurethane and anti-abrasion polyurethane. Anti-seepage polyurethane is suggested to be used as a sealant in either chemical tanks, as it has good resitance to chemical corrosion (Zhiheng, 2015) or in dams to prevent water leaks through the concrete. Anti-abrasion polyurethane can be used on locations where high corrosion is expected. Locations of such can be water ducts from dams, on ships, due to the force of water while ship is in transit, and so forth.

2.5. Infrared camera technology

All bodies emit radiation, the most familiar being the light we see in the visible spectrum, with wavelength from $380nm$ to $700nm$. See the figure below (NASA, 2010).

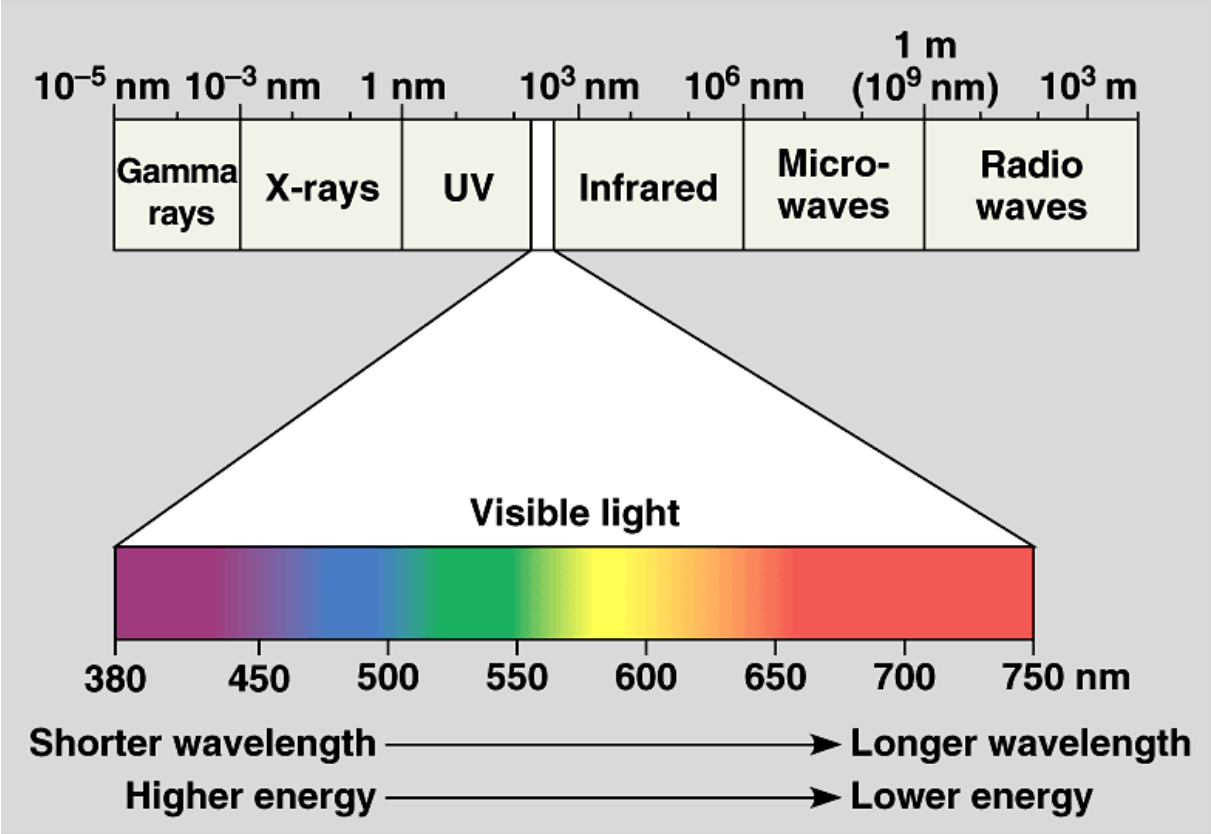

Figure 2: the electromagnetic spectrum, showing different wavelength for different types of radiation .

By using a camera that can "see" beyond what our eyes can see, a thermal camera (infrared camera), a visual representation of the thermal radiation can be obtained. Thermal cameras report a temperature value. Instead of seeing the visible light of an object, the camera estimates the infrared radiation an object is emitting. This is because any temperature above zero kelvin, glows. Our eyes cannot pick up this radiation because the emitted photons are not in our visible range. However, the intensity of radiation (e.g. temperature difference) can be linked to a color, see fig. 10 on page 17. In this figure, a darker color represents colder temperatures, and lighter colors represents hotter temperatures.

Chapter 3: Methodology

3.1. Heat Transfer and Thermal Conductivity

Heat is energy. This energy comes from the net average motion (e.g. translational, rotational, and/or vibrational motion) of the atoms and molecules that make up a medium. For instance, a unit mass of iron with a temperature of 300K will contain atoms with a higher net motion that the same unit mass of iron at temperature 273K. For sake of example, if these two iron specimen were put in direct contact with each other, heat will transfer to the medium with higher energy, to the one with lower energy. In that case, heat transfer is established. Energy will "flow" from the 300K specimen to the 273K specimen. Thus, the definition of heat transfer can be written as

Heat transfer is energy in transit due to a temperature difference (Moran, et al., 2003).

There are different types of modes of heat transfer, however, this paper will focus on heat transfer due to conduction. To compute the amount of heat transferred per unit time, rate equations, such as Fourier's Law (see section 2.2.1.) can be applied.

Thermal conductivity is a material's ability to transmit heat throughout its volume. It is defined as "watts per kelvin-meter", $W \cdot K^{-1} \cdot m^{-1}$ (Snoke, 2009). Different matters have different thermal conductivity. For example, the heating element in a water boiler (kettle) needs to have a high thermal conductivity to transfer heat to the water. However, the plastic handle needs to have a relatively low thermal conductivity to ensure that the device is safe to use. Likewise, workplaces where hot pipes and instruments are present needs to be insulated. See figure 3.

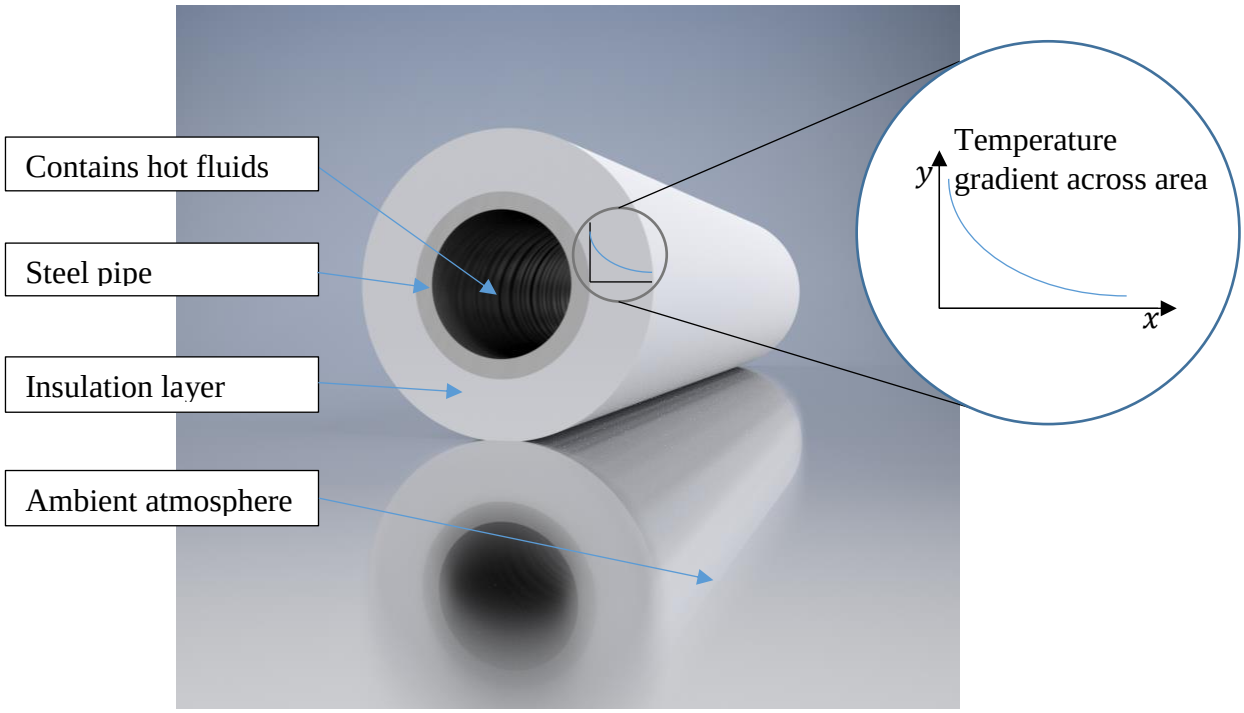

Figure 3: insulated pipe with description of the heat loss through the insulated layer. Rendered in Autodesk Inventor Professional 2017.

As it can be seen in the illustration above, the temperature across the insulated area decreases. One could argue that the temperature of the insulated layer should reach the temperature of the steel pipe when time t is very large. However, because the surrounding atmosphere absorb heat, due to radiation, there will always be a temperature difference. Additionally, the steel pipe will absorb heat faster than the insulated layer. This is not illustrated here.

3.1.1. Fourier's Law

As mentioned in the introduction to this sub-chapter, Fourier's Law (Fourier, 2007 (1822)) can be applied to describe the heat transfer in a spatial direction ($x, y\ and/or\ z$) per unit area perpendicular to the direction of transfer. Further, the heat transfer it proportional to the temperature gradient (Moran, et al., 2003). Fourier's Law, in $x - direction$, and one-dimension, can be seen in equation 13

$$q''_x = -k\frac{dT}{dx} \tag{1}$$

Where

- Fourier's Law, which is also called the heat flux (W/m^2)
- k is the thermal conductivity ($W/m \cdot K$)

- T is time.

The reason to the minus sign is because energy is transferred from media with higher temperature to a lower temperature medium.

3.1.2. Derivation of the heat equation

The derivation of the heat equation is based on the principle of conservation of energy, e.g.

$$\begin{gathered} Rate\ of\ energy\ accumulation \\ = \\ Flow\ of\ energy\ into\ system \\ - \\ Flow\ of\ energy\ out\ of\ system \\ + \\ Rate\ of\ energy\ "generated" \end{gathered} \tag{2}$$

The last term, $Rate\ of\ energy\ "generated"$, describes the thermal energy generated from an external, different source. Examples of such energies can be chemical reactions, nuclear fission, and/or electrical. To simplify the understanding of eq. 2, an infinitesimally small control volume can be drawn, as seen on the figure below.

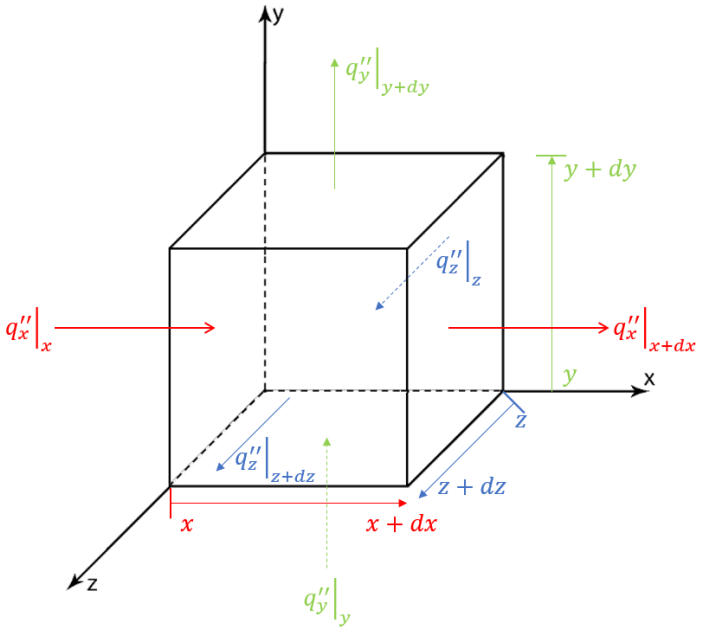

Figure 4: infinitesimally small control volume, in the cartesian space x, y, and z.

As it can be seen in figure 4, dx, dy, and dz represents a very (infinitesimally) small change in direction. For further derivation, the heat flowing into the system, denoted $q''_x|_x$, will be the only direction considered in this explanation. This is because the energy flowing in y, and z direction will be derived in the same manner as the x −direction. Thus, the flow of energy entering the system (in x −direction) is $q''_x|_x$, evaluated at position x, and the energy leaving the system is $q''_x|_{x+dx}$, evaluated at position $x + dx$. To find the relationship between the energy at position x and $x + dx$, e.g. $q''_x|_x \xrightarrow{?} q''_x|_{x+dx}$, the use of a Taylor series expansion could be applied. Looking at the first term in this series, the heat evaluated at position $q''_x|_{x+dx}$ is simply,

$$q''_x|_{x+dx} = q''_x|_x + \frac{\partial q_x}{\partial x} dx \tag{3}$$

The term on the right-hand side is the rate of which energy changes as a function of x multiplied by dx. The figure below shows equation (3). From the first term in the Taylor series, which assumes a linear relationship between the two points, $q''_x|_x$ and $q''_x|_{x+dx}$, figure 5 can be drawn.

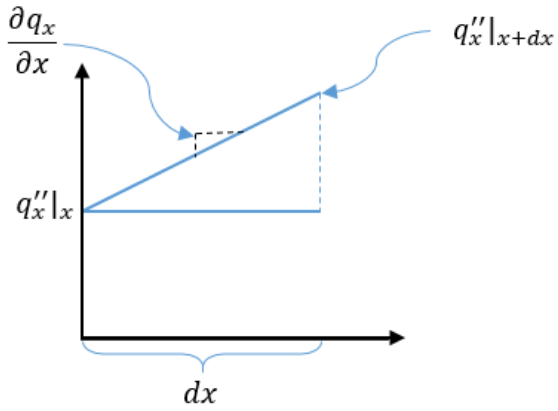

Figure 5: visual representation of equation (3)

The next step would be to look at the net flow of energy into the system. Remember that the net flow of energy, from eq. (2), is the flow of energy into the system, minus flow of energy out of the system. Thus, the net flow of energy is

$$q''_x|_x - q''_x|_{x+dx} = q''_x|_x - \left(q''_x|_x + \frac{\partial q''_x}{\partial x} dx \right) \tag{4}$$

Rearranging eq. (4) to eq. (5)

$$q''_x|_x - q''_x|_{x+dx} = -\frac{\partial q''_x}{\partial x} dx \tag{5}$$

Remember from eq. (2), that $q''_x|_x - q''_x|_{x+dx}$ is

$$Flow\ of\ energy\ into\ system - Flow\ of\ energy\ out\ of\ system$$

Referring to eq. (2), there are two terms left to be described mathematically.

- *The first is the rate of which energy is being generated.*

The generated energy can be described as $\dot{q}$ multiplied by $volume$. Where $\dot{q}$ is the energy per unit volume. For an infinitesimally small control volume (see fig. 2), the volume is $dx \cdot dy \cdot dz$. Thus,

$$Rate\ of\ energy\ "generated"\ = \dot{q} \cdot dx \cdot dy \cdot dz \tag{6}$$

The last term left to describe is

- $Rate\ of\ energy\ accumulated.$

This is the rate of which internal energy increases, or decreases, with time. So,

$$\frac{du}{dt} \cdot \rho \cdot dx \cdot dy \cdot dz \tag{7}$$

Where

- $\rho \cdot dx \cdot dy \cdot dz$ is the mass of the control volume, ρ being the density.

Further, the internal energy, u, is defined as $c_p \cdot T$. Therefore, the rate of which energy is accumulated can be expressed as following

$$Rate\ of\ energy\ accumulated = \rho \cdot C_p \frac{dT}{dt} dx \cdot dy \cdot dz \tag{8}$$

Remember Fourier's Law, shown in eq. (1), $q''_x = -k\frac{dT}{dx}$. This is restricted to a one-dimension system, and since this derivation concern a three-dimensional control volume, eq. (2) needs to be modified. Recall that the energy transfers perpendicular to the direction of transfer.

Additionally, energy flowing in $x - direction$ can only flow through the area $dy \cdot dz$ (Smith, et al., 2013), (Moran, et al., 2003). Therefore, Fourier's Law can be rewritten to

$$q_x'' = -k(dy \cdot dz)\frac{\partial T}{\partial x} \tag{9}$$

A relationship between the flow of energy and the temperature have now been established in eq. (9). This equation can substitute q_x'' in eq. (3), (4), and (5). Add together and cancel out equal terms, the result is the heat equation in $x - direction$ is obtained:

$$\rho c_p \frac{\partial T}{\partial t} = \dot{q} + \frac{\partial}{\partial x}\left(k\frac{\partial T}{\partial x}\right) \tag{10}$$

Apply the same strategy for y, and z −direction, the heat equation for a three-dimensional volume is obtained:

$$\rho c_p \frac{\partial T}{\partial t} = \dot{q} + \frac{\partial}{\partial x}\left(k\frac{\partial T}{\partial x}\right) + \frac{\partial}{\partial y}\left(k\frac{\partial T}{\partial y}\right) + \frac{\partial}{\partial z}\left(k\frac{\partial T}{\partial z}\right) \tag{11}$$

For most cases, there heat generation term, $\dot{q}$, can be neglected. Thus, we end up with the final heat equation used in this paper:

$$\frac{\partial T}{\partial t} = \alpha\left(\frac{\partial^2 T}{\partial x^2} + \frac{\partial^2 T}{\partial y^2} + \frac{\partial^2 T}{\partial z^2}\right) \tag{12}$$

Where

- ρ is the density of the material (kg/m^3)
- c_p is the specific heat capacity $(J/(kg\ K))$
- T is the temperature (K)
- t is time (s)
- $\dot{q}$ is the volumetric energy generation (W/m^3)
- k is the thermal conductivity $(W/m \cdot K)$
- x, y, z is the coordinates of which the temperature is calculated (m)
- α is volumetric heat capacity (see section 3.1.4.).

This is a partial differential equation (PDE), one which currently have no analytical (exact) solution. However, different methods can be applied to solve the equation. This will be done it section 2.3.

3.1.3. Boundary and Initial conditions

To solve the heat equation, the temperatures at the boundaries, and the temperature of the surface (or any position) at time zero of the system, is needed. Refer to fig. 6, the boundary conditions can be applied to all six sides of the cube. In addition, we are no longer dealing with an infinitesimally small control volume. Thus, the convective boundary conditions were applied to this system (Moran, et al., 2003). This can be seen in eq. 13.

$$-k\frac{\partial T_s}{\partial x} = h(T_\infty - T_s) \tag{13}$$

Where

- T_s is the surface temperature, K
- T_∞ is the temperature of the surrounding atmosphere, K
- h is convective heat transfer coefficient, $W/m^2 \cdot K$.

For sake of example, at time $t = 0$, the initial condition will be $T_{initial} = T_s|_{@t=0}$.

3.1.4. Thermal conductivity and heat transfer

There are two important constants that determine the temperature of a body subjected to heat change; the thermal conductivity and the heat transfer. The symbols are k ($W \cdot m^{-1} \cdot K^{-1}$) and H ($W \cdot m^{-2} \cdot K^{-1}$), respectively. The heat transfer coefficient describes the rate of which the heat transfers *to* the body, whereas the thermal conductivity describes the rate the transferred heat dissipates within the body.

The product of ρc, with units $J/m^3 \cdot K$, is often described as the materials ability to store heat (energy), and is called the *volumetric heat capacity* (Moran, et al., 2003). Further, to describe the time a material needs to reach equilibrium temperature (e.g. adapt to ambient atmosphere), the *thermal diffusivity constant*, α can be derived:

$$\alpha = \frac{k}{\rho c} \tag{14}$$

Usually, materials with a large α will absorb heat at a faster rate compared to materials with a small α (Moran, et al., 2003).

3.2. Solution to the Heat equation

As it was shown in sec. 3.1.2., the heat equation is a partial differential equation (PDE), and further, a PDE with no analytical solution. To solve problems with the Heat equation, and other PDEs for that matter, different numerical methods can be applied. One such numerical method is the *Finite Difference Method* (FDM). When the FDM is applied to a continuous PDE, the numerical solution is replaced with a discrete approximation (Recktenwald, 2004). This means that the numerical solution is only known at a finite number of positions (boundary and initial conditions). When FDM is applied to a PDE, the first step would be to divide the physical domain into a finite set of elements, or replace the physical domain with a grid. See fig. 5 on the next page. Here, a two-dimensional plane is divided into a set of finite elements, or nodes. The resolution (number of elements) in this example is $11x11$. Further, the initial condition here is in the middle, and the boundary conditions are on all edges of the plane. This is because the red square indicates hot areas, and blue indicate colder areas.

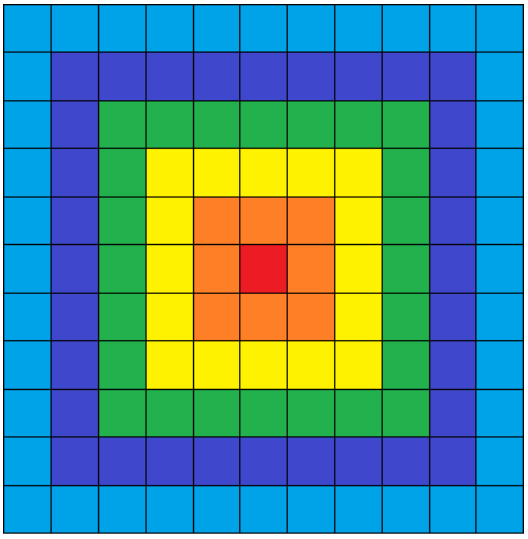

Figure 6: grid applied to a two-dimensional plane, with the heat source (initial condition) in the middle.

At each of the points, the discrete solution is evaluated. There are two important parameters that govern the accuracy of the results, namely Δx and Δt. For sake of example, if the grid in fig. 5 is $11\ cm\ x\ 11cm$, Δx would be 1. Thus, if it was desirable to have double resolution, Δx should be 0.5, and the resulting grid would be $22x22$. Δt, on the other hand, governs the time it takes to go from one position to the next. With lesser time steps (usually around $1\ sec$), more information is gathered in the solution, and thus, a more accurate solution is obtained. For sake

of example, imagine two cameras, one with capture rate of 30 *frames per second* and the other camera having 120 *frames per second*. An identical event recorded with either cameras, the camera with 120 frames per second will contain 4 times as much information as the other camera. Simply put, the same goes for FDM and solution resolution. Naturally, with smaller Δx and Δt, the time required to solve the model increases (computationally heavier).

Further, the discrete solution to a PDE, $\frac{\partial \varphi}{\partial x}$, (at each node) can we shown to be (Recktenwald, 2004)

$$\frac{\partial \varphi}{\partial x} \approx \frac{\varphi_{i+1} - \varphi_i}{\Delta x} \tag{15}$$

Where

- $\varphi(x,t)$ is the true (continuous) solution
- $\varphi(x_i, t_m)$ is the continuous solution calculated at each node in the mesh
- φ_i^m is the approximated numerical solution given by solving the FEM equation

To help the understanding of eq. 15, and the derivation of the approximation of the heat equation, a general grid can be drawn:

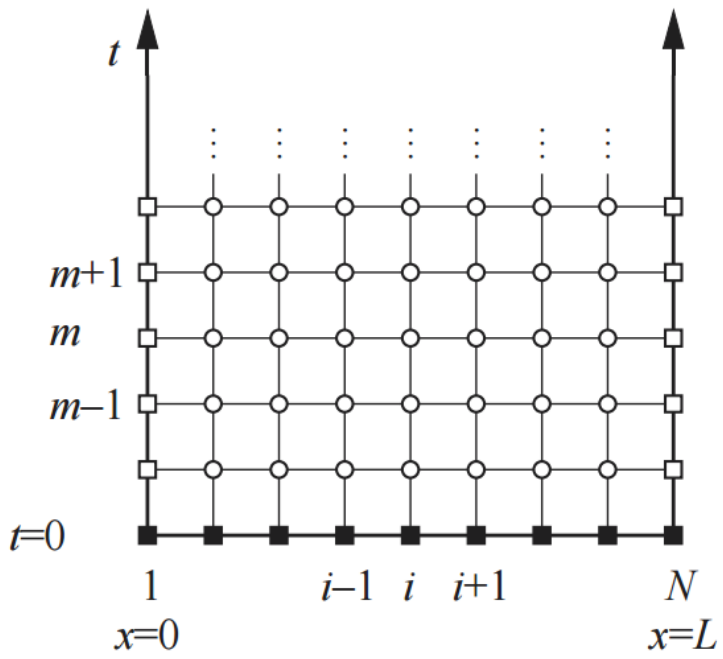

Figure 7: general grid for a one-dimensional Heat equation problem (Recktenwald, 2004)

In figure 7, the initial condition is displayed as solid squares, and the non-solids squares indicate the boundary conditions. i denote the grid position, m denote the time. The work done by Recktenwald (2004) introduces the FDM. The following section is thus purely based on his work. To obtain the finite difference approximation to the Heat equation, the first step is to consider a Taylor series expansion $\varphi(x)$ about point x_i (Recktenwald, 2004)

$$\varphi(x_i + \delta_x) = \varphi(x) + \delta x \frac{\partial \varphi}{\partial x}\bigg|_{x_i} + \frac{\delta x^2}{2}\frac{\partial^2 \varphi}{\partial x^2}\bigg|_{x_i} + \frac{\delta x^3}{3!}\frac{\partial^3 \varphi}{\partial x^3}\bigg|_{x_i} + \cdots \tag{16}$$

Where δ_x is the change of x relative to x_i, thus δ_x can be assumed to be Δx and consider the value of φ at position x_{i+1} on the mesh line, and solve for $\frac{\partial \varphi}{\partial x}\Big|_{x_i}$. Thus, eq. 16 can be rewritten to eq. 17

$$\frac{\partial \varphi}{\partial x}\bigg|_{x_i} \approx \frac{\varphi_{i+1} - \varphi_i}{\Delta x} - \frac{\Delta x}{2}\frac{\partial^2 \varphi}{\partial x^2}\bigg|_{x_i} - \frac{\Delta x}{3!}\frac{\partial^3 \varphi}{\partial x^3}\bigg|_{x_i} + \cdots \tag{17}$$

Notice the approximated approach, and that the first term on the right side is the approximated solution to $\varphi_{i+1} \approx \varphi(x_i + \Delta x)$ and $\varphi(x_i) \approx \varphi_{i+1}$. Since this derivation deals with a Taylor series expansion, the mean value theorem can be applied to replace the higher order derivatives (Recktenwald, 2004). Simply put, the mean value theorem states that in a function $f(x)$ is a differentiable on the open interval (a, b), and continuous on the closed interval $[a, b]$ there is a point, c, in (a, b), such that $f'(c) = \frac{f(b)-f(a)}{b-a}$ (Weisstein, 2011). Thus,

$$\frac{\partial \varphi}{\partial x}\bigg|_{\xi} = \frac{\varphi_{i+1} - \varphi_i}{\Delta x} + \frac{\Delta x}{2}\frac{\partial^2 \varphi}{\partial x^2}\bigg|_{\xi} \tag{18}$$

The term on the far-right side is called the *truncation error*. This is an error that is the result of using the mean value theorem, and this error is not known. However, the truncation error term contains the parameter Δx, and is the only parameter that determines the error. This is a parameter that can be changed by the user, and thus, this error term is usually neglected. Therefore,

$$\frac{\partial \varphi}{\partial x}\bigg|_{x_i} \approx \frac{\varphi_{i+1} - \varphi_i}{\Delta x} \tag{19}$$

If the simulated solution is clearly unstable, the user should decrease the timestep, or lower Δx. Therefore, the argument of removing the truncation error is thus validated. Eq. 19 is called the *forward difference,* for the approximation, since it contains x_i and x_{i+1}. The backwards difference, however is

$$\left.\frac{\partial \varphi}{\partial x}\right|_{x_i} = \frac{\varphi_i - \varphi_{i-1}}{\Delta x} \tag{20}$$

The last form of the approximation is called the *central difference.* This form is derived by writing the Taylor series expansion for φ_{i+1} and φ_{i-1} (Recktenwald, 2004). The derivation follows the same route as the derivation of eq. 16 and 17, so,

$$\left.\frac{\partial \varphi}{\partial x}\right| = \frac{\varphi_{i+1} - \varphi_{i-1}}{2\Delta x} \tag{21}$$

By applying the same strategy, and further manipulation of the Taylor series in eq. 16, second order PDE can be approximated (Recktenwald, 2004):

$$\varphi_{i+1} + \varphi_{i-1} = 2\varphi_i + (\partial\delta)^2 \left.\frac{\partial^2 \varphi}{\partial x^2}\right|_{x_i} \tag{22}$$

Solving for $\frac{\partial^2 \varphi}{\partial x^2}$ yields

$$\left.\frac{\partial^2 \varphi}{\partial x^2}\right|_{x_i} = \frac{\varphi_{i+1} - 2\varphi_i + \varphi_{i-1}}{\Delta x^2} \tag{23}$$

In this section, the heat equation was estimated, by first describing a first degree approach, and then a second degree approach.

3.2.1. Forward-Time Central-Space (FTCS)

Eq. 20 to eq. 23 is are different types of finite difference approximation. This approximation can be applied to eq. 12, the Heat equation in $x - direction$. However, the Heat equation will be written in a manner called the *forward difference.* By using this technique, the temperature at each node can be estimated *one timestep* forward, e.g.

$$\frac{\varphi_i^{m+1} - \varphi_i^m}{\Delta t} \tag{24}$$

Remember from fig. 8 that m denotes timestep. With this statement in mind, eq. 23 can be applied to the Heat equation in $x - direction$

$$\frac{\varphi_i^{m+1} - \varphi_i^m}{\Delta t} = \frac{\varphi_{i+1} - 2\varphi_i + \varphi_{i-1}}{\Delta x^2} \tag{25}$$

Substitute appropriate term (according to the heat equation):

$$T_i^{t+1} = T_i^t + \alpha \left(\frac{T_{i+1}^t - 2T_i^t + T_{i-1}}{(\Delta x)^2} \right) \Delta t \tag{26}$$

Where

- T is the temperature
- i is the space (grid) coordinate of which the temperature is calculated
- t is the time
- α is volumetric heat capacity (see section 3.1.4.).

Remember that this equation (eq. 26) only is applicable for a one-dimensional problem. To bring this approximation to a three-dimensional problem, the space coordinates j and k is introduced. Thus, the final FTCS FEM can be derived (Rashid, et al., 2016), (Recktenwald, 2004):

$$\begin{aligned} T_{i,j,k}^{t+1} = T_i^t &+ \alpha\left(\frac{T_{i+1}^t - 2T_i^t + T_{i-1}}{(\Delta x)^2}\right)\Delta t \\ &+ \alpha\left(\frac{T_{j+1}^t - 2T_j^t + T_{j-1}}{(\Delta x)^2}\right)\Delta t \\ &+ \alpha\left(\frac{T_{k+1}^t - 2T_k^t + T_{k-1}}{(\Delta x)^2}\right)\Delta t \end{aligned} \tag{27}$$

The advantages of using FTCS is that the values of φ_i^{m+1}, or T_i^{t+1}, can be updated independently of each other (Recktenwald, 2004).

3.3. IR Imaging and Setup

The method that was elected to determine the heat transfer and thermal conductivity was developed and described in (Rashid, et al., 2016), and the basics steps in shown in the flow chart below.

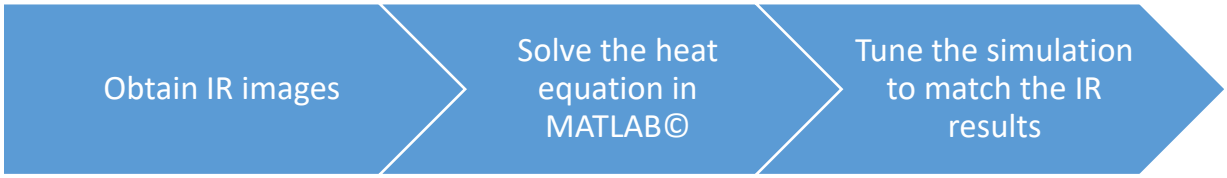

Figure 8: flow chart of determination of heat transfer coefficient, H, and thermal conductivity, K.

The experiment used a FLIR T1030Sc camera to capture the infrared radiation of the polyurethane sample. The sample was oriented normal to the camera lens. The data was gathered inside the software. The schematic figure of the setup can be seen in figure 9 below.

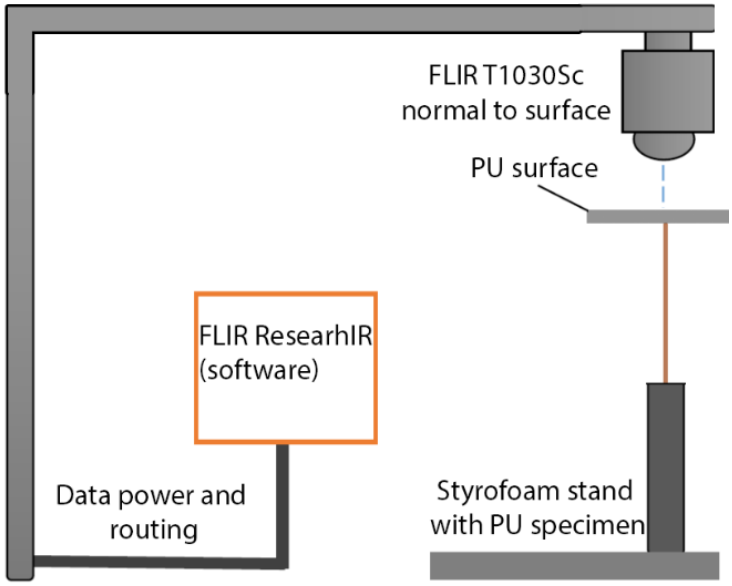

Figure 9: schematic setup of IR capture

From figure 8, there are only three steps. There are, however, multiple small, but equally important steps. Before the IR images can be captured, the sample needs to be at a different temperature than the surrounding atmosphere. There are several ways this could be done. However, to obtain the temperature difference for this experiment, the specimen was put in a freezer over-night (approximately 24hrs.). The freezer can hold temperatures of $-20°C$ to $-30°C$. The surrounding atmosphere (the location of where the IR images would be captured) was a steady $24°C$. With a temperature difference between the sample and the atmosphere was established, capturing of the IR signatures could be done. Within the software to the IR camera, the sampling rate was set $2Hz$. That means, at every half second the software would capture the IR signature of the specimen. After about 7 minutes, the entire polyurethane specimen had reached $0°C$, and the recording was stopped. The next step would be to extract the temperature data of the specimen.

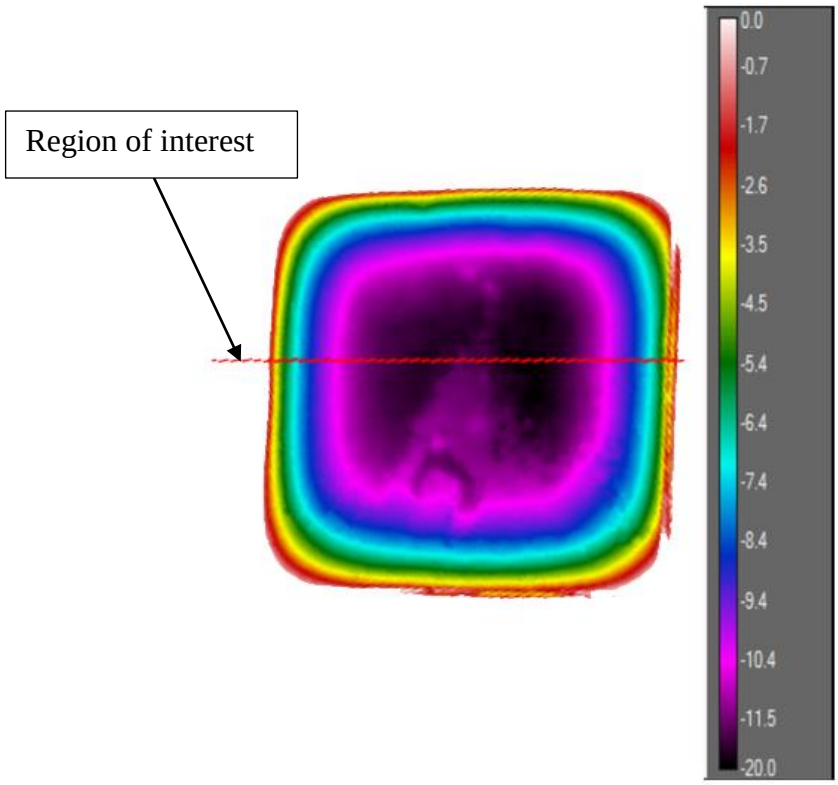

Figure 10: FLIR capture and region of interests where the temperature was read.

The red line shown in fig. 10, called the *Region of interest,* or *ROI* for short, and is the location of where the temperature profile for the anti-abrasion specimen was captured. The ROI was at constant position. This was to ensure that the captured temperature was at the same location on the specimen, throughout all the time. For the anti-abrasion sample, there was captured 9 different temperature profiles, and for the anti-seepage it was captured 13 temperature profiles. The reason for the different captures was because the two different samples reached zero degrees C at different rates, due to size difference and different thermal properties (see section 4.). The next step would be to import the temperature profiles into MATLAB© for further processing. In figure 8, the ROI is outside of the specimen. To obtain results where only the temperature of the specimen, not the air surrounding it, would be visible when comparing simulated data and experimental data. To manage this, the plotted experimental data was cut off at the edges of the specimens. When the experimental data and the simulated data was initially compared, without altering the two constants H and k, it was naturally a significant difference occurred. However, after tinkering with the constants, the results were obtained.

In preparation for the tests, the specimens were cut into $50x50mm$ cubes and labeled A, B and C. The corners of the materials were numbered 1 to 4, and it the center was labeled 5. The numbers indicated the point if which the measurements of the thickness. This was done for both

the anti-seepage and the anti-abrasion materials. The results of these measurements, in millimeters, can be viewed in table 2 below.

Table 2: measurements of thickness (mm)

	Anti-abrasion		
	A	B	C
1	7,15	8,87	10,83
2	8,52	10,35	10,76
3	9,7	8,36	7,9
4	10,025	8,61	8,65
5	10,73	10,73	10,05

	Anti-seepage		
	A	B	C
1	5,25	5,5	5,45
2	5,41	5,65	5,52
3	5,45	6,27	6,4
4	5,38	5,34	6,28
5	5,98	5,45	5,78

When measuring the rate of which heat travels through a material, the thickness of the tested specimen is important. In addition to the length, width and thickness, the masses were measured. The mass for the anti-abrasion material was $16g$ and for anti-seepage was $13g$. Thus, the density of anti-abrasion is

- $\rho_{anti-abrasion} = 1283kg/m^3$

and for anti-seepage

- $\rho_{anti-seepage} = 1150kg/m^3$.

3.4. Heat Equation in MATLAB©

The solution the FDM approximated equations that was obtained in sections 2.2., was solved in MATLAB®. To write the FTCS FEM only two basic code loops are necessary. One loop loops over Δt, while the other loop loops over Δx. However, since this problem deals with a three-dimensional problem, unique loops for each spatial domain (x, y, z or i, j, k) needs to be constructed. The code was developed by Hassan Abbas Khawaja, however, the author of the paper fine-tuned the parameters in the code. The step-by-step approach to simulate the temperature in the two materials anti-seepage and anti-abrasion is identical, with the three unique parameters *heat transfer*, *thermal conductivity* and *density* being different. In table 3 below, it can be shown that there are only 4 basic steps to solve the FEM Heat equation.

Table 3: the logic steps to solve the FTCS FEM

Step	Event	Description
1	Define parameters	$\Delta t, \Delta x$ the spatial domains $spacex, spacey, spacez$ k and h ρ and c The discretized space Initial temperature and initial conditions.
2	Create a matrix, T, containing zeroes	The matrix T, initially only contains zeros. However, in step 3, the temperature at each node will replace the zeroes with the simulated temperature.
3	Create loops	This step is what solves the FTCS FEM. In these loops both the $\Delta t, \Delta x$ are contained. In addition to these, the boundary conditions are included.
4	Plot experimental data vs. simulated data	The last step plots the experimental data and compares it with the simulated data from step 1 to 3.

Chapter 4: Results and Discussion

4.1. Thermal Imaging

To determine the thermal properties of polyurethane, the samples was taken out of the freezer and put in room temperature. The IR capture software was used to measure the established temperature gradient of the two polyurethane specimens. After reviewing the results and comparing it with the simulation, k and h was matched to fit the experimental data.

Table 4: the coefficient of Heat transfer for anti-abrasion, and anti-seepage polyurethane

Coefficient of heat transfer (h)	Value $(W/(m^2 \cdot K)$
Anti-seepage	19.95
Anti-abrasion	5.2

Applying the same logic to estimate the thermal conductivity, k:

Table 5: the coefficient of Heat transfer for anti-abrasion, and anti-seepage polyurethane

Coefficient of thermal conductivity (k)	Value $(W/(m \cdot K)$
Anti-seepage	25.0
Anti-abrasion	11.0

The simulated thermal image, as well as the captured thermal image from the ReseachIR® software are displayed in the figures on the next page.

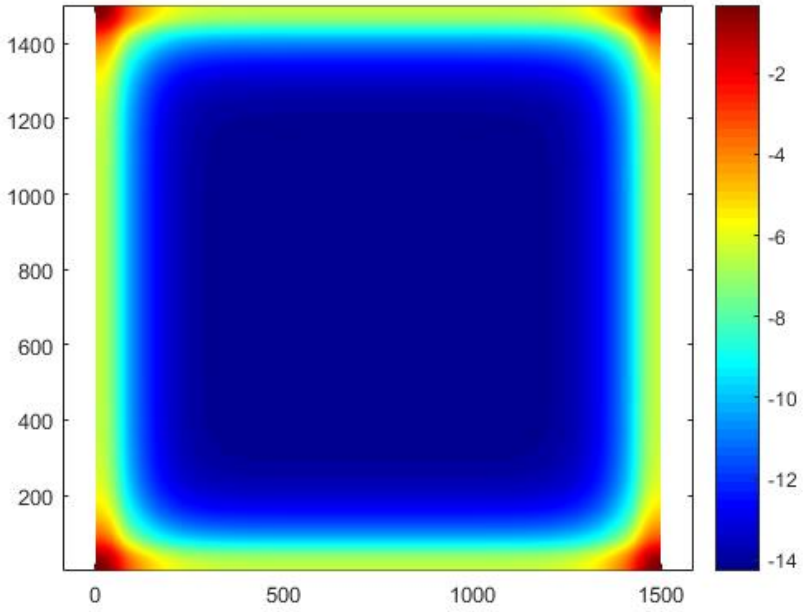

Figure 11: the variation of temperature in the anti-seepage polyurethane after 100 seconds

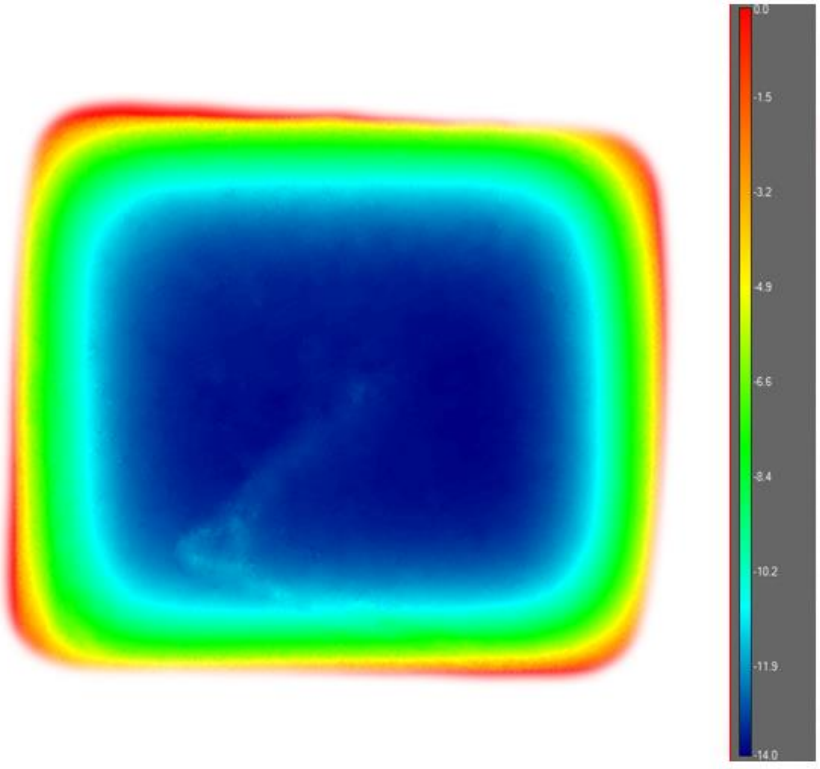

Figure 12: IR capture (FLIR T1030Sc) of anti-seepage at the same time as the simulation.

The following two figures shows the plotted temperature in the middle of both materials, one as a function of time (fig. 13 and 15), and one as a function of position and time (fig. 14 and 16).

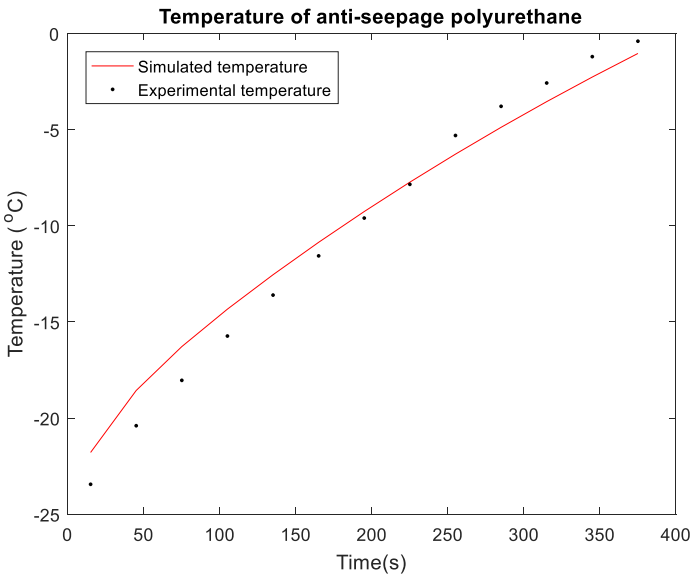

Figure 13: temperature in anti-seepage polyurethane as a function of time.

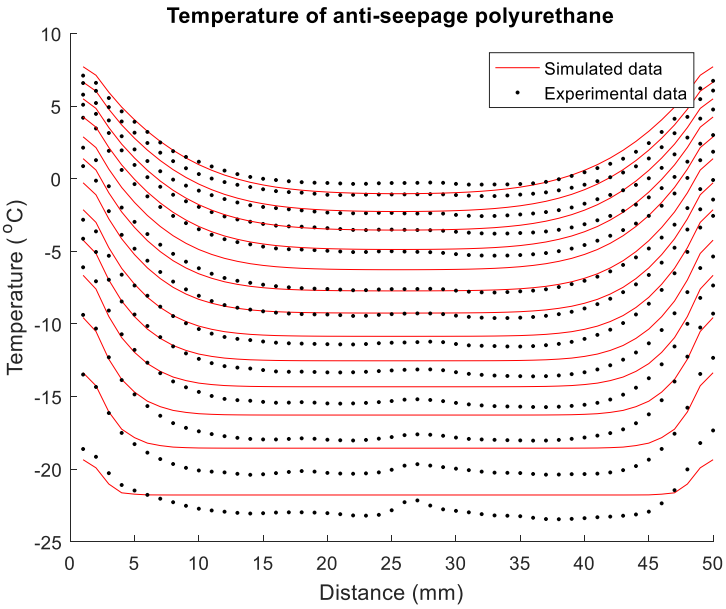

Figure 14: temperature in anti-seepage polyurethane as a function of position.

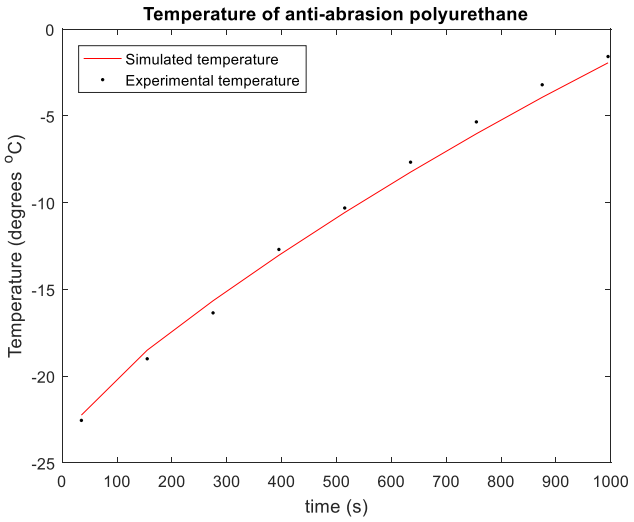

Figure 15: temperature in anti-abrasion polyurethane as a function of time.

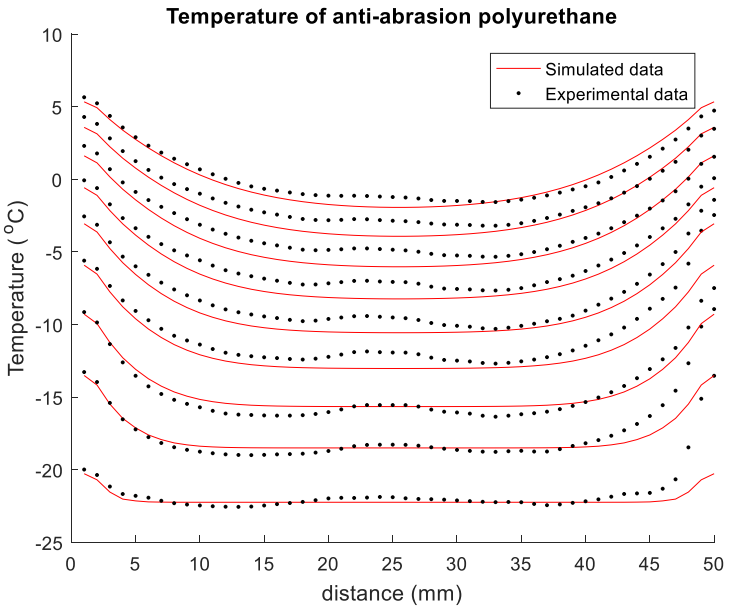

Figure 16: temperature in anti-abrasion polyurethane as a function of position.

The results reveal that the heat transfer coefficient for anti-abrasion polyurethane is almost four times that for anti-seepage polyurethane, and the thermal conductivity for the respective have a difference of a factor of two.

Chapter 5: Conclusions and Future work

5.1. Conclusions

By applying a finite difference approach to the heat equation, and using IR-capture technology, the two thermal constants, heat transfer coefficient and the thermal conductivity coefficient was estimated for anti-abrasion and anti-seepage polyurethane. These constants were found for the two materials *anti-abrasion polyurethane* and *anti-seepage polyurethane.* However, from fig. 14 and 16, it appears to be a difference in the two compared temperatures. This is because the samples that were tested were non-uniform. This non-uniformity can be because there are air bubbles from the production of the polyurethane. The computational load required to model air bubbles are unnecessary high, therefore this difference will be present in the solution.

5.2. Future Work

Based on the results and methods that have been described, a proposition of future work is presented below

- How this material can be utilized in the Arctic region with regard to coating of hot pipes
- More sophisticated methods to obtain a more accurate representation of the thermal properties

Bibliography

Bayer, O., 1947. Das Di-Isocyanat-Polyadditionsverfahren (Polyurethane). *Angewandte Chemie,* 59(9), pp. 257 - 272.

Dulong, P. L. & Petit, A. T., 1819. Recherches sur quelques points importants de la Théorie de la Chaleur. *Annales de Chimie et de Physique,* Issue 10, pp. 395 - 413.

Engineering Toolbox, 2017. *Engineerig Toolbox.* [Online]
Available at: http://www.engineeringtoolbox.com/thermal-conductivity-d_429.html
[Accessed 2 5 2017].

Fourier, J., 2007 (1822). *The Analytical Theory of Heat.* s.l.:Cosimo Classics.

Gebhart, B., 1993. *Heat conduction and mass diffusion.* 1st ed. New York: McGraw-Hill.

Gum, W., Wolfram, R. & Ulrich, H., 1992. *Reaction Polymers.* New York: Oxford University Press.

Harrington, R. & Hock, K., 1991. *Flexible Polyurethane Foams.* Midland: The Dow Chemical Company.

Moran, M. J., Shaprio, H. N., Munson, B. R. & DeWitt, D. P., 2003. *Introduction to Thermal systems Engineering. Thermodynamics, Fluid Mechanics, and Heat Transfer.* 1st ed. s.l.:Wiley & Sons, Inc..

NASA, 2010. *NASA.* [Online]
Available at: https://science.hq.nasa.gov/kids/imagers/ems/visible.html
[Accessed 28 4 2017].

Nave, R., 2016. *hyperphysics.phy-astr.gsu.* [Online]
Available at: http://hyperphysics.phy-astr.gsu.edu/hbase/thermo/Dulong.html#c1
[Accessed 11 02 2017].

Prisacariu, C., 2011. *Polyurethane Elastomers. From Morphology to Mechanical Aspects.* Wien: Springer.

Rashid, T., Khawaja, H. & Edvardsen, K., 2016. Determination of Thermal Properties of Fresh Water and Sea Water Ice using Multiphysics Analysis. *International Journal of Multiphysics,* 10(3), pp. 277 - 290.

Recktenwald, G. W., 2004. *Finite-Difference Approximations to the Heat Equation,* s.l.: s.n.

Seymore, R. B. & Kauffman, G. B., 1992. Polyurethanes: A class of modern versatile materials. *Journal of Chemical Education,* 69(11), p. 909.

Smith, R., Inomata, H. & Peters, C., 2013. Chapter 8 – Heat Transfer and Finite-Difference Methods. *Supercritical Fluid Science and Technology,* Volume 4, pp. 557-615.

Snoke, D. W., 2009. *Solid State Physics: Essential Concepts.* 1st ed. s.l.:Addison-Wesley.

Soto, M., Sebastián, R. M. & Marquet, J., 2014. Photochemical Activation of Extremely Weak Nucleophiles: Highly Fluorinated Urethanes and Polyurethanes from Polyfluoro Alcohols. *The Journal of Organic Chemistry,* 11(79), pp. 5019 - 5027.

Weisstein, E. W., 2011. *Mean-Value Theorem.* [Online]
Available at: http://mathworld.wolfram.com/Mean-ValueTheorem.html
[Accessed 15 03 2017].

Woods, G., 1990. *The ICI Polyurethanes Book.* New York: John Wiley & Sons.

Zhiheng, S., 2015. *The SK one component polyurea and its application in hydraulic and hydropower project structures.* Beijing, China Institute of Water Resources & Hydropower Research.

Özisik, N. M., 1993. *Heat Conduction.* 2nd ed. New York: John Wiley & Sons, Inc..

Appendix I

The MATLAB© code that was used to determine h and k for Anti-seepage polyurethane is displayed below

Polyurethane Anti-Abrasion heat simulation

```
clear all
close all

delta_t = 1;                          % time step (1 sec)
time_steps = 6000/delta_t;            % timesteps
n = 5;
m = [10.83 10.76 7.9 8.65 10.05];  % actual thickness of C specimen (anti-abrasion)
mm
%i = size(m);
q = int32(mean(m)/10);                % average thickness of C specimen (anti-abrasion)
cm, and then rouning up to nearest integer



spacex = 5*n;                         % array size (in cm)
spacey = 5*n;
spacez = q*n;

T = zeros(spacex, spacey, spacez, time_steps);

                                    % Constants (multiple of hundreds to convert to cm)
k = 0.11*100;                       % conductivity constant of polyurethane (W/(m.K)),
varies                    slightly                    with                    temperature
(http://www.efunda.com/materials/polymers/properties/polymer_datasheet.cfm?MajorID=
pu&MinorID=1)
h = 5.2;                             % convective (overall) heat transfer coefficient
of air (W/(m2.K)), varies with conditions (CAUTION: tune it later)

r = 950/1000000;                  % density (Kg/m3)(current value, 1286 is calculated)
(1030       -       1500),       varies       slightly       with       temperature
(http://www.efunda.com/materials/polymers/properties/polymer_datasheet.cfm?MajorID=
pu&MinorID=1)
c = 1800*10000;                       % heat capacity polyurethane (J/Kg/K), varies
slightly with temperature (http://www.engineeringtoolbox.com/specific-heat-capacity-
d_391.html)
Dx = 1/n;                             % discretisised space (in cm)
Dy = Dx;
```

```
Dz = Dx;
To = 273+23;                        % Room Temperature in K



% Initial conditions
T(:,:,:,1) = 273-24;                % Temperature of polyurethane when taken out of
freezer in K




tic
% Solution
for t = 2 : time_steps


sx = 2 : spacex-1;
sy = 2 : spacey-1;
sz = 2 : spacez-1;


T(sx, sy, sz, t) = T(sx, sy, sz, t-1) ...
    + k/r/c * (T(sx+1, sy, sz, t-1) - 2*T(sx, sy, sz, t-1) + T(sx-1, sy, sz, t-1)) /
(Dx*Dx) * delta_t ...
    + k/r/c * (T(sx, sy+1, sz, t-1) - 2*T(sx, sy, sz, t-1) + T(sx, sy-1, sz, t-1)) /
(Dy*Dy) * delta_t ...
    + k/r/c * (T(sx, sy, sz+1, t-1) - 2*T(sx, sy, sz, t-1) + T(sx, sy, sz-1, t-1)) /
(Dz*Dz) * delta_t;

% Boundary conditions

% 8 Corner Cells
T(1,1,1,t) = T(1,1,1,t-1)...
    + (h/r/c/Dx * (To - T(1,1,1,t-1)) + k/r/c/Dx/Dx * (T(2,1,1,t-1) - T(1,1,1,t-
1)))*delta_t ...
    + (h/r/c/Dy * (To - T(1,1,1,t-1)) + k/r/c/Dy/Dy * (T(1,2,1,t-1) - T(1,1,1,t-
1)))*delta_t ...
    + (h/r/c/Dz * (To - T(1,1,1,t-1)) + k/r/c/Dz/Dz * (T(1,1,2,t-1) - T(1,1,1,t-
1)))*delta_t;



T(spacex,1,1,t) = T(spacex,1,1,t-1)...
```

```
    - (-h/r/c/Dx * (To - T(spacex,1,1,t-1)) + k/r/c/Dx/Dx * (T(spacex,1,1,t-1) -
T(spacex-1,1,1,t-1)))*delta_t ...
    + (h/r/c/Dy * (To - T(spacex,1,1,t-1)) + k/r/c/Dy/Dy * (T(spacex,2,1,t-1) -
T(spacex,1,1,t-1)))*delta_t ...
    + (h/r/c/Dz * (To - T(spacex,1,1,t-1)) + k/r/c/Dz/Dz * (T(spacex,1,2,t-1) -
T(spacex,1,1,t-1)))*delta_t;



T(1,spacey,1,t) = T(1,spacey,1,t-1)...
    + (h/r/c/Dx * (To - T(1,spacey,1,t-1)) + k/r/c/Dx/Dx * (T(2,spacey,1,t-1) -
T(1,spacey,1,t-1)))*delta_t ...
    - (-h/r/c/Dy * (To - T(1,spacey,1,t-1)) + k/r/c/Dy/Dy * (T(1,spacey,1,t-1) -
T(1,spacey-1,1,t-1)))*delta_t ...
    + (h/r/c/Dz * (To - T(1,spacey,1,t-1)) + k/r/c/Dz/Dz * (T(1,spacey,2,t-1) -
T(1,spacey,1,t-1)))*delta_t;



T(spacex,spacey,1,t) = T(spacex,spacey,1,t-1)...
    - (-h/r/c/Dx * (To - T(spacex,spacey,1,t-1)) + k/r/c/Dx/Dx * (T(spacex,spacey,1,t-
1) - T(spacex-1,spacey,1,t-1)))*delta_t ...
    - (-h/r/c/Dy * (To - T(spacex,spacey,1,t-1)) + k/r/c/Dy/Dy * (T(spacex,spacey,1,t-
1) - T(spacex,spacey-1,1,t-1)))*delta_t ...
    + (h/r/c/Dz * (To - T(spacex,spacey,1,t-1)) + k/r/c/Dz/Dz * (T(spacex,spacey,2,t-
1) - T(spacex,spacey,1,t-1)))*delta_t;



T(1,1,spacez,t) = T(1,1,spacez,t-1)...
    + (h/r/c/Dx * (To - T(1,1,spacez,t-1)) + k/r/c/Dx/Dx * (T(2,1,spacez,t-1) -
T(1,1,spacez,t-1)))*delta_t ...
    + (h/r/c/Dy * (To - T(1,1,spacez,t-1)) + k/r/c/Dy/Dy * (T(1,2,spacez,t-1) -
T(1,1,spacez,t-1)))*delta_t ...
    - (-h/r/c/Dz * (To - T(1,1,spacez,t-1)) + k/r/c/Dz/Dz * (T(1,1,spacez,t-1) -
T(1,1,spacez-1,t-1)))*delta_t;



T(spacex,1,spacez,t) = T(spacex,1,spacez,t-1)...
    - (-h/r/c/Dx * (To - T(spacex,1,spacez,t-1)) + k/r/c/Dx/Dx * (T(spacex,1,spacez,t-
1) - T(spacex-1,1,spacez,t-1)))*delta_t ...
    + (h/r/c/Dy * (To - T(spacex,1,spacez,t-1)) + k/r/c/Dy/Dy * (T(spacex,2,spacez,t-
1) - T(spacex,1,spacez,t-1)))*delta_t ...
    - (-h/r/c/Dz * (To - T(spacex,1,spacez,t-1)) + k/r/c/Dz/Dz * (T(spacex,1,spacez,t-
1) - T(spacex,1,spacez-1,t-1)))*delta_t;
```

```
T(1,spacey,spacez,t) = T(1,spacey,spacez,t-1)...
    + (h/r/c/Dx * (To - T(1,spacey,spacez,t-1)) + k/r/c/Dx/Dx * (T(2,spacey,spacez,t-
1) - T(1,spacey,spacez,t-1)))*delta_t ...
    - (-h/r/c/Dy * (To - T(1,spacey,spacez,t-1)) + k/r/c/Dy/Dy * (T(1,spacey,spacez,t-
1) - T(1,spacey-1,spacez,t-1)))*delta_t ...
    - (-h/r/c/Dz * (To - T(1,spacey,spacez,t-1)) + k/r/c/Dz/Dz * (T(1,spacey,spacez,t-
1) - T(1,spacey,spacez-1,t-1)))*delta_t;



T(spacex,spacey,spacez,t) = T(spacex,spacey,spacez,t-1)...
    -   (-h/r/c/Dx   *   (To   -   T(spacex,spacey,spacez,t-1))   +   k/r/c/Dx/Dx   *
(T(spacex,spacey,spacez,t-1) - T(spacex-1,spacey,spacez,t-1)))*delta_t ...
    -   (-h/r/c/Dy   *   (To   -   T(spacex,spacey,spacez,t-1))   +   k/r/c/Dy/Dy   *
(T(spacex,spacey,spacez,t-1) - T(spacex,spacey-1,spacez,t-1)))*delta_t ...
    -   (-h/r/c/Dz   *   (To   -   T(spacex,spacey,spacez,t-1))   +   k/r/c/Dz/Dz   *
(T(spacex,spacey,spacez,t-1) - T(spacex,spacey,spacez-1,t-1)))*delta_t;

%12 edges

% sx = 2 : spacex-1;

T(sx,1,1,t) = T(sx,1,1,t-1) ...
    + k/r/c * (T(sx+1, 1, 1, t-1) - 2*T(sx, 1, 1, t-1) + T(sx-1, 1, 1, t-1)) / (Dx*Dx)
* delta_t ...
    + (h/r/c/Dy * (To - T(sx,1,1,t-1)) + k/r/c/Dy/Dy * (T(sx,2,1,t-1) - T(sx,1,1,t-
1)))*delta_t ...
    + (h/r/c/Dz * (To - T(sx,1,1,t-1)) + k/r/c/Dz/Dz * (T(sx,1,2,t-1) - T(sx,1,1,t-
1)))*delta_t;

T(sx,spacey,1,t) = T(sx,spacey,1,t-1)...
    + k/r/c * (T(sx+1, spacey, 1, t-1) - 2*T(sx, spacey, 1, t-1) + T(sx-1, spacey, 1,
t-1)) / (Dx*Dx) * delta_t ...
    - (-h/r/c/Dy * (To - T(sx,spacey,1,t-1)) + k/r/c/Dy/Dy * (T(sx,spacey,1,t-1) -
T(sx,spacey-1,1,t-1)))*delta_t ...
    + (h/r/c/Dz * (To - T(sx,spacey,1,t-1)) + k/r/c/Dz/Dz * (T(sx,spacey,2,t-1) -
T(sx,spacey,1,t-1)))*delta_t;

T(sx,1,spacez,t) = T(sx,1,spacez,t-1)...
    + k/r/c * (T(sx+1, 1,spacez, t-1) - 2*T(sx, 1,spacez, t-1) + T(sx-1, 1,spacez, t-
1)) / (Dx*Dx) * delta_t ...
    + (h/r/c/Dy * (To - T(sx,1,spacez,t-1)) + k/r/c/Dy/Dy * (T(sx,2,spacez,t-1) -
T(sx,1,spacez,t-1)))*delta_t ...
```

```
    - (-h/r/c/Dz * (To - T(sx,1,spacez,t-1)) + k/r/c/Dz/Dz * (T(sx,1,spacez,t-1) -
T(sx,1,spacez-1,t-1)))*delta_t;

T(sx,spacey,spacez,t)= T(sx,spacey,spacez,t-1)...
    + k/r/c * (T(sx+1, spacey,spacez, t-1) - 2*T(sx, spacey,spacez, t-1) + T(sx-1,
spacey,spacez, t-1)) / (Dx*Dx) * delta_t ...
    -   (-h/r/c/Dy   *   (To   -   T(sx,spacey,spacez,t-1))   +   k/r/c/Dy/Dy   *
(T(sx,spacey,spacez,t-1) - T(sx,spacey-1,spacez,t-1)))*delta_t ...
    -   (-h/r/c/Dz   *   (To   -   T(sx,spacey,spacez,t-1))   +   k/r/c/Dz/Dz   *
(T(sx,spacey,spacez,t-1) - T(sx,spacey,spacez-1,t-1)))*delta_t;

% sy = 2 : spacey-1

T(1,sy,1,t) = T(1,sy,1,t-1)...
    + (h/r/c/Dx * (To - T(1,sy,1,t-1)) + k/r/c/Dx/Dx * (T(2,sy,1,t-1) - T(1,sy,1,t-
1)))*delta_t ...
    + k/r/c * (T(1, sy+1, 1, t-1) - 2*T(1, sy, 1, t-1) + T(1, sy-1, 1, t-1)) / (Dy*Dy)
* delta_t ...
    + (h/r/c/Dz * (To - T(1,sy,1,t-1)) + k/r/c/Dz/Dz * (T(1,sy,2,t-1) - T(1,sy,1,t-
1)))*delta_t;

T(spacex,sy,1,t) = T(spacex,sy,1,t-1)...
    - (-h/r/c/Dx * (To - T(spacex,sy,1,t-1)) + k/r/c/Dx/Dx * (T(spacex,sy,1,t-1) -
T(spacex-1,sy,1,t-1)))*delta_t ...
    + k/r/c * (T(spacex, sy+1, 1, t-1) - 2*T(spacex, sy, 1, t-1) + T(spacex, sy-1, 1,
t-1)) / (Dy*Dy) * delta_t ...
    + (h/r/c/Dz * (To - T(spacex,sy,1,t-1)) + k/r/c/Dz/Dz * (T(spacex,sy,2,t-1) -
T(spacex,sy,1,t-1)))*delta_t;

T(1,sy,spacez,t) = T(1,sy,spacez,t-1)...
    + (h/r/c/Dx * (To - T(1,sy,spacez,t-1)) + k/r/c/Dx/Dx * (T(2,sy,spacez,t-1) -
T(1,sy,spacez,t-1)))*delta_t ...
    + k/r/c * (T(1, sy+1, spacez, t-1) - 2*T(1, sy, spacez, t-1) + T(1, sy-1, spacez,
t-1)) / (Dy*Dy) * delta_t ...
    - (-h/r/c/Dz * (To - T(1,sy,spacez,t-1)) + k/r/c/Dz/Dz * (T(1,sy,spacez,t-1) -
T(1,sy,spacez-1,t-1)))*delta_t;

T(spacex,sy,spacez,t) = T(spacex,sy,spacez,t-1)...
    -   (-h/r/c/Dx   *   (To   -   T(spacex,sy,spacez,t-1))   +   k/r/c/Dx/Dx   *
(T(spacex,sy,spacez,t-1) - T(spacex-1,sy,spacez,t-1)))*delta_t ...
    + k/r/c * (T(spacex,sy+1,spacez, t-1) - 2*T(spacex,sy,spacez, t-1) + T(spacex,sy-
1,spacez, t-1)) / (Dy*Dy) * delta_t ...
    -   (-h/r/c/Dz   *   (To   -   T(spacex,sy,spacez,t-1))   +   k/r/c/Dz/Dz   *
(T(spacex,sy,spacez,t-1) - T(spacex,sy,spacez-1,t-1)))*delta_t;

%sz = 2 : spacez-1
```

```
T(1,1,sz,t) = T(1,1,sz,t-1)...
    + (h/r/c/Dx * (To - T(1,1,sz,t-1)) + k/r/c/Dx/Dx * (T(2,1,sz,t-1) - T(1,1,sz,t-
1)))*delta_t ...
    + (h/r/c/Dy * (To - T(1,1,sz,t-1)) + k/r/c/Dy/Dy * (T(1,2,sz,t-1) - T(1,1,sz,t-
1)))*delta_t ...
    + k/r/c * (T(1, 1, sz+1, t-1) - 2*T(1, 1, sz, t-1) + T(1, 1, sz-1, t-1)) / (Dz*Dz)
* delta_t;


T(spacex,1,sz,t) = T(spacex,1,sz,t-1)...
    - (-h/r/c/Dx * (To - T(spacex,1,sz,t-1)) + k/r/c/Dx/Dx * (T(spacex,1,sz,t-1) -
T(spacex-1,1,sz,t-1)))*delta_t ...
    + (h/r/c/Dy * (To - T(spacex,1,sz,t-1)) + k/r/c/Dy/Dy * (T(spacex,2,sz,t-1) -
T(spacex,1,sz,t-1)))*delta_t ...
    + k/r/c * (T(spacex, 1, sz+1, t-1) - 2*T(spacex, 1, sz, t-1) + T(spacex, 1, sz-
1, t-1)) / (Dz*Dz) * delta_t;


T(1,spacey,sz,t) = T(1,spacey,sz,t-1)...
    + (h/r/c/Dx * (To - T(1,spacey,sz,t-1)) + k/r/c/Dx/Dx * (T(2,spacey,sz,t-1) -
T(1,spacey,sz,t-1)))*delta_t ...
    - (-h/r/c/Dy * (To - T(1,spacey,sz,t-1)) + k/r/c/Dy/Dy * (T(1,spacey,sz,t-1) -
T(1,spacey-1,sz,t-1)))*delta_t ...
    + k/r/c * (T(1,spacey, sz+1, t-1) - 2*T(1,spacey, sz, t-1) + T(1,spacey, sz-1, t-
1)) / (Dz*Dz) * delta_t;


T(spacex,spacey,sz,t) = T(spacex,spacey,sz,t-1)...
    - (-h/r/c/Dx * (To - T(spacex,spacey,sz,t-1)) + k/r/c/Dx/Dx *
(T(spacex,spacey,sz,t-1) - T(spacex-1,spacey,sz,t-1)))*delta_t ...
    - (-h/r/c/Dy * (To - T(spacex,spacey,sz,t-1)) + k/r/c/Dy/Dy *
(T(spacex,spacey,sz,t-1) - T(spacex,spacey-1,sz,t-1)))*delta_t ...
    + k/r/c * (T(spacex,spacey, sz+1, t-1) - 2*T(spacex,spacey, sz, t-1) +
T(spacex,spacey, sz-1, t-1)) / (Dz*Dz) * delta_t;

%6 faces

T(sx,sy,1,t) = T(sx,sy,1,t-1)...
    + k/r/c * (T(sx+1, sy, 1, t-1) - 2*T(sx, sy, 1, t-1) + T(sx-1, sy, 1, t-1)) /
(Dx*Dx) * delta_t ...
    + k/r/c * (T(sx, sy+1, 1, t-1) - 2*T(sx, sy, 1, t-1) + T(sx, sy-1, 1, t-1)) /
(Dy*Dy) * delta_t ...
    + (h/r/c/Dz * (To - T(sx,sy,1,t-1)) + k/r/c/Dz/Dz * (T(sx,sy,2,t-1) - T(sx,sy,1,t-
1)))*delta_t;
```

```
T(sx,sy,spacez,t) = T(sx,sy,spacez,t-1)...
    + k/r/c * (T(sx+1, sy, spacez, t-1) - 2*T(sx, sy, spacez, t-1) + T(sx-1, sy,
spacez, t-1)) / (Dx*Dx) * delta_t ...
    + k/r/c * (T(sx, sy+1, spacez, t-1) - 2*T(sx, sy, spacez, t-1) + T(sx, sy-1,
spacez, t-1)) / (Dy*Dy) * delta_t ...
    - (-h/r/c/Dz * (To - T(sx,sy,spacez,t-1)) + k/r/c/Dz/Dz * (T(sx,sy,spacez,t-1) -
T(sx,sy,spacez-1,t-1)))*delta_t;


T(sx,1,sz,t) = T(sx,1,sz,t-1)...
    + k/r/c * (T(sx+1, 1, sz, t-1) - 2*T(sx, 1, sz, t-1) + T(sx-1, 1, sz, t-1)) /
(Dx*Dx) * delta_t ...
    + (h/r/c/Dy * (To - T(sx,1,sz,t-1)) + k/r/c/Dy/Dy * (T(sx,2,sz,t-1) - T(sx,1,sz,t-
1)))*delta_t...
    + k/r/c * (T(sx,1,sz+1, t-1) - 2*T(sx, 1, sz, t-1) + T(sx, 1, sz-1, t-1)) /
(Dz*Dz) * delta_t;


T(sx,spacey,sz,t) = T(sx,spacey,sz,t-1)...
    + k/r/c * (T(sx+1, spacey, sz, t-1) - 2*T(sx, spacey, sz, t-1) + T(sx-1, spacey,
sz, t-1)) / (Dx*Dx) * delta_t ...
    - (-h/r/c/Dy * (To - T(sx,spacey,sz,t-1)) + k/r/c/Dy/Dy * (T(sx,spacey,sz,t-1) -
T(sx,spacey-1,sz,t-1)))*delta_t...
    + k/r/c * (T(sx,spacey,sz+1, t-1) - 2*T(sx, spacey, sz, t-1) + T(sx, spacey, sz-
1, t-1)) / (Dz*Dz) * delta_t;


T(1,sy,sz,t) = T(1,sy,sz,t-1)...
    + (h/r/c/Dx * (To - T(1,sy,sz,t-1)) + k/r/c/Dx/Dx * (T(2,sy,sz,t-1) - T(1,sy,sz,t-
1)))*delta_t ...
    + k/r/c * (T(1, sy+1, sz, t-1) - 2*T(1, sy, sz, t-1) + T(1, sy-1, sz, t-1)) /
(Dy*Dy) * delta_t ...
    + k/r/c * (T(1, sy, sz+1, t-1) - 2*T(1, sy, sz, t-1) + T(1, sy, sz-1, t-1)) /
(Dz*Dz) * delta_t;


T(spacex,sy,sz,t) = T(spacex,sy,sz,t-1)...
    - (-h/r/c/Dx * (To - T(spacex,sy,sz,t-1)) + k/r/c/Dx/Dx * (T(spacex,sy,sz,t-1) -
T(spacex-1,sy,sz,t-1)))*delta_t ...
    + k/r/c * (T(spacex, sy+1, sz, t-1) - 2*T(spacex, sy, sz, t-1) + T(spacex, sy-1,
sz, t-1)) / (Dy*Dy) * delta_t ...
    + k/r/c * (T(spacex, sy, sz+1, t-1) - 2*T(spacex, sy, sz, t-1) + T(spacex, sy,
sz-1, t-1)) / (Dz*Dz) * delta_t;
```

```
end

toc
```

```
Elapsed time is 4.166959 seconds.
```

```
load 'experimental_data_anti_abrasion.mat'

figure()
lapse = 35;                          % adjust accordingly
frames = 9;                          % from experiments
void_1 = imresize(temp_2, [9 50]);  % experiment



void_2     =     reshape(T(:,int32(spacey/2),spacez,lapse:120:lapse+(frames-1)*120)-
273.15,25,9);
void_3 = imresize(void_2, [50 9]);  % simulation

temp_3 = zeros(9,3);

for g = 1:frames
    hold on
    plot (void_3(:,g),'red')
    plot (void_1(g,:),'k.');
    temp_3(g,1) = min ((T(:,int32(spacey/2),spacez,lapse+(g-1)*120)-273.15));
    temp_3(g,2) = min (temp_2(g,:));
    temp_3(g,3) = lapse+(g-1)*120;
    legend('Simulated data','Experimental data')
        xlabel('distance (mm)')
        ylabel('Temperature (^oC)')
    title('Temperature of anti-abrasion polyurethane')
end

hold off

figure()
plot (temp_3(:,3),temp_3(:,1),'red')
hold on
plot (temp_3(:,3),temp_3(:,2),'k.')
legend('Simulated temperature','Experimental temperature','location','northwest')
        xlabel('time (s)')
    ylabel('Temperature (degrees ^oC)')
title('Temperature of anti-abrasion polyurethane')
```

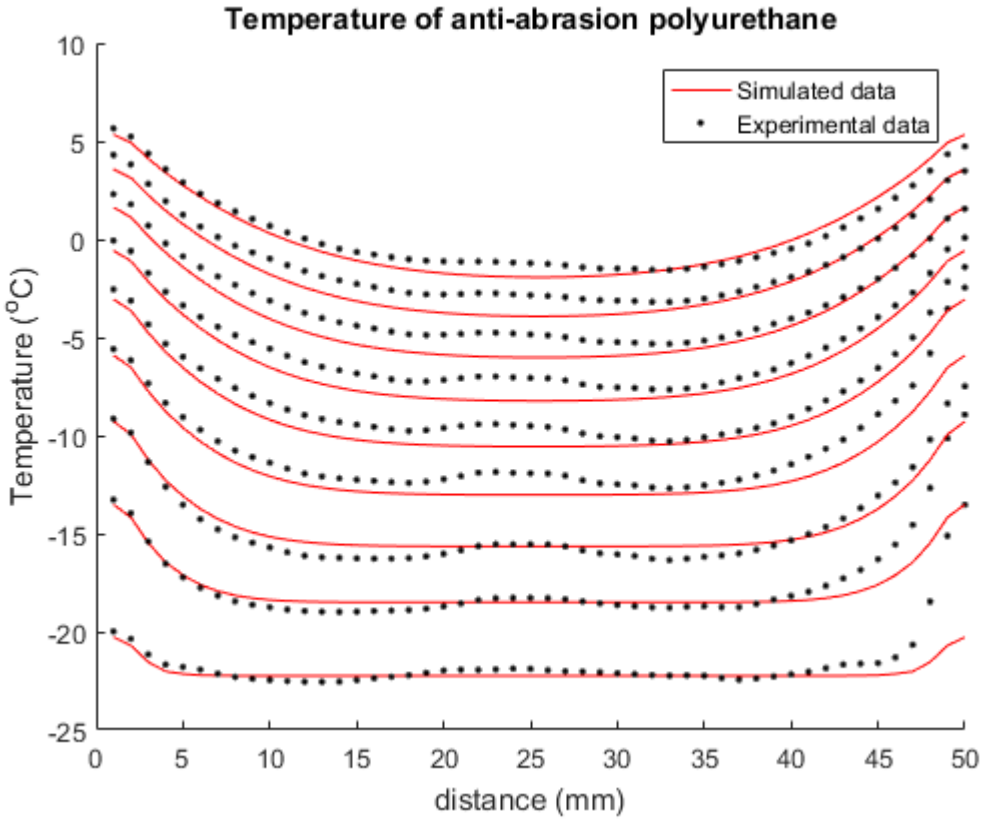

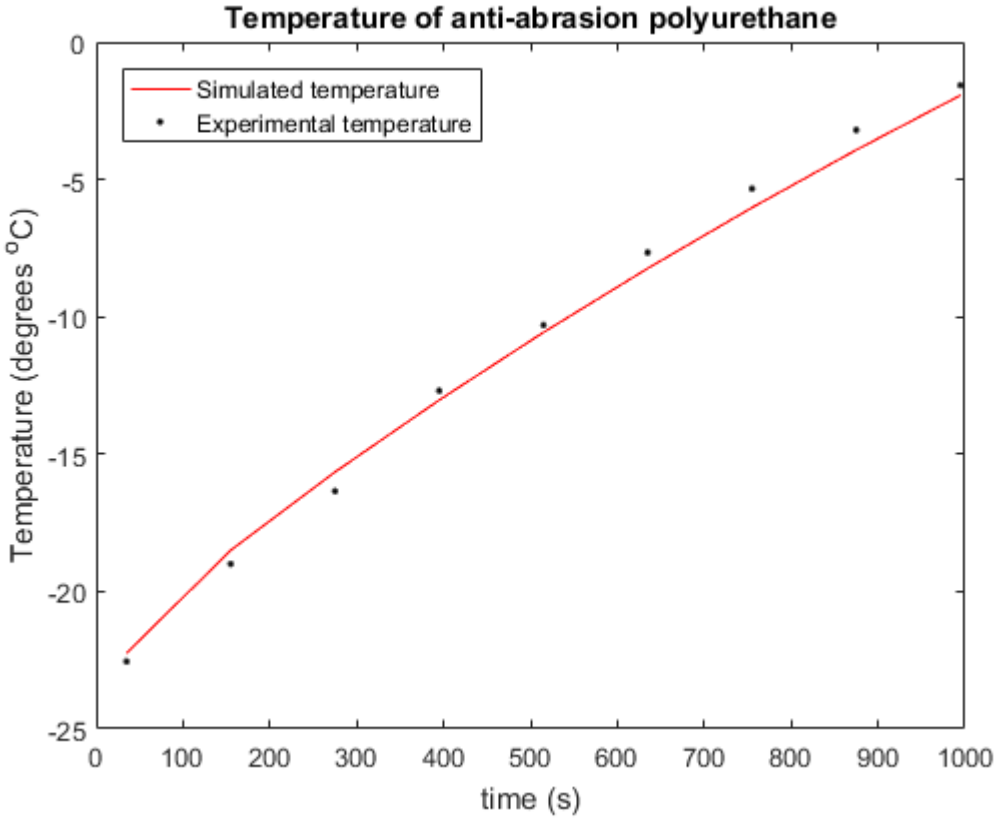


```
frame = int32(309/2);    %at what time the temperature should be calculated. Refer to
Data_1.m, which refers to the experimantal data.
figure;
```

```
dummy_T3 = reshape(T(:,:,1,100)-273, spacex, spacey); %time 100 in simulation refers
to frame 233 in experimental data
void = imresize(dummy_T3, [1500 1500]);
pcolor (void), shading flat

colormap jet
colorbar
axis equal

figure;
plot (dummy_T3(:,25))
title('Temperature at pos. 13')
```

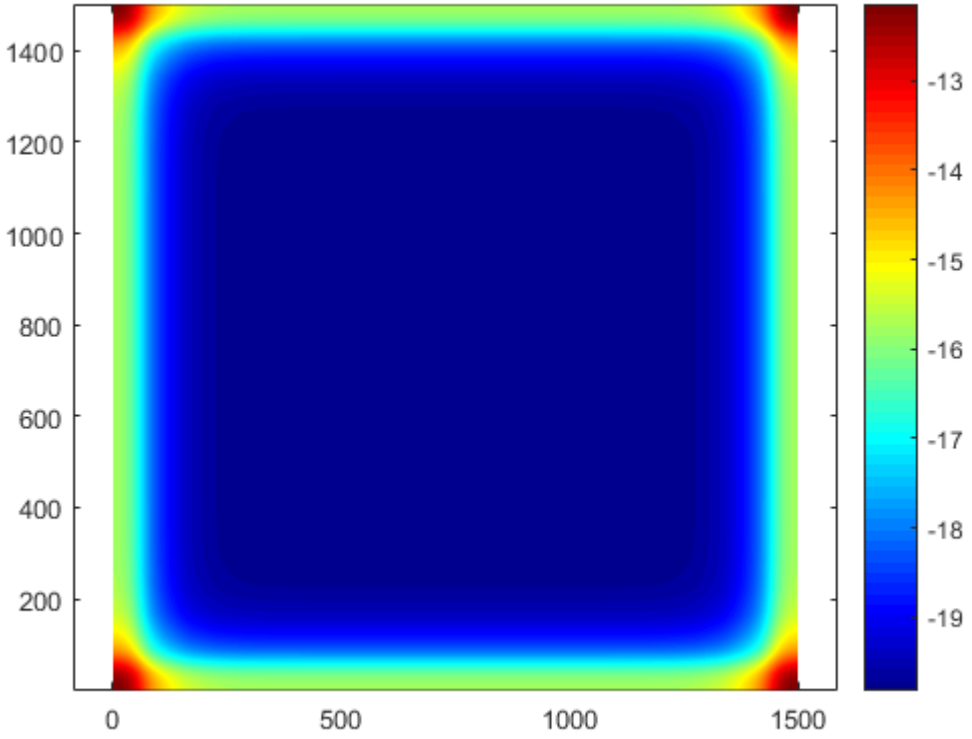

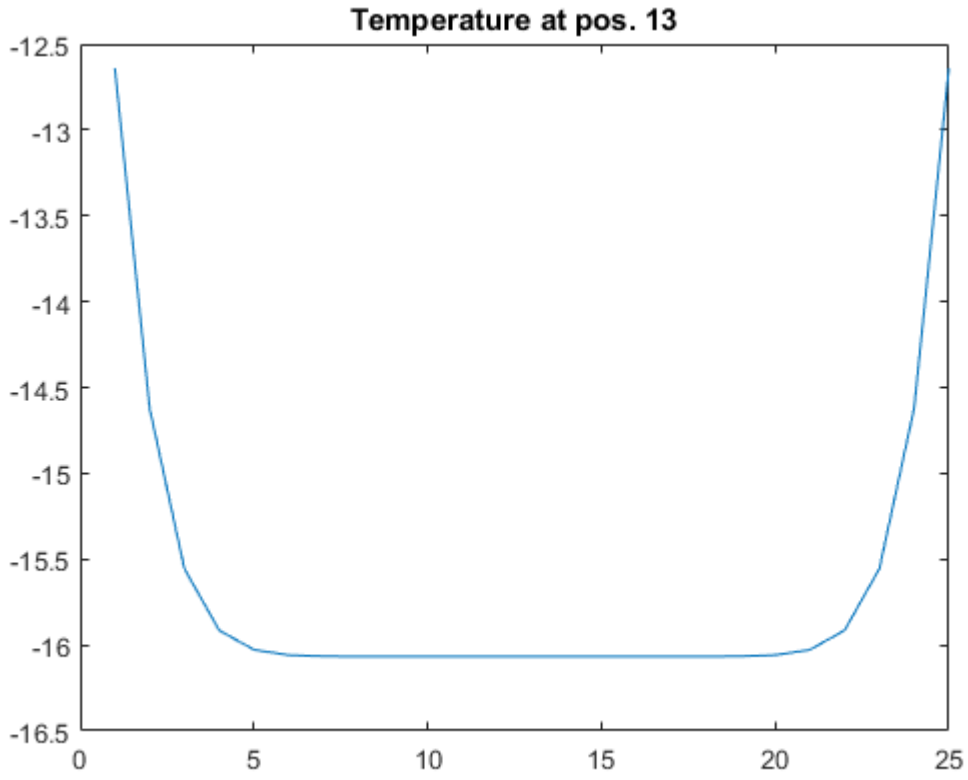

Published with MATLAB® R2016b